Electronic Supplementary Material (ESI) for ChemComm.

Supporting Information for

Isostructural σ-hydrocarbyl phospholide complexes of uranium, neptunium, and plutonium

Michaela Černá,[a] John A. Seed,[a] Sara Garrido Fernandez,[a] Michael T. Janicke,[b] Brian L. Scott,[c] George F. S. Whitehead,[a] Andrew J. Gaunt,[b] and Conrad A. P. Goodwin*[a,b]

[a] Centre for Radiochemistry Research, Department of Chemistry, The University of Manchester, Oxford Road, Manchester, M13 9PL (UK).

[b] Chemistry Division, Los Alamos National Laboratory, Los Alamos, New Mexico, 87545 (USA).

[c] Materials Physics & Applications Division, Los Alamos National Laboratory, Los Alamos, New Mexico, 87545 (USA).

*To whom correspondence should be addressed:

conrad.goodwin@manchester.ac.uk

Table of contents

S1. Experimental details

Radiological considerations

Caution! The U (natural abundance, assumed standard composition: 0.7204% ^{235}U, $t_{½}$ = 7.04×10^{8}; 99.2742% ^{238}U, $t_{½}$ = 4.468×10^{9} – depleted U was also used, which has similar hazards), ^{237}Np ($t_{½}$ = 2.144×10^{6} years), and ^{239}Pu ($t_{½}$ = 2.411×10^{5} years) radionuclides – and their daughters – present serious health threats due to their α-, β-, and γ-emissions. ^{237}Np establishes a secular equilibrium (asymptotical concentration at 34.6 ppb) with the potent β-emitter ^{233}Pa ($t_{1/2}$ = 26.975(13) days, A = 777 TBq g^{-1}), which pertains also to an intense γ-ray emission. Accordingly, the primary occupational hazard of these systems is due to severe radiotoxic (α-particles) and heavy-metal toxicity effects, though for ^{237}Np cumulative tissue absorptive dose rates must be considered and protected against. Hence, all studies that involved manipulation of these isotopes were conducted in a radiation laboratory equipped with high efficiency particulate air (HEPA) filtered hoods and in negative pressure gloveboxes. Additional safeguards included continuous air monitoring and use of hand-held radiation monitoring equipment. Entrance to the laboratory space was controlled with a hand and foot radiation monitoring instrumentation and a full body personal contamination monitoring station. The handling of free-flowing solids was restricted to be within negative pressure gloveboxes equipped with HEPA filters. In addition to standard laboratory PPE, aqueous solutions were handled using multiple layers of latex gloves combined with DuPont™ Tyvek® 400 sleeves to provide overlapping coverage of the arms. Due to these radiological hazards, elemental analyses were not possible for ^{237}Np- and ^{239}Pu-containing materials.

Chemical reagents except solvents

[LnI$_3$(THF)$_4$] (Ln = La, Ce, Pr),[1] [U(BH$_4$)$_4$]$_n$,[2] [AnI$_3$(THF)$_4$] (An = Np, Pu),[3], and UI$_3$(OEt$_2$)$_x$ (*X* assumed to = 1 by mass determination),[4] were prepared as described elsewhere. KTMP

(KPC_4Me_4) was prepared according to a literature procedure,[5] and the crystal structure of its THF-adduct, $[K(THF)_2(TMP)]_n$ (**4**), is reported here for the first time. Lewis-base free KBn (KC_7H_7) was prepared from a slight excess (1.05 equiv.) of *n*-BuLi (2.5 M, Sigma Aldrich) and *t*-BuOK in toluene at room temperature followed by exhaustive washing of the precipitated orange powder with toluene and then *n*-hexane to remove *t*-BuOLi and residual *n*-BuLi. 3 or 4 Å molecular sieves were activated by heating for 8–36 hours (240 °C at 10^{-3} to 10^{-4} mbar until vacuum pressure stable).

Equipment, materials, and solvents used with transuranium elements

A negative-pressure, transuranium capable, helium atmosphere glovebox (UHP helium – AirGas) was used for all work involving the synthesis of transuranium compounds. The glovebox atmosphere was maintained with a standalone Vacuum Atmosphere Genesis™ oxygen and moisture removal system, and atmosphere suitability was verified using a dilute toluene solution of $[Ti(Cp)_2(\mu\text{-}Cl)]_2$ (200 mg of commercial $[Ti(Cp)_2(Cl)_2]$ reduced over an excess of Zn powder in 20 mL of toluene, and filtered) prior to any manipulations such that the residue dried to a dark green colour each time (a colour change to yellow or orange indicates decomposition of the Ti test compound and atmospheric O_2/H_2O removal is required). Anhydrous THF (Sigma Aldrich), anhydrous *n*-hexane (Sigma Aldrich), and anhydrous toluene (Sigma Aldrich) were transferred onto activated 3 or 4 Å molecular sieves, stored for 1 week and degassed before use. C_6D_6, C_4D_8O, (Sigma Aldrich) were stored over activated 4 Å molecular sieves and degassed before use – all solvents were tested with a dilute THF solution of Na_2Ph_2CO (150 mg Ph_2CO in 20 mL of THF with an excess of Na metal) such that THF required 1 drop / mL to retain purple colouration and hydrocarbon solvents required 1 drop / 2 mL.

All glassware, and glass-fibre filter discs, was stored in a vacuum oven (>150 °C) for 24 hours prior to being brought into the glovebox, and FEP (fluorinated ethylene propylene) NMR liners were brought into the box *via* overnight or multi-hour vacuum cycles. A vacuum oven was not used for reactions involving non-transuranium elements. Transuranium crystals for single-crystal X-ray diffraction were mounted in Paratone-N or NVH oil inside 0.5 mm quartz capillaries (Charles Supper). The quartz capillaries were inserted through silicone stoppers and placed inside test tubes to allow handling inside the transuranium glovebox while mounting crystals without contaminating the exterior surface of the capillary. The capillaries were then cut to appropriate size for later goniometer mounting with nail clippers. The ends of the cut capillaries were sealed with hot capillary wax before being removed from the glovebox for coating in clear nail varnish (Hard as Nails™) to provide shatter-resilience.[6] During the clipping and wax sealing steps, care must be taken to avoid the capillary touching any contaminated surfaces (this is achieved by the introduction of fresh petri dishes, forceps, clippers, and wax, as needed in conjunction with careful handling techniques to avoid contamination transfer). Solution phase UV-vis-NIR spectra were collected at ambient temperature using a Varian Cary 6000i UV-vis-NIR spectrometer. The solution was contained in a low volume (1 mL) screw-capped quartz cuvette (1 cm path length) that was loaded in a transuranium glovebox (or HEPA filtered fume hood as appropriate) using Parafilm to protect the exterior surface of the cuvette and cap from radioactive contamination (parafilm removed in fume hood prior to data acquisition). Data was collected from 40,000 to 6,250 cm^{-1} (250 to 1,600 nm). Where ε values are reported for molecular complexes below there is a modest error due to the small quantities of weighed material, as is nearly always the case when these values are reported from synthetic chemistry (as opposed analytical determination methods). Nonetheless it is a useful metric to determine based on weight of crystal dissolved and solvent weight. For NMR spectroscopy, solution was loaded into a fresh FEP NMR liner that was protected from surface contamination with Parafilm while inside a transuranium glovebox. The liner was sealed with

two PTFE plugs, brought out of the glovebox, and verified to be free of surface contamination before the parafilm was removed. The liner was then loaded into a J. Young tap appended 5 mm NMR tube, the headspace was then evacuated and refilled with He to provide an inert atmosphere headspace above the sample. NMR spectroscopy data collection was performed on a Bruker Avance II (400 MHz) at 295 K to 299 K (temperature indicated on figure captions and experimental section).

Equipment, materials, and solvents used with lanthanide elements or uranium

All Schlenk glassware and spectroscopy vessels (UV-vis-NIR cuvettes and NMR tubes) were stored in an oven (150 °C) for 12 hours prior to use. Schlenk vessels were also heated under vacuum (10^{-3} mbar) using a butane flame and allowed to cool before final use. An MBraun UniLab glovebox (argon or dinitrogen – Linde) equipped with solvent scrubber and integral O_2/H_2O sensors was used for sample preparation and storage, while syntheses were performed using standard Schlenk techniques. The inert gas supply (argon – Linde) for Schlenk work was purified by passage through a column of activated molecular sieves and glovebox oxygen removal catalyst. THF, toluene, Et_2O and *n*-pentane solvents were dried by passage through activated Al_2O_3 towers (INERT Corp.), while *n*-hexane was distilled from potassium. All solvents were stored over potassium mirrors except for THF which was stored over activated 4 Å sieves – solvents were degassed before use. Deuterated solvents C_6D_6 and C_4D_8O were distilled from potassium, degassed by three freeze-pump-thaw cycles, and stored under argon prior to use. ATR-IR spectra were recorded on microcrystalline samples using a Bruker Alpha II spectrometer with a Platinum-ATR module in a glovebox. UV-vis-NIR spectroscopy was performed on samples in Youngs tap appended 10 mm path length quartz cuvettes on an Agilent Technologies Cary Series UV-vis-NIR spectrophotometer at 57,143–3,333 cm^{-1} (175–3,000 nm). Elemental microanalyses (C/H/N) were carried out by Martin

Jennings and Anne Davies at the University of Manchester. NMR spectroscopy data collection was performed on a Bruker Avance III (400 MHz or 500 MHz) at 295 K to 299 K (temperature indicated on figure captions and experimental section). Static and variable-temperature magnetic moment data were recorded in an applied dc field of 0.5 T on a Quantum Design MPMS superconducting quantum interference device (SQUID) magnetometer. Care was taken to ensure the sample was at thermal equilibrium before each data point was measured, and samples were immobilised in an eicosane matrix to prevent sample reorientation during measurements. Diamagnetic corrections were applied using tabulated Pascal constants, and measurements were corrected for the effect of the blank sample holders (flame sealed Wilmad NMR tube and straw) and eicosane matrix.

A note on NMR spectroscopy of paramagnetic samples

All spectra were referenced to internal solvent residuals (^{1}H and ^{13}C) or externally to 10% TMS in $CDCl_3$ (^{31}P) *via* Equation S1, which is the IUPAC recommended convention.

Equation S1. $$\Delta\ (Hz) = \frac{SR^{1H}}{SF^{1H}} \times SF^{NUC}$$

Where SR^{1H} is the spectrum reference frequency (in Hz) of a reference ^{1}H NMR spectrum collected with TMS set to 0 ppm collected under the same experimental conditions; SF^{1H} is the spectrometer frequency (in MHz) for the ^{1}H nucleus; SF^{NUC} is the spectrometer frequency (in MHz) of the nucleus in question. The answer is given in Hz.

Paramagnetic samples become magnetised in the presence of an external magnetic field, such as that of an NMR spectrometer. The level of magnetisation will approximately follow Curie's law when saturation of magnetisation is not reached ($\mu_B \leq k_BT$). The magnetic response of a

sample is proportional to: (i) sample temperature; (ii) external field strength; and (iii) sample concentration. This necessarily affects the reproducibility of the chemical shifts given for paramagnetic samples – a sample run at a different concentration, or a different field strength, or at a different temperature, will produce a different paramagnetic contribution to the observed chemical shift. Moreover, the direction that an individual chemical shift will change (upfield or downfield) cannot easily be predicted.[7] Finally, modern convention to reference chemical shift relative to solvent residual peaks further complicates the comparison of multiple samples as the factors listed above will also change the absolute shift of the solvent peak (relative to the spectrometer proton frequency) as the susceptibility of solvent molecules may differ from the ligand atoms surrounding a paramagnetic ion. Though, solvent effects even in diamagnetic NMR samples can vary chemical shift by several ppm for some nuclei.[8]

Considering these caveats, we report our data as it is output from experiment with rounding to two decimal places as this is convention. We defer to the expertise of the reader to interpret the data reported here in a way that is appropriate for their needs.

*Synthesis of complexes **1–3***

Synthesis of $[Np(TMP)_2Cl_2K(Et_2O)]_n$ (1). In an inert atmosphere transuranium glovebox: Et_2O (4 mL) was added to a mixture of $[NpCl_4(DME)_2]$ (35.0 mg, 63 μmol) and KTMP (33.0 mg, 188 μmol, 3 equiv.) in a 20 mL glass scintillation vial with a Teflon-coated stir bar. An immediate pale orange/brown colour developed in the solution which changed to intense blue/purple over the course of 5 minutes. The mixture was stirred for 16 hours, then filtered into a 4 mL glass vial through Celite® packed atop 2 half-discs of glass microfiber mounted in a glass pipette. Volatiles were removed *in vacuo*, which left a blue solid. Toluene (2 mL) was added to the solids and warmed gently until most of the material had dissolved to form a dark solution. The solution was filtered into a 4 mL glass vial through Celite® packed atop 2 half-discs of glass microfiber mounted in a glass pipette, and the filter material washed with hot toluene (1 mL). Dark purple solids remained on the filter material and in the vial previously extracted with toluene. Et_2O (3 mL) was used to extract the purple solids from the vial and filter. Both the Et_2O and toluene extracts were stored at –35 °C for 7 days. Several crystals of $[Np(TMP)_2Cl_2K(Et_2O)]_n$ (**1**) formed from the Et_2O fraction, and the structure was determined, but no crystalline material could be recovered from the toluene fraction.

Synthesis of $[Np(TMP)_2Cl_2K(DME)]_n$ (2). In an inert atmosphere transuranium glovebox: solid KTMP (23.9 mg, 134 μmol, 3 equiv.) was added to a pale pink solution of $[NpCl_4(DME)_2]$ (25.0 mg, 45 μmol) in THF (1.5 mL) in a 20 mL glass scintillation vial with a Teflon-coated stir bar. The solution immediately turned an intense dark red/purple colour. The mixture was stirred for 30 minutes, and then volatiles were removed *in vacuo* to afford a purple solid. Toluene (1.5 mL) was added and heated to 100 °C for 1 minute which afforded a dark purple solution which was filtered into a 4 mL glass vial through 2 half-discs of glass microfiber mounted in a glass pipette. The purple solution was concentrated to 2 mL and stored at –35 °C for 16 hours which

gave a small crop of dark blue/black plate-shaped crystals, which were found to be $[Np(TMP)_2Cl_2K(DME)]_n$ (**2**). The crystals were then isolated by decanting the supernatant followed by drying *in vacuo* for several hours (yield 3.2 mg, 11%).

^{1}H NMR (C_4D_8O, 400.13 MHz, 295 K): δ = –5.67 (d, $^3J_{HP}$ = 7.7 Hz, 12 H, TMP 2,5-C(C$\underline{H}_3$)), 3.10 (s, 12 H, TMP 3,4-C(C$\underline{H}_3$)), 3.27 (s, 1.5 H, DME O(C$\underline{H}_3$)), 3.43 (s, 1 H, DME (C$\underline{H}_2$)$_2$) – note that the integrals for the DME protons do not match their theoretical values of 6 H and 4 H, presumably due to loss of some coordinated DME during drying of the crystals.

^{13}C{^{1}H} NMR (C_4D_8O, 100.62 MHz, 296 K): δ = –46.03 (d, J_{CP} = 15.1 Hz, TMP C($\underline{C}$H$_3$)), –15.23 (TMP C($\underline{C}$H$_3$)), 58.94 (DME O($\underline{C}$H$_3$)), 72.81 (DME ($\underline{C}$H$_2$)$_2$), 187.98 (TMP $\underline{C}$(CH$_3$)), 195.74 (d, J_{CP} = 48.9 Hz, TMP $\underline{C}$(CH$_3$)).

^{31}P NMR (C_4D_8O, 161.98 MHz, 295 K): δ = 445.35 (TMP P).

UV-vis-NIR (THF) λ_{max} / nm (cm^{-1}, ε / M^{-1} cm^{-1}) = 419 (23,866, *1,446*), 519 (19,268, *1,054*), 544 (18,396, *967*), 550 (18,182, *951*), 561 (17,838, *897*), 591 (16,915, *646*), 642 (15,567, *364*), 680 (14,715, *193*), 801 (12,484, *161*), 820 (12,189, *217*), 831 (12,031, *257*), 851 (11,751, *126*), 877 (11,397, *247*), 910 (10,987, *157*), 920 (10,870, *120*), 932 (10,730, *84*), 967 (10,343, *95*), 1,025 (9,756, *448*), 1,064 (9,397, *94*), 1,210 (8,266, *40*), 1,391 (7,188, *287*), 1,483 (6,745, *41*).

Synthesis of [{Np(TMP)$_2$}$_2$(μ-Cl)(μ-O$_2$PC$_4$Me$_4$-κ*O*,*O*')] (3). '$NpCl_3(THF)_n$' was prepared similarly to previous reports,[9-10] alkali-metal graphite reduction of $[NpCl_4(DME)_2]$. In an inert atmosphere transuranium glovebox: $[NpCl_4(DME)_2]$ (70 mg, 125 μmol) in a 20 mL glass scintillation vial with a Teflon-coated stir bar was triturated twice with THF (1.5 mL), forming a pink oily solid after each drying period. The pink semi-solid was then dissolved in THF (2 mL) and solid KC_8 (16.9 mg, 125 μmol, 1 equiv.) was tapped in with stirring, which caused an immediate colour change to yellow/green which upon settling revealed a yellow solution with black solids. After stirring for 5 minutes, the yellow solution was filtered into a 20 mL glass

scintillation vial through Celite® packed atop 2 half-discs of glass microfiber mounted in a glass pipette, and the filter was washed with THF until the filtrate was colourless (*ca*. 2 mL). The bright yellow solution was concentrated *in vacuo* to *ca*. 1 mL, then *n*-hexane (5 mL) was added with stirring which caused a yellow precipitate to form. The supernatant was decanted, and the solids were washed with *n*-hexane (3 mL) then dried to give crude '$NpCl_3(THF)_n$' (32 mg).

Half (16 mg) of the as-prepared '$NpCl_3(THF)_n$' described above was combined with KTMP (20 mg, 112 μmol, 2 equiv. w.r.t. half of the Np-content from the first step) in a 20 mL glass scintillation vial with a Teflon-coated stir bar. THF (3 mL) was added which afforded a burgundy solution immediately, which was stirred for 10 minutes. The volatiles were removed *in vacuo* then extracted at room temperature with toluene (3 mL) which was filtered into a 4 mL glass vial through 2 half-discs of glass microfiber mounted in a glass pipette. Concentration of the dark blue solution followed by storage at –35 °C gave several crystals of **3** and no other identifiable products.

*Synthesis of $[U(TMP)_2(I)(THF)]$ (**5**) and $[U(TMP)_2Bn_2K(benzene)]$ (**7U**)* in situ *from $UI_3(OEt_2)_x$*

Synthesis of $[U(TMP)_2(I)(THF)]$ (5) and $[U(TMP)_2Bn_2K(benzene)]$ (7U) *in situ* from $UI_3(OEt_2)_x$. In a transuranium glovebox, THF (1.5 mL) was added to a mixture of solid KTMP (25.7 mg, 144 μmol, 2 equiv.) and $UI_3(OEt_2)_x$ (50.0 mg, 72 μmol) in a 20 mL glass scintillation vial with a Teflon-coated stir bar. The solution immediately turned an intense dark red/brown colour with precipitation of pale solids. The mixture was stirred for 5 minutes, then a small aliquot (<0.1 mL) was filtered into a 4 mL glass vial through 2 half-discs of glass microfiber mounted in a glass pipette along with a rinse of the filter material with THF (*ca*. 0.2 mL). Volatiles were removed from the aliquot, which was redissolved in Et_2O (*ca*. 0.2 mL) to give a dark green solution which was stored at –35 °C and afforded a green block of $[U(TMP)_2(I)(THF)]$ (**5**) as determined by single-crystal X-ray diffraction. The remaining THF

solution was treated with solid KBn (18.7 mg, 144 μmol, 2 equiv.) which caused a slight change in the solution colour to a darker shade of red, along with the precipitation of pale solids. After stirring for 5 minutes, volatiles were removed *in vacuo* to afford a brown/red solid. Benzene (2.5 mL) was added to the solids and heated to a gentle boil for 1 minute and then filtered hot into a 4 mL glass vial through 2 half-discs of glass microfiber mounted in a glass pipette. The red/brown solution was concentrated to 1.5 mL, some solids were warmed gently back into solution and the mixture was left to stand at room temperature which gave a small crop of black crystals (yield 7.0 mg), whose composition was inferred to be [U(TMP)$_2$Bn$_2$K(benzene)] (**7U**) by UV-vis-NIR spectroscopic comparison with a genuine sample of [U(TMP)$_2$Bn$_2$K(toluene)] (**6U**) (*vide supra*) – no other data could be gathered from this sample, hence **6U** was synthesised independently by an alternative route.

*Synthesis of [M(TMP)$_2$Bn$_2$K(toluene)] (**6M**, M = La, Ce, Pr) from [MI$_3$(THF)$_4$]*

Synthesis of [La(TMP)$_2$Bn$_2$K(toluene)] (6La). THF (15 mL) was added to a pre-cooled (–98 °C) mixture of [LaI$_3$(THF)$_4$] (0.4040 g, 0.5 mmol) and KTMP (0.1782 g, 1 mmol, 2 equiv.) in a Schlenk flask with a Teflon-coated stirrer bar. The pale-yellow mixture was stirred and allowed to warm to room temperature. After 3.5 hours, the mixture was cooled to –98 °C then a solution of KBn (0.1302 g, 1 mmol, 2 equiv.) in THF (15 mL) was added which caused a darkening of the solution and precipitation of a pale powder. The mixture was warmed to room temperature then stirred for 16 hours. Volatiles were removed *in vacuo* from the pale brown mixture to afford a brown solid. Toluene (25 mL) was added to the flask which was then vigorously stirred at reflux for several minutes, allowed to settle briefly, then filtered hot to a small Schlenk flask. Concentration of the pale brown solution gave a small crop of yellow crystals of **6La** at room temperature, further crops were obtained by cooling the mixture to –28 °C which were isolated

by decanting the supernatant followed by drying *in vacuo* for several hours (combined yield 0.188 g, 51%).

Found: C, 58.41; H, 6.16. Calc. for $LaKP_2C_{30}H_{38}\cdot(C_7H_8)_{0.5}$: C, 58.77; H, 6.18.

^{1}H NMR (C_4D_8O, 400.13 MHz, 295 K): δ = 1.04 (s, 4 H, Bn C$\underline{H}_2$), 1.96 (s, 12 H, TMP 3,4-C(C$\underline{H}_3$)), 2.08 (d, $^3J_{HP}$ = 9.7 Hz, 12 H, TMP 2,5-C(C$\underline{H}_3$)), 2.30 (s, 3 H, toluene C$\underline{H}_3$), 6.14 (t, $^3J_{HH}$ = 7.2 Hz, 2 H, Bn *p*-C$\underline{H}$), 6.40 (d, $^3J_{HH}$ = 8.2 Hz, 4 H, Bn *o*-C$\underline{H}$), 6.67 (t, $^3J_{HH}$ = 7.7 Hz, 4 H, Bn *m*-C$\underline{H}$), 7.04–7.22 (m, 5H, toluene C$\underline{H}$).

^{13}C{^{1}H} NMR (C_4D_8O, 100.61 MHz, 296 K): δ = 15.04 (TMP C($\underline{C}H_3$)), 16.41 (d, J_{CP} = 28.9 Hz, TMP C($\underline{C}H_3$)), 21.54 (toluene $\underline{C}H_3$), 114.25 (Ar $\underline{C}$H), 123.09 (Ar $\underline{C}$H), 126.08 (Ar $\underline{C}$H), 128.34 (Ar $\underline{C}$H), 128.95 (Ar $\underline{C}$H), 129.72 (Ar $\underline{C}$H), 133.38 (TMP $\underline{C}(CH_3)$), 138.48 (Ar $\underline{C}$H), 141.66 (d, J_{CP} = 47.7 Hz, TMP $\underline{C}(CH_3)$), 155.63 (Bn $\underline{C}H_2$).

^{31}P NMR (C_4D_8O, 161.98 MHz, 295 K): δ = 93.66 (TMP P).

UV-vis-NIR (THF) λ_{max} / nm (cm^{-1}, ε / M^{-1} cm^{-1}) = no peaks could be observed, just a broad featureless LMCT band that tails into *ca*. 606 nm (16,500 cm^{-1}).

ATR-IR ($\bar{\nu}$, cm^{-1}) = 3,057 (vw), 2,967 (w), 2,910 (w), 2,855 (w), 2,718 (vw), 1,584 (m), 1,550 (w), 1,474 (m), 1,450 (m), 1,447 (m), 1,399 (w), 1,376 (w), 1,366 (w), 1,324 (vw), 1,292 (w), 1,249 (vw), 1,227 (m), 1,176 (m), 1,149 (w), 1,095 (w), 1,081 (vw), 1,020 (w), 994 (w), 955 (vw), 881 (m), 819 (m), 786 (s), 737 (vs), 698 (vs), 537 (m), 516 (m), 509 (s), 470 (m).

Synthesis of [Ce(TMP)$_2$Bn$_2$K(toluene)] (6Ce). The same procedure and scale as above was followed, orange crystals (yield 0.180 g, 49%).

Found: C, 58.79; H, 6.07. Calc. for $CeKP_2C_{30}H_{38}\cdot(C_7H_8)_{0.5}$: C, 58.67; H, 6.17.

Magnetic moment (Evans method, 299 K, C_4D_8O) μ_{eff} = 2.79(1) μ_B.

^{1}H NMR (C_4D_8O, 400.13 MHz, 299 K): δ = 1.22 (s, 12 H, TMP C(C$\underline{H}_3$)), 2.30 (s, 3 H, toluene C$\underline{H}_3$), 2.94 (br s, $\nu_{½}$ = 17 Hz, 12 H, TMP C(C$\underline{H}_3$)), 3.65 (br s, $\nu_{½}$ = 17 Hz, 4 H, Bn *o/m*-C$\underline{H}$), 4.57

(t, $^{3}J_{HH}$ = 6.8 Hz, 2 H, Bn *o*-C*H*), 6.07 (br s, $v_{½}$ = 9 Hz, 4 H, Bn *o/m*-C*H*), 7.03–7.22 (m, 5H, toluene C*H*), 14.13 (br s, $v_{½}$ = 59 Hz, 4 H, Bn CH_2).

$^{13}C\{^{1}H\}$ NMR (C_4D_8O, 100.61 MHz, 298 K): δ = 7.84 (TMP C(*C*H_3)), 21.54 (toluene *C*H_3), 119.61 (Ar *C*H), 121.11 (Ar *C*H), 126.08 (Ar *C*H), 128.95 (Ar *C*H), 129.72 (Ar *C*H), 138.48 (Ar *C*H) – we could not conclusively locate any remaining peaks, such as the Bn *C*H_2.

^{31}P NMR (C_4D_8O, 161.98 MHz, 299 K): δ = 175.30 (TMP P).

UV-vis-NIR (THF) λ_{max} / nm (cm^{-1}, ε / M^{-1} cm^{-1}) = 480 (20,812, *317*).

ATR-IR ($\bar{\nu}$, cm^{-1}) = 3,058 (vw), 2,966 (w), 2,949 (w), 2,909 (w), 2,853 (w), 2,717 (vw), 1,583 (m), 1,551 (w), 1,534 (vw), 1,491 (w), 1,486 (w), 1,474 (m), 1,450 (m), 1,444 (m), 1,398 (w), 1,376 (w), 1,366 (w), 1,324 (vw), 1,292 (w), 1,248 (vw), 1,226 (m), 1,176 (m), 1,149 (w), 1,116 (w), 1,094 (w), 1,081 (w), 1,059 (vw), 1,054 (vw), 1,039 (w), 1,020 (w), 995 (w), 974 (vw), 954 (w), 905 (vw), 883 (m), 856 (vw), 822 (s), 788 (s), 738 (vs), 698 (vs), 617 (m), 551 (m), 538 (m), 531 (m), 509 (s), 491 (m), 480 (m), 470 (s), 438 (m), 437 (m), 427 (m), 422 (m), 419 (m), 415 (m), 408 (m), 401 (m).

Synthesis of [Pr(TMP)$_2$Bn$_2$K(toluene)] (6Pr). The same procedure and scale as above was followed, green/orange crystals (yield 0.196 g, 53%).

Found: C, 58.70; H, 6.05. Calc. for $PrKP_2C_{30}H_{38}\cdot(C_7H_8)_{0.5}$: C, 58.60; H, 6.17.

Magnetic moment (Evans method, 299 K, C_4D_8O) μ_{eff} = 3.82(2) μ_B.

^{1}H NMR (C_4D_8O, 400.13 MHz, 299 K): δ = 1.46 (s, 12 H, TMP C(C*H*$_3$)), 2.29–2.30 (overlapping s, 12 H + 3 H, TMP C(C*H*$_3$) + toluene C*H*$_3$), 2.78 (t, $^{3}J_{HH}$ = 7.2 Hz, 2 H, Bn *p*-C*H*), 3.32 (d, $^{3}J_{HH}$ = 7.7 Hz, 4 H, Bn *o*-C*H*), 7.04–7.18 (m, 5H, toluene C*H*), 7.22 (t, $^{3}J_{HH}$ = 7.2 Hz, 4 H, Bn *m*-C*H*), 7.48 (br s, $v_{½}$ = 22 Hz, 4 H, Bn C*H*$_2$).

$^{13}C\{^{1}H\}$ NMR (C_4D_8O, 100.61 MHz, 298 K): δ = –6.81 (TMP C(*C*H_3)), –3.89 (TMP C(*C*H_3)), 21.53 (toluene *C*H_3), 111.67 (Ar *C*H), 126.07 (Ar *C*H), 126.93 (Ar *C*H), 128.94 (Ar *C*H), 129.70

(Ar *C*H), 133.55 (TMP *C*(CH_3)), 138.46 (Ar *C*H), 143.92 (TMP *C*(CH_3)) – we could not conclusively locate any remaining peaks, such as the Bn *C*H_2.

^{31}P NMR (C_4D_8O, 161.98 MHz, 299 K): δ = 293.52 (TMP P).

UV-vis-NIR (THF) λ_{max} / nm (cm^{-1}, ε / M^{-1} cm^{-1}) = 462 (21,622, *145*), 491 (20,367, *52*), 505 (19,802, *40*), 597 (16,750, *10*), 600 (16,653, *11*), 604 (16,543, *10*), 607 (16,461, *11*), 835 (11,969, *11*), 1,478 (6,766, *11*), 1,571 (6,367, *14*), 1,596 (6,266, *15*).

ATR-IR ($\bar{\nu}$, cm^{-1}) = 3,058 (vw), 2,967 (vw), 2,910 (w), 2,854 (w), 2,716 (vw), 1,583 (m), 1,552 (w), 1,474 (m), 1,444 (m), 1,399 (w), 1,376 (w), 1,365 (w), 1,293 (w), 1,251 (vw), 1,226 (m), 1,176 (m), 1,148 (w), 1,096 (w), 1,081 (w), 1,021 (w), 1,010 (w), 995 (w), 989 (vw), 966 (vw), 956 (vw), 885 (m), 850 (w), 833 (m), 824 (s), 789 (s), 738 (vs), 699 (vs), 539 (m), 515 (m), 509 (s), 493 (m), 470 (s).

*Synthesis of **6U** from [U(BH_4)$_4$]*

Due to material scarcity issues with U-metal, the traditional precursor for [UI_3(THF)$_4$] which would be the analogous starting material for the synthesis of **6U** following the methods above, was not available. An alternative method was developed using the thermal decomposition of [U(BH_4)$_4$] to generate a U^{III} precursor *in situ*.[2]

Synthesis of [U(TMP)$_2$Bn$_2$K(toluene)] (6U). A Teflon-stoppered high-pressure Schlenk tube was loaded with [U(BH_4)$_4$] (0.149 g, 0.5 mmol), a Teflon-coated stirrer bar, and toluene (10 mL) at room temperature to form a very pale brown suspension. With the vessel open to a dynamic overpressure of argon, the mixture was heated and stirred to 80 °C at which point all the solid dissolved, but the solution remained pale. The heat was increased to 110 °C which resulted in a rapid darkening of the solution to very dark brown/black. After the solution had darkened, the vessel was sealed and left stirring at 110 °C for 1 hour after which all the volatiles were removed

in vacuo to afford a dark brown/red powder. Solid KTMP (0.1783 g, 1 mmol, 2 equiv.) was then loaded on top of the powder, and the mixture was cooled to –98 °C. THF (15 mL) was added, and the dark brown suspension was stirred and allowed to warm to room temperature. After 3.5 hours, the mixture was cooled to –98 °C then a solution of KBn (0.1302 g, 1 mmol, 2 equiv.) in THF (10 mL) was added which caused a darkening of the solution and precipitation of pale powder. The mixture was warmed to room temperature then stirred for 16 hours. Volatiles were removed *in vacuo* from the intense brown/black mixture to afford a brown solid. Toluene (25 mL) was added to the flask which was then vigorously stirred at reflux for several minutes, allowed to settle briefly, then filtered hot to a small Schlenk flask. Concentration of the dark brown solution gave a small crop of dark brown crystals of **6U** at room temperature, further crops were obtained by cooling the mixture to –28 °C which were isolated by decanting the supernatant followed by drying *in vacuo* for several hours (yield 0.119 g, 29%).

Found: C, 51.34; H, 5.40. Calc. for $UKP_2C_{30}H_{38}\cdot(C_7H_8)_{0.5}$: C, 51.34; H, 5.40.

Magnetic moment (Evans method, 299 K, C_4D_8O) μ_{eff} = 3.40(1) μ_B.

^{1}H NMR (C_4D_8O, 400.13 MHz, 299 K): δ = –55.31 (br s, $\nu_{½}$ = 50 Hz, 4 H, Bn C*H*$_2$), –22.74 (s, 12 H, TMP C(C*H*$_3$)), –3.76 (s, 12 H, TMP C(C*H*$_3$)), –3.13 (d, $^3J_{HH}$ = 7.6 Hz, 4 H, Bn *o*-C*H*), 1.10 (t, $^3J_{HH}$ = 7.0 Hz, 2 H, Bn *p*-C*H*), 2.31 (s, 3 H, toluene C*H*$_3$), 6.54 (t, $^3J_{HH}$ = 7.0 Hz, 4 H, Bn *m*-C*H*), 7.05–7.22 (m, 5H, toluene C*H*).

^{13}C{^{1}H} NMR (C_4D_8O, 100.61 MHz, 298 K): δ = 21.53, 101.87, 126.10, 128.96, 129.73, 136.72, 139.88.– we could not conclusively locate any remaining peaks, such as the Bn *C*H$_2$.

^{31}P{^{1}H} NMR (C_4D_8O, 161.98 MHz, 298 K): δ = 738.77 (TMP P).

UV-vis-NIR (THF) λ_{max} / nm (cm^{-1}, ε / M^{-1} cm^{-1}) = 476 (21,008, *1,386*), 525 (19,048, *1,137*), 662 (15,106, *451*), 834 (11,990, *546*), 981 (10,194, *331*), 1,095 (9,132, *234*), 1,220 (8,200, *207*), 2,026 (4,936, *82*).

ATR-IR ($\bar{\nu}$, cm^{-1}) = 2,962 (w), 2,952 (w), 2,908 (m), 2,853 (m), 1,581 (m), 1,474 (m), 1,443 (m), 1,395 (w), 1,375 (w), 1,365 (w), 1,294 (w), 1,220 (m), 1,175 (m), 1,149 (w), 1,092 (w),

1,020 (w), 996 (w), 891 (s), 840 (s), 792 (s), 738 (vs), 698 (vs), 541 (s), 506 (vs), 470 (s), 461 (s), 419 (s).

*Synthesis of **6Np**, **6Pu**, and **7M** (M = Np, Pu)*

Synthesis of [Np(TMP)$_2$Bn$_2$K(toluene)] (6Np) and [Np(TMP)$_2$Bn$_2$K(benzene)] (7Np). In an inert atmosphere transuranium glovebox: THF (1.5 mL) was added to a mixture of [NpI$_3$(THF)$_4$] (40 mg, 44 μmol) and KTMP (15.7 mg, 88 μmol, 2 equiv.) in a 20 mL glass scintillation vial with a Teflon-coated stir bar. The mixture briefly formed a teal solution, then changed to a blue/black suspension with pale solids and was stirred for 15 minutes. Solid KBn (11.5 mg, 88 μmol, 2 equiv.) was added which caused an instantaneous colour change to vivid emerald-green with more pale solids. The mixture was stirred for a further 15 minutes and then the volatiles were removed *in vacuo* to afford a green powder. Toluene (1.5 mL) was added which gave an almost colourless solution at room temperature but upon heating to a gentle boil a white powder could be seen below a green solution. The solution was filtered at room temperature into a 4 mL glass vial through 2 half-discs of glass microfiber mounted in a glass pipette, concentrated by *ca*. 0.2 mL which caused some green crystals to form, and the whole mixture was stored at –35 °C for 16 hours. Green blocks of **6Np** were isolated by decanting the toluene supernatant and then drying *in vacuo* for several hours, a second crop was obtained by layering the supernatant with *n*-hexane and storing the mixture at –35 °C overnight (combined yield 8.9 mg, 24%). Material not consumed in structural determination, or in spectroscopic studies – *ca*. 1.6 mg remained – was recrystallised from C_6H_6 and the structure was confirmed to be [Np(TMP)$_2$Bn$_2$K(benzene)] (**7Np**).

Magnetic moment (Evans method, 298 K, C_6D_6O) μ_{eff} = 2.42(2) μ_B.

^{1}H NMR (C_6D_6 + C_4D_8O, 400.13 MHz, 295 K): δ = –60.30 (s, 4 H, Bn C$\underline{H}_2$), –7.61 (d, $^{3}J_{HH}$ = 6.9 Hz, 12 H, TMP C(C$\underline{H}_3$)), 2.18 (s, 12 H, TMP C(C$\underline{H}_3$)), 2.56 (t, $^{3}J_{HH}$ = 7.0 Hz, 2 H, Bn *p*-C$\underline{H}$), 2.63 (d, $^{3}J_{HH}$ = 7.6 Hz, 4 H, Bn *o*-C$\underline{H}$), 7.86 (t, $^{3}J_{HH}$ = 7.5 Hz, 4 H, Bn *m*-C$\underline{H}$).

^{13}C{^{1}H} NMR (C_6D_6 + C_4D_8O, 100.61 MHz, 295 K): δ = –52.54 (TMP C($\underline{C}$H$_3$)), –14.41 (TMP C($\underline{C}$H$_3$)), 109.48 (Ar $\underline{C}$H), 134.05 (Ar $\underline{C}$H), 143.22 (Ar $\underline{C}$H), 192.76, 201.96, 202.40 – we cannot with certainty assign the peaks at 192.76, 201.96, and 202.40 as the TMP $\underline{C}$(CH$_3$), the benzylic $\underline{C}$H$_2$, Ar $\underline{C}$H, or Ar $\underline{C}$.

^{31}P{^{1}H} NMR (C_6D_6 + C_4D_8O, 161.98 MHz, 296 K): δ = –497.90 (TMP P).

UV-vis-NIR (THF) λ_{max} / nm (cm^{-1}, $\boldsymbol{\varepsilon}$ / M^{-1} cm^{-1}) = 431 (23,223, *1,129*), 547 (18,275, *215*), 612 (16,340, *297*), 648 (15,442, *269*), 840 (11,908, *100*), 902 (11,084, *92*), 965 (10,365, *36*), 1,035 (9,666, *91*), 1,273 (7,855, *16*), 1,411 (7,086, *77*).

Synthesis of [Pu(TMP)$_2$Bn$_2$K(toluene)] (6Pu) and [Pu(TMP)$_2$Bn$_2$K(benzene)] (7Pu). In an inert atmosphere transuranium glovebox: THF (1.5 mL) was added to a mixture of [PuI$_3$(THF)$_4$] (40 mg, 44 μmol) and KTMP (15.7 mg, 88 μmol, 2 equiv.) in a 20 mL glass scintillation vial with a Teflon-coated stir bar. The mixture promptly changed an apple green suspension with pale solids and was stirred for 10 minutes. Solid KBn (11.5 mg, 88 μmol, 2 equiv.) was added which caused an instantaneous colour change to muddy golden green with more pale solids. The mixture was stirred for a further 10 minutes and then the volatiles were removed *in vacuo* to afford a muddy green powder. Toluene (2 mL) was added which gave an almost colourless solution at room temperature but upon heating to a gentle boil a white powder could be seen below a black/brown solution. The solution was filtered while warm into a 4 mL glass vial through 2 half-discs of glass microfiber mounted in a glass pipette, concentrated by *ca*. 0.5 mL which caused some brown crystals to form, and the whole mixture was stored at room temperature for 16 hours. Brown blocks of **6Pu** were isolated by decanting the toluene

supernatant and then drying *in vacuo* for several hours, a second crop was obtained by layering the supernatant with *n*-hexane and storing the mixture at –35 °C overnight (combined yield 6.0 mg, 16%). Material not consumed in structural determination, or in spectroscopic studies – *ca*. 2 mg remained – was recrystallised from C_6H_6 and the structure was confirmed to be [Pu(TMP)$_2$Bn$_2$K(benzene)] (**7Pu**).

^{1}H NMR (C_6D_6 + C_4D_8O, 400.13 MHz, 296 K): δ = –18.75 (s, 4 H, Bn C*H*$_2$), 0.72 (s, 12 H, TMP C(C*H*$_3$)), 2.12 (s, 5 H – should be 3 H, toluene C*H*$_3$), 2.60 (s, 12 H, TMP C(C*H*$_3$)), 5.04 (t, $^3J_{HH}$ = 7.0 Hz, 2 H, Bn *p*-C*H*), 5.68 (d, $^3J_{HH}$ = 7.6 Hz, 4 H, Bn *o*-C*H*) – we tentatively assign the triplet at 7.86 ppm ($^3J_{HH}$ = 7.4 Hz) as the *m*-C*H* resonance, however it overlaps with the C_6D_6 protio residual signal and due to material conservation issues we could not repeat the experiment in a different NMR solvent to confirm this. Alternatively, a triplet at 0.85 ppm ($^3J_{HH}$ = 6.5 Hz) has an appropriate integration but unfortunately this is coincident with the triplet resonance of *n*-pentane which is present in the glovebox and hence cannot be ruled out as an impurity in the atmosphere during sample preparation. Due to the requirements of transuranium sample preparation, it is not always possible to exclude air/moisture for long-enough to obtain high-quality NMR spectra. In this data we can see the toluene resonance (by the C*H*$_3$ signal at 2.31) is larger than just from **6Pu** dissolved, presumably due to decomposition/protonation of the benzyl complex by adventitious water.

^{31}P{^{1}H} NMR (C_6D_6 + C_4D_8O, 161.98 MHz, 296 K): For the reasons above, the ^{31}P{^{1}H} spectrum shows at least 5 signals. One (73.46 ppm) is readily attributed to KTMP by comparison with an authentic sample. Two very sharp signals at 12.21 and 14.00 ppm are unlikely to correspond to paramagnetic **6Pu**, which leaves signals at 150.15 and 186.23 ppm as plausibly originating from **6Pu** – but we are unable to determine which by repeating the experiment due to material conservation issues.

UV-vis-NIR (THF) λ_{max} / nm (cm^{-1}, ε / M^{-1} cm^{-1}) = 450 (22,242, *616*), 479 (20,886, *493*), 541 (18,484, *115*), 566 (17,680, *65*), 580 (17,241, *108*), 623 (16,057, *88*), 686 (14,569, *37*), 803

(12,456, *46*), 845 (11,829, *33*), 921 (10,858, *38*), 1,057 (9,461, *56*), 1,132 (8,837, *28*), 1,170 (8,546, *31*), 1,182 (8,459, *32*), 1,460 (6,850, *43*), 1,499 (6,669, *43*).

S2. Photographs taken during synthesis

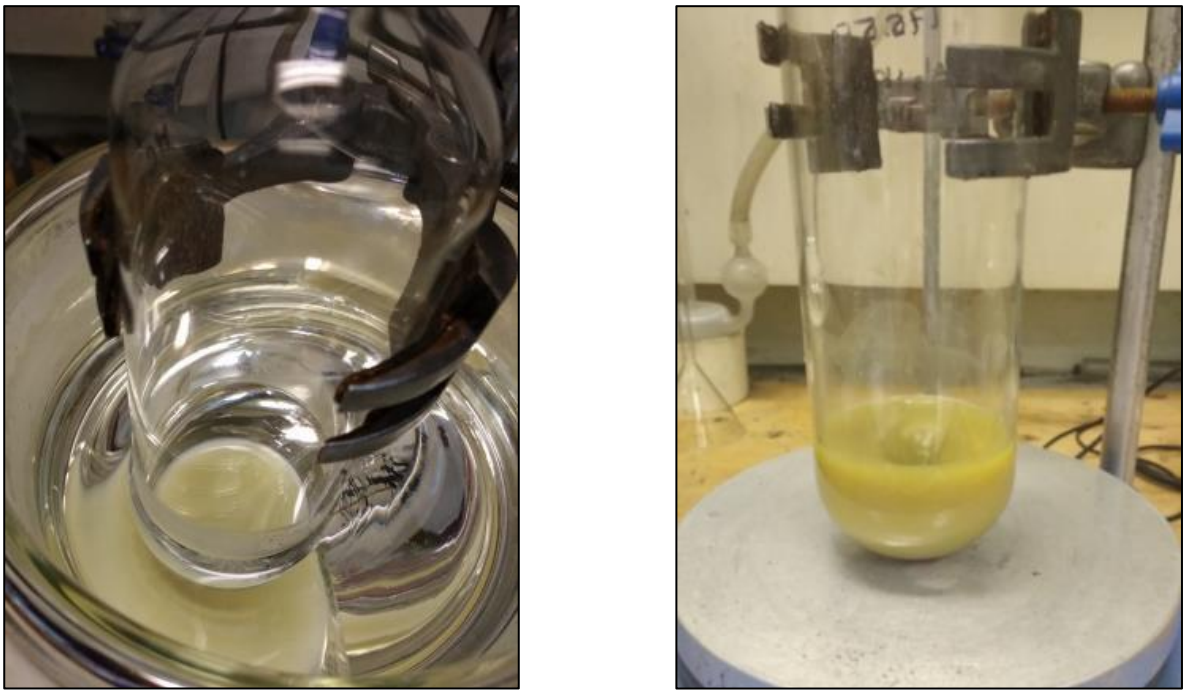

Figure S1. (Left) The reaction mixture of $[LaI_3(THF)_4]$ + 2 KTMP in THF shortly after the addition of THF; (Right) The same mixture after the addition of 2 KBn and warmed to room temperature.

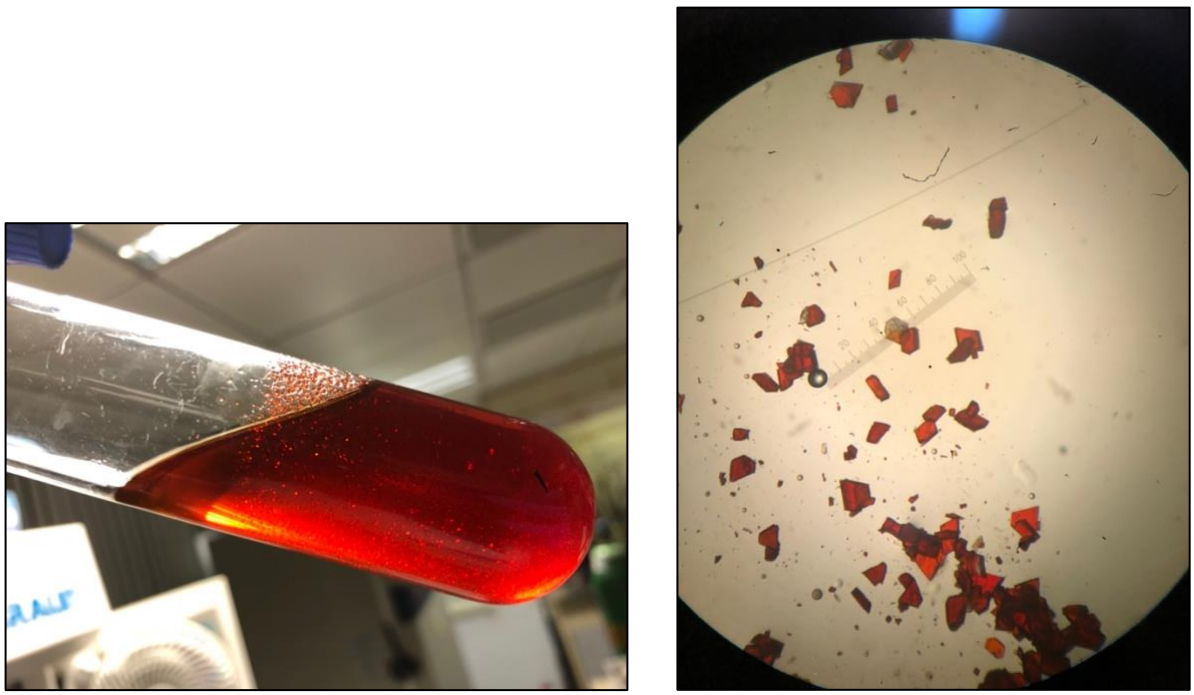

Figure S2. (Left) Crystals of $[La(TMP)_2Bn_2K(toluene)]$ (**6La**) grown at room temperature; (Right) Crystals of **6La** in Fomblin® oil under a microscope.

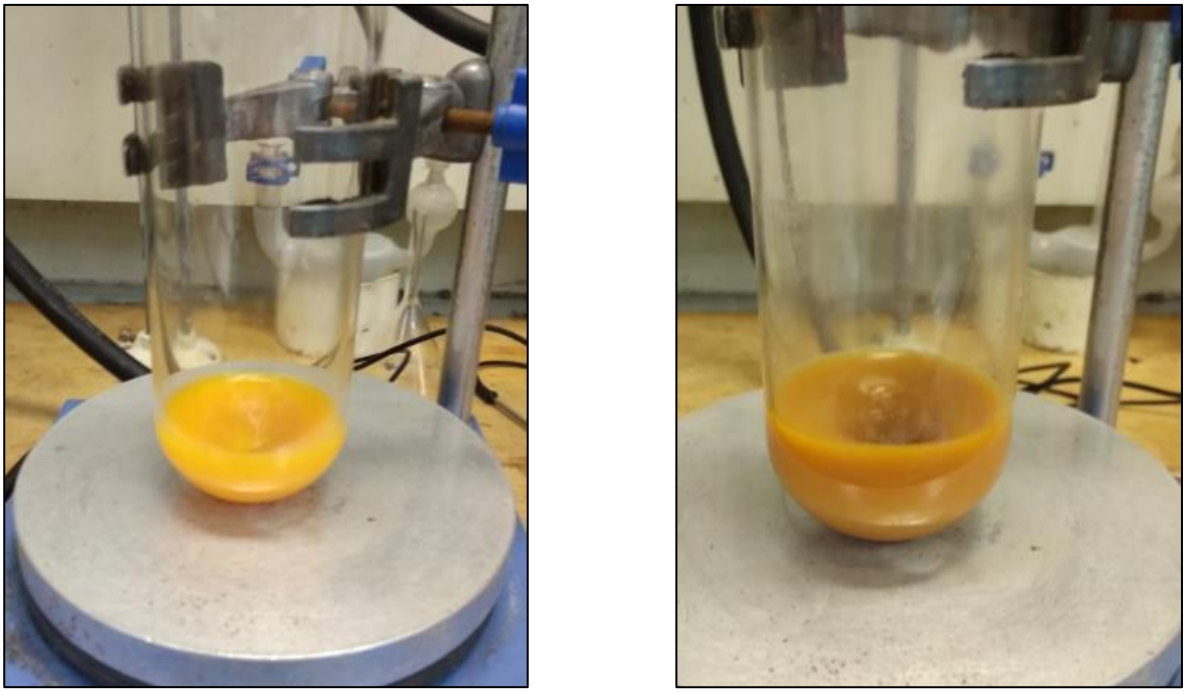

Figure S3. (Left) The reaction mixture of $[CeI_3(THF)_4]$ + 2 KTMP in THF shortly after the addition of THF; (Right) The same mixture after the addition of 2 KBn and warmed to room temperature.

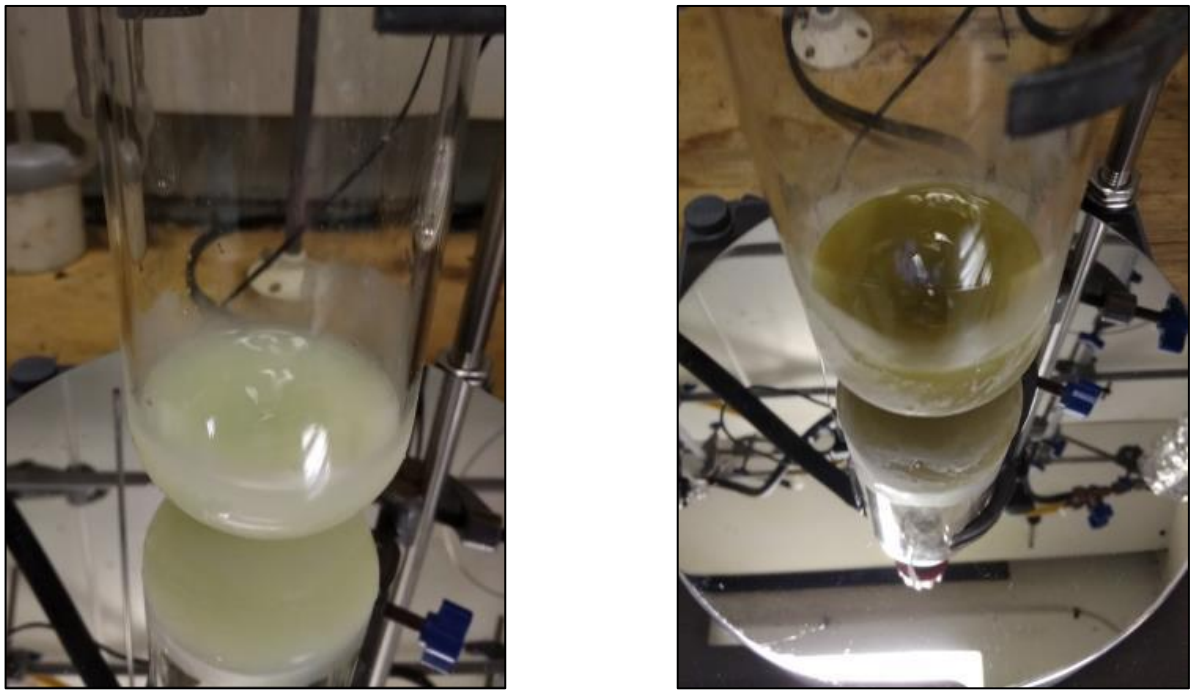

Figure S4. (Left) The reaction mixture of $[PrI_3(THF)_4]$ + 2 KTMP in THF shortly after the addition of THF; (Right) The same mixture after the addition of 2 KBn and warmed to room temperature.

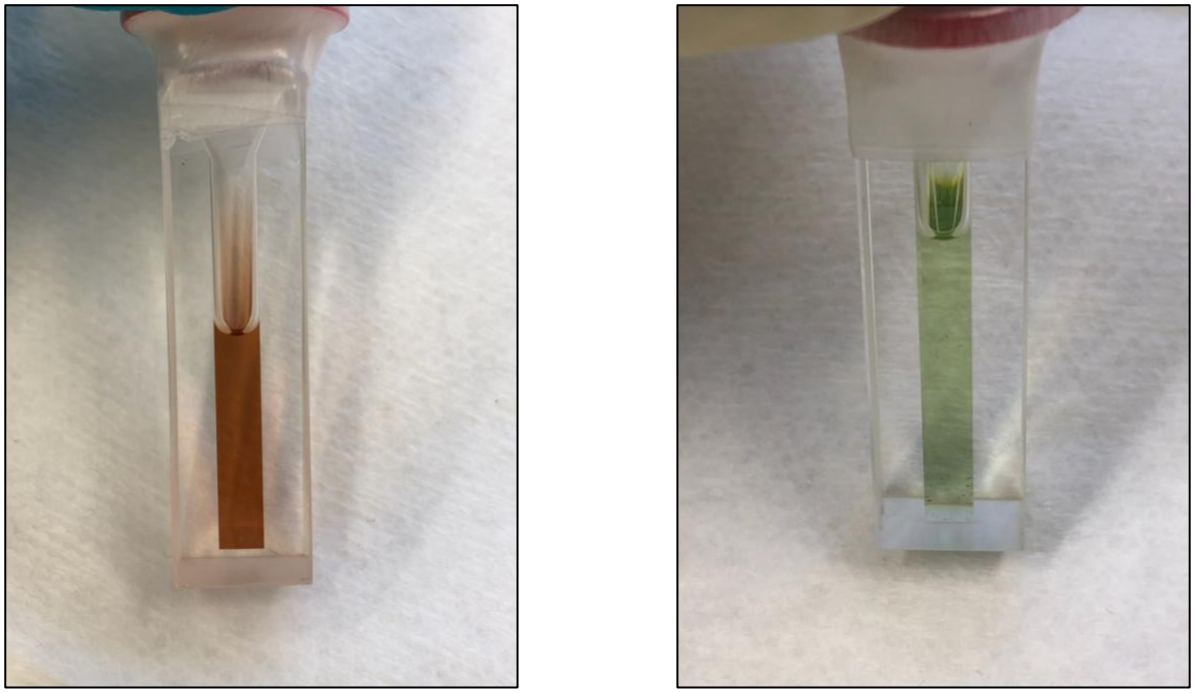

Figure S5. (Left) Solution of putative **7U** in toluene at room temperature; (Right) Solution of **6Np** in toluene at room temperature used for UV-vis-NIR measurements.

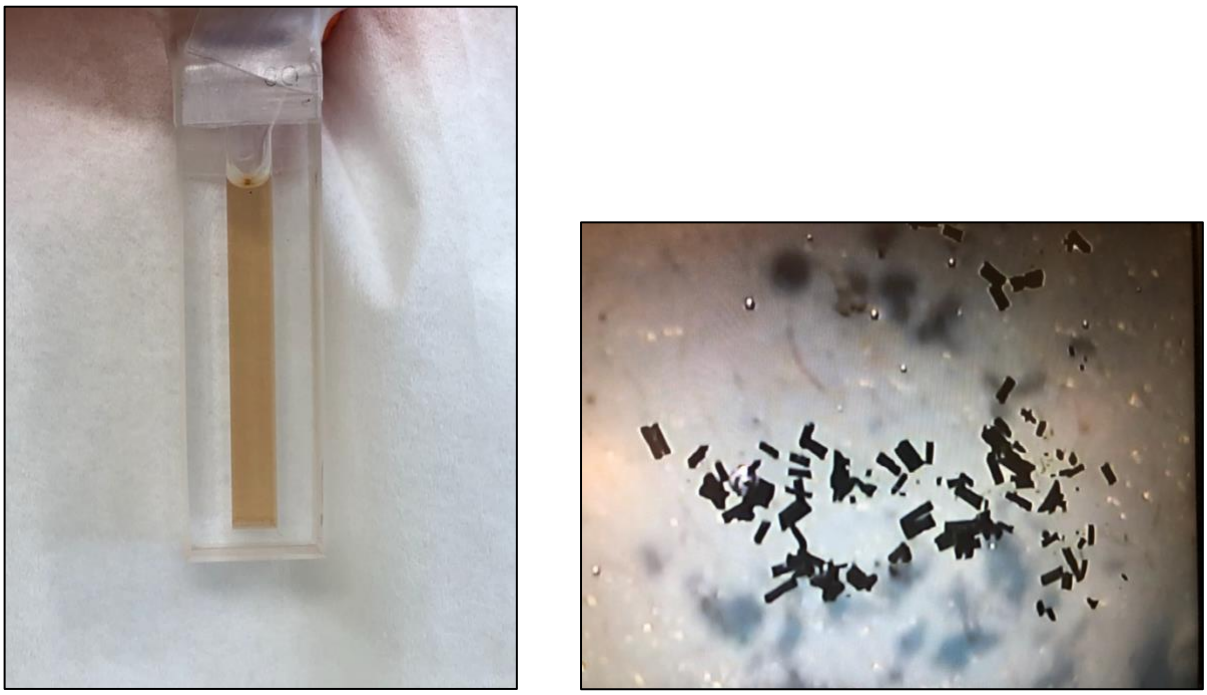

Figure S6. (Left) Solution of **6Pu** in toluene at room temperature used for UV-vis-NIR measurements; (Right) Crystals of **6Np** in NVH oil used for single-crystal X-ray diffraction studies.

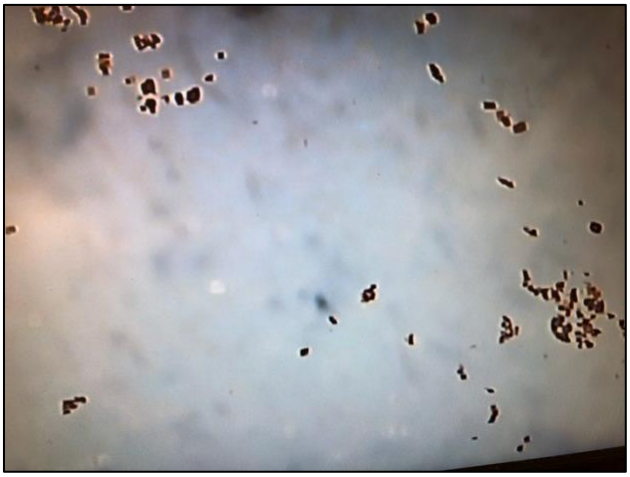

Figure S7. Crystals of **6Pu** in NVH oil used for single-crystal X-ray diffraction studies.

S3. Crystallography

General considerations

Data for **2**, **6Np**, **7Np**, **6Pu**, **7Pu** and **7U** were collected using a Bruker D8 Quest diffractometer, equipped with a Incoatec IμS Mo Kα radiation source (λ = 0.71073 Å), using a 3-circle fixed-χ goniometer, a Photon-III hybrid pixel array detector operating in shutterless mode and an Oxford Cryosystems Cyostream 800 nitrogen gas flow system at a temperature of 120K or 150K. Data for **1**, **3** and **5** were collected using a Bruker D8 Quest diffractometer, equipped with a graphite monochromated sealed-tube Mo Kα radiation source (λ = 0.71073 Å), using a 3-circle fixed-χ goniometer, a Photon-100 CMOS detector operating in shutterless mode and an Oxford Cryosystems Cyostream 700 nitrogen gas flow system at a temperature of 150K. Data for **6La**, **6Pr**, and **6U** were collected using a Rigaku XtaLAB Synergy DW diffractometer, equipped with a PhotonJet Cu Kα radiation source (λ = 1.54184 Å), using a 4-circle κ goniometer, a HyPix-6000HE hybrid pixel array detector operating in shutterless mode and an Oxford Cryosystems Cryostream 800 nitrogen flow gas system at a temperature of 100K. Data for **6Ce** were collected using a Rigaku FR-X DW diffractometer, equipped with an FR-X high intensity rotating anode Cu Kα radiation source (λ = 1.54184 Å) and VariMAX^{TM} microfocus optics, using an AFC-11 4-circle κ goniometer, a HyPix-6000HE hybrid pixel array detector operating in shutterless mode and an Oxford Cryosystems Cryostream 800 plus nitrogen flow gas system at a temperature of 100K. Data for **1**, **2**, **3**, **5**, **6Np**, **7Np**, **6Pu**, **7Pu**, and **7U** were collected using Bruker APEX III software, and data for **6La**, **6Pr**, **6U**, and **6Ce** were collected using Rigaku Oxford Diffraction CrysAlisPro v1.171.42. All data were integrated and reduced using Rigaku Oxford Diffraction CryAlisPro v1.171.42.[11] Intensities were integrated from data recorded from ω, or ω and φ rotation at the frame width and exposure times outlined in Table S1. The crystal data for complexes **1–5**, **6M** (M = La, Ce, Pr, U, Np, Pu), and **7M** (M = U, Np, Pu) are compiled in Table S2 to Table S6.

Table S1. Data collection parameters for all structures herein.

	Formula	Frame width (°)	Exposure time (s)
1	$[Np(TMP)_2Cl_2K(Et_2O)]_n$	0.5	30
2	$[Np(TMP)_2Cl_2K(DME)]_n$	0.5	30
3	$[\{Np(TMP)_2\}_2(\mu\text{-}Cl)(\mu\text{-}O_2PC_4Me_4\text{-}\kappa O,O')]$	0.5	10
4	$[K(THF)_2(TMP)]_n$	1.0	15, 30
5	$[U(TMP)_2(I)(THF)]$	0.5	10
6La	$[La(TMP)_2Bn_2K(toluene)]$	0.5	1, 2
6Ce	$[Ce(TMP)_2Bn_2K(toluene)]$	0.5	1, 2
6Pr	$[Pr(TMP)_2Bn_2K(toluene)]$	0.5	1, 2
6U	$[U(TMP)_2Bn_2K(toluene)]$	0.5	0.5, 1
7U	$[U(TMP)_2Bn_2K(benzene)]$	0.5	3
6Np	$[Np(TMP)_2Bn_2K(toluene)]$	0.5	40
7Np	$[Np(TMP)_2Bn_2K(benzene)]$	0.5	10
6Pu	$[Pu(TMP)_2Bn_2K(toluene)]$	0.5	20
7Pu	$[Pu(TMP)_2Bn_2K(benzene)]$	0.5	10

CrysAlisPro was used for final unit cell determination and parameters were refined from the observed positions of all strong reflections in each data set.[11] An analytical absorption correction was applied.[11] The Olex2[12] GUI was used for structure solution and refinement utilizing the ShelX software packages.[13-14] The structures were solved using ShelXT[13], and datasets were refined by ShelXL[14] using full-matrix least-squares on all unique F^2 values with anisotropic displacement parameters for all non-hydrogen atoms, and with constrained riding hydrogen geometries; U_{iso}(H) set at 1.2 (1.5 for methyl groups where applicable) times Ueq of the parent atom. The largest features in final difference syntheses were close to heavy atoms and were of no chemical significance. Olex2 combined with Inkscape was employed for molecular graphics.[12, 15]. CCDC entries 2193335–2193346, and 2202840 contain the supplementary crystal data for this article. **1** (2193335), **2** (2193336), **3** (2193337), **4** (2193338), **5** (2193339), **6La** (2193340), **6Ce** (2193341), **6Pr** (2193342), **6U** (2193343), **7U** (2202840) **6Np** (2193344), **7Np** (2193345), and **7Pu** (2193346). These data can be obtained free of charge from the Cambridge Crystallographic Data Centre via www.ccdc.cam.ac.uk/data_request/cif. The data for **6Pu** are not of sufficient quality for deposition to the CCDC.

*Note on choice of space group and symmetry for **6M** and **7M** series*

All **6M** datasets show a similar pseudo symmetry in the structural model. While the structures can all be solved and refined in *P*nma with appropriate modelling of closely overlapping disorder, the resultant fits of the atomic displacement parameters are not satisfactory, with *P*na2_1 and an applied inversion twin giving a better fit to the data.

Similarly, all the **7M** datasets can be solved and refined in *P*na2_1 without mirror symmetry, however the resultant fits of the atomic displacement parameters are less satisfactory. We also believe that it is good practice to solve data in the highest symmetry that results in a sound fit to the data, and thus for **7M** we have opted to use *P*nma.

The combined error from two individual metrics that have their own associated errors (estimated standard deviation, or standard uncertainty used interchangeably here) can be calculated as the root of the sum of the square of each error (Equation S2). This is not strictly appropriate for combining more than two individual errors.[16]

Equation S2. $$\sigma_{tot} = \sqrt{{\sigma_1}^2 + {\sigma_2}^2}$$

The combined error for the numerical average for multiple (independent) bond lengths, such as the five independent M–C bonds in an M–($\eta^5C_5H_5$) complex, is calculated using the alternate weighted standard deviation from Parsons and Clegg (Equation S3).[16]

Equation S3. $$\sigma_{tot} = 1/\sqrt{\sum_{1\to n} W_n} \qquad W_n = 1/{\sigma_n}^2$$

Table S2. Crystallographic data for **1**, **2**, and **3**.

	1	**2**	**3**
CCDC ref code	2193335	2193336	2193337
Identification code	dq0876	ms0711	dq1016
Formula	$C_{20}H_{34}Cl_2KNpOP_2$	$C_{18}H_{29}Cl_2KNpOP_2$	$C_{47}H_{68}ClNp_2O_2P_5$
Fw	699.41	670.35	1329.31
Temperature / K	101.0(10)	150(1)	100.0(2)
Crystal system	monoclinic	triclinic	triclinic
Space group	$P2_1/n$	P-1	P-1
a / Å	16.1677(3)	8.5818(2)	11.1814(3)
b / Å	8.70020(10)	19.2369(4)	13.0223(4)
c / Å	18.9428(3)	29.3792(7)	17.8428(4)
α / °	90	89.425(2)	76.498(3)
β / °	101.370(2)	89.166(2)	81.654(2)
γ / °	90	79.460(2)	85.265(3)
Volume / Å^3	2612.24(7)	4767.66(19)	2496.27(13)
Z	4	8	2
ρ_{calcg} / cm^3	1.778	1.868	1.769
μ / mm^{-1}	4.473	4.897	4.389
F(000)	1352.0	2568.0	1288.0
Crystal size / mm^3	0.5 × 0.09 × 0.05	0.254 × 0.235 × 0.085	0.31 × 0.28 × 0.14
Radiation	MoKα (λ = 0.71073)	MoKα (λ = 0.71073)	MoKα (λ = 0.71073)
2Θ range / °	9.026 to 52.714	3.498 to 43.932	5.442 to 52.858
Index ranges	-20 ≤ h ≤ 20, -10 ≤ k ≤ 10, -23 ≤ l ≤ 23	-9 ≤ h ≤ 9, -20 ≤ k ≤ 20, -30 ≤ l ≤ 30	-14 ≤ h ≤ 13, -16 ≤ k ≤ 16, -22 ≤ l ≤ 22
No. reflections	10354	31266	17718
Unique reflections	10354 [R_{int} = 0.0623, R_{sigma} = 0.1902]	31266 [R_{int} = 0.1403, R_{sigma} = 0.2497]	17718 [R_{int} = 0.0530, R_{sigma} = 0.1255]
Data / restraints / parameters	10354/0/255	31266/3558/1111	17718/0/536
GOOF on F^2	0.763	1.168	0.847
Final R indexes [I ≥ 2σ (I)][a]	0.0347, 0.0715	0.0946, 0.2822	0.0333, 0.0787
Final R indexes [all data]	0.0635, 0.0759	0.1497, 0.3036	0.0462, 0.0795
Largest diff. (peak / hole) / e Å^{-3}	2.21/-0.92	4.70/-2.50	2.24/-0.85

[a] $R = \sum||F_O| - |F_C||/\sum|F_O|$; $R_W = [\sum w(F_O^2 - F_C^2)^2/\sum w(F_O^2)^2]^{0.5}$; GOOF = $[\sum w(F_O^2 - F_C^2)^2/(\text{no. data} - \text{no. params})]^{0.5}$ for all data.

Table S3. Crystallographic data for **4**, **5**, and **6La**.

	4	**5**	**6La**
CCDC ref code	2193338	2193339	2193340
Identification code	ccapg2	dq0844	ccapg4
Formula	$C_{16}H_{28}KO_2P$	$C_{20}H_{32}IOP_2U$	$C_{37}H_{46}KIaP_2$
Fw	322.45	715.32	730.69
Temperature / K	100.15	100(1)	100.00(10)
Crystal system	monoclinic	triclinic	orthorhombic
Space group	$P2_1/n$	P-1	$Pna2_1$
a / Å	9.1277(6)	11.6875(8)	23.4224(2)
b / Å	10.5943(5)	13.1727(11)	10.06770(10)
c / Å	18.8451(10)	15.8575(14)	14.90600(10)
α / °	90	99.655(7)	90
β / °	101.128(6)	96.384(6)	90
γ / °	90	99.298(6)	90
Volume / Å^3	1788.09(18)	2351.0(3)	3514.98(5)
Z	4	4	4
ρ_{calcg} / cm^3	1.198	2.021	1.381
μ / mm^{-1}	3.433	8.359	11.473
F(000)	696.0	1340.0	1496.0
Crystal size / mm^3	0.256 × 0.254 × 0.121	0.18 × 0.11 × 0.1	0.197 × 0.091 × 0.071
Radiation	CuKα (λ = 1.54184)	MoKα (λ = 0.71073)	CuKα (λ = 1.54184)
2Θ range / °	9.566 to 160.724	4.326 to 52.74	7.548 to 160.008
Index ranges	-11 ≤ h ≤ 11, -13 ≤ k ≤ 13, -23 ≤ l ≤ 23	-14 ≤ h ≤ 14, -16 ≤ k ≤ 16, -19 ≤ l ≤ 19	-29 ≤ h ≤ 29, -12 ≤ k ≤ 12, -18 ≤ l ≤ 14
No. reflections	6337	29950	29350
Unique reflections	6337 [R_{int} = 0.0615, R_{sigma} = 0.0222]	9440 [R_{int} = 0.0445, R_{sigma} = 0.0567]	6468 [R_{int} = 0.0354, R_{sigma} = 0.0194]
Data / restraints / parameters	6337/0/186	9440/111/486	6468/385/445
GOOF on F^2	1.062	0.962	1.115
Final R indexes [I ≥ 2σ (I)][a]	0.0582, 0.1574	0.0264, 0.0540	0.0363, 0.0982
Final R indexes [all data]	0.0665, 0.1648	0.0375, 0.0576	0.0370, 0.0988
Largest diff. (peak / hole) / e Å^{-3}	0.44/-0.35	1.45/-0.75	1.02/-1.29
Flack parameter	-	-	0.341(9)

[a] $R = \sum||F_O| - |F_C||/\sum|F_O|$; $R_W = [\sum w(F_O^2 - F_C^2)^2/\sum w(F_O^2)^2]^{0.5}$; GOOF = $[\sum w(F_O^2 - F_C^2)^2/(\text{no. data} - \text{no. params})]^{0.5}$ for all data.

Table S4. Crystallographic data for **6Ce**, **6Pr**, and **6U**.

	6Ce	**6Pr**	**6U**
CCDC ref code	2193341	2193342	2193343
Identification code	rcapg3	ccapg6	ccapg26
Formula	$C_{37}H_{46}CeKP_2$	$C_{37}H_{46}KP_2Pr$	$C_{37}H_{46}KP_2U$
Fw	731.90	732.69	829.81
Temperature / K	100.00(10)	100.00(10)	100.00(10)
Crystal system	orthorhombic	orthorhombic	orthorhombic
Space group	*P*na2$_1$	*P*na2$_1$	*P*na2$_1$
a / Å	23.4368(2)	23.40830(18)	23.43610(10)
b / Å	10.04890(10)	10.04593(7)	9.99740(10)
c / Å	14.85740(10)	14.80861(11)	14.85090(10)
α / °	90	90	90
β / °	90	90	90
γ / °	90	90	90
Volume / Å^3	3499.13(5)	3482.37(4)	3479.57(4)
Z	4	4	4
ρ_{calcg} / cm^3	1.389	1.398	1.584
μ / mm^{-1}	12.142	12.832	15.234
F(000)	1500.0	1504.0	1636.0
Crystal size / mm^3	0.25 × 0.168 × 0.13	0.178 × 0.117 × 0.03	0.25 × 0.168 × 0.13
Radiation	CuKα (λ = 1.54184)	CuKα (λ = 1.54184)	CuKα (λ = 1.54184)
2Θ range / °	7.544 to 151.612	7.554 to 140.134	7.544 to 140.112
Index ranges	-29 ≤ h ≤ 28, -12 ≤ k ≤ 11, -17 ≤ l ≤ 15	-28 ≤ h ≤ 28, -12 ≤ k ≤ 12, -18 ≤ l ≤ 17	-28 ≤ h ≤ 27, -12 ≤ k ≤ 12, -18 ≤ l ≤ 18
No. reflections	32686	31776	40897
Unique reflections	5642 [R_{int} = 0.0504, R_{sigma} = 0.0239]	6169 [R_{int} = 0.0315, R_{sigma} = 0.0215]	6346 [R_{int} = 0.0369, R_{sigma} = 0.0174]
Data / restraints / parameters	5642/321/397	6169/385/445	6346/447/397
GOOF on F^2	1.174	1.052	1.080
Final R indexes [I ≥ 2σ (I)][a]	0.0429, 0.1509	0.0303, 0.0794	0.0222, 0.0594
Final R indexes [all data]	0.0432, 0.1511	0.0305, 0.0797	0.0222, 0.0595
Largest diff. (peak / hole) / e Å^{-3}	2.04/-1.41	1.30/-0.94	0.98/-1.56
Flack parameter	0.282(9)	0.372(5)	0.471(8)

[a] $R = \sum||F_O| - |F_C||/\sum|F_O|$; $R_W = [\sum w(F_O^2 - F_C^2)^2/\sum w(F_O^2)^2]^{0.5}$; GOOF = $[\sum w(F_O^2 - F_C^2)^2/(\text{no. data} - \text{no. params})]^{0.5}$ for all data.

Table S5. Crystallographic data for **6Np**, **6Pu**, and **7U**.

	6Np	**6Pu**	**7U**
CCDC ref code	2193344	N/A	2202840
Identification code	ms0681	dq1490	ms0702
Formula	$C_{37}H_{46}KNpP_2$	$C_{37}H_{46}KP_2Pu$	$C_{36}H_{44}KP_2U$
Fw	828.78	833.78	815.78
Temperature / K	119(5)	150.15(10)	150(1)
Crystal system	orthorhombic	orthorhombic	orthorhombic
Space group	*P*na2$_1$	*P*na2$_1$	*P*nma
a / Å	23.4277(12)	23.3939(13)	23.4180(6)
b / Å	10.0191(4)	10.0493(5)	15.1866(5)
c / Å	14.8503(6)	14.9440(9)	9.8667(2)
α / °	90	90	90
β / °	90	90	90
γ / °	90	90	90
Volume / Å^3	3485.7(3)	3513.2(3)	3508.99(17)
Z	4	4	4
ρ_{calcg} / cm^3	1.579	1.576	1.544
μ / mm^{-1}	3.216	2.109	4.857
F(000)	1640.0	1644.0	1604
Crystal size / mm^3	0.135 × 0.125 × 0.05	0.135 × 0.125 × 0.05	0.125 × 0.123 × 0.122
Radiation	MoKα (λ = 0.71073)	MoKα (λ = 0.71073)	Mo Kα (λ = 0.71073)
2Θ range / °	4.422 to 51.354	4.884 to 51.354	4.48 to 51.36
Index ranges	-26 ≤ h ≤ 28, -12 ≤ k ≤ 12, -18 ≤ l ≤ 17	-28 ≤ h ≤ 28, -12 ≤ k ≤ 12, -18 ≤ l ≤ 18	-28 ≤ h ≤ 28, -18 ≤ k ≤ 16, -11 ≤ l ≤ 12
No. reflections	18677	21206	29124
Unique reflections	6532 [R_{int} = 0.0600, R_{sigma} = 0.0755]	5309 [R_{int} = 0.2653, R_{sigma} = 0.1412]	3456 [R_{int} = 0.0522, R_{sigma} = 0.0261]
Data / restraints / parameters	6532/735/397	5309/1641/397	3456/409/281
GOOF on F^2	1.029	1.085	1.065
Final R indexes [I ≥ 2σ (I)][a]	0.0401, 0.0569	0.0945, 0.1864	0.0231, 0.0552
Final R indexes [all data]	0.0636, 0.0631	0.1376, 0.2182	0.0245, 0.0561
Largest diff. (peak / hole) / e Å^{-3}	0.77/-0.73	1.34/-1.89	1.76/-0.82
Flack parameter	0.45(3)	0.48(14)	-

[a] $R = \sum||F_O| - |F_C||/\sum|F_O|$; $R_W = [\sum w(F_O^2 - F_C^2)^2/\sum w(F_O^2)^2]^{0.5}$; GOOF = $[\sum w(F_O^2 - F_C^2)^2/(\text{no. data} - \text{no. params})]^{0.5}$ for all data.

Table S6. Crystallographic data for **7Np**, and **7Pu**.

	7Np	**7Pu**
CCDC ref code	2193345	2193346
Identification code	ms0699	ms0701
Formula	$C_{36}H_{44}KNpP_2$	$C_{36}H_{44}KP_2Pu$
Fw	814.75	819.75
Temperature / K	150(1)	150.15(10)
Crystal system	orthorhombic	orthorhombic
Space group	*P*nma	*P*nma
a / Å	23.0479(7)	23.3784(7)
b / Å	14.9689(6)	15.1956(6)
c / Å	9.7383(3)	9.8873(3)
α / °	90	90
β / °	90	90
γ / °	90	90
Volume / Å^3	3359.7(2)	3512.45(19)
Z	4	4
ρ_{calcg} / cm^3	1.611	1.550
μ / mm^{-1}	3.335	2.108
F(000)	1608.0	1612.0
Crystal size / mm^3	0.235 × 0.223 × 0.198	0.125 × 0.123 × 0.122
Radiation	MoKα (λ = 0.71073)	MoKα (λ = 0.71073)
2Θ range / °	4.54 to 51.36	4.396 to 51.358
Index ranges	-28 ≤ h ≤ 28, -18 ≤ k ≤ 18, -11 ≤ l ≤ 11	-28 ≤ h ≤ 28, -18 ≤ k ≤ 18, -12 ≤ l ≤ 12
No. reflections	24903	25437
Unique reflections	3313 [R_{int} = 0.0905, R_{sigma} = 0.0461]	3460 [R_{int} = 0.0722, R_{sigma} = 0.0379]
Data / restraints / parameters	3313/342/281	3460/409/281
GOOF on F^2	1.064	1.021
Final R indexes [I ≥ 2σ (I)][a]	0.0238, 0.0491	0.0251, 0.0544
Final R indexes [all data]	0.0292, 0.0512	0.0322, 0.0571
Largest diff. (peak / hole) / e Å^{-3}	0.49/-0.75	1.06/-0.81
Flack parameter	-	-

[a] $R = \sum||F_O| - |F_C||/\sum|F_O|$; $R_W = [\sum w(F_O^2 - F_C^2)^2/\sum w(F_O^2)^2]^{0.5}$; GOOF = $[\sum w(F_O^2 - F_C^2)^2/(\text{no. data} - \text{no. params})]^{0.5}$ for all data.

S4. Molecular structures

*Complex **1***

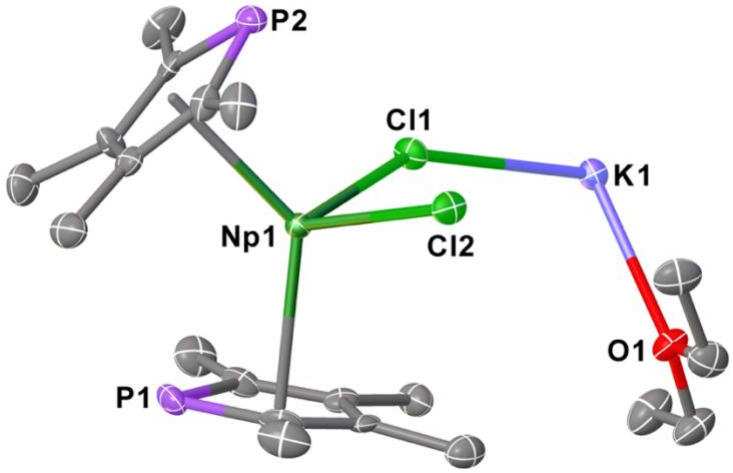

Figure S8. Molecular structure of the monomeric unit of **1**. Ellipsoids set at 50% probability and H-atoms removed for clarity (operations: X,Y,Z).

Lengths (Å): Np1–P1 = 2.9388(15); Np1–P2 = 2.9688(19); Np1–TMP_{cent1} = 2.528(3); Np1–TMP_{cent2} = 2.522(3); Np1–Cl1 = 2.7004(15); Np1–Cl2 = 2.7082(17); K1–Cl1 = 3.134(2); K1–O1 = 2.799(5).

Angles (°): Cl1–Np1–Cl2 = 90.65(5); TMP_{cent}–Np–TMP_{cent} = 131.22(9).

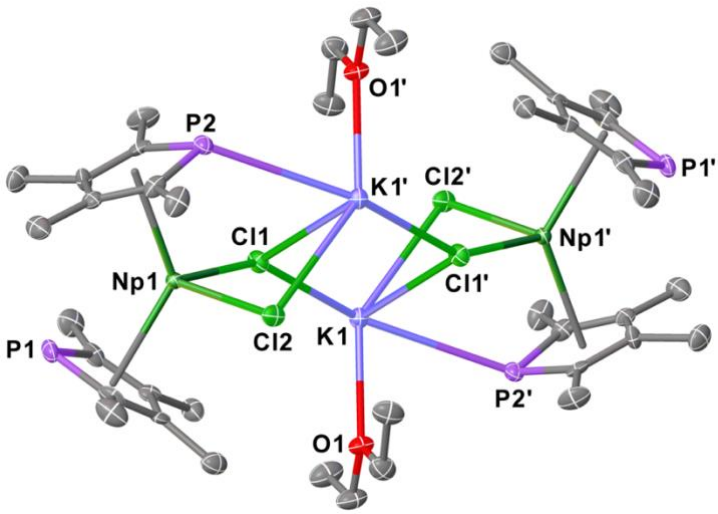

Figure S9. Molecular structure of the dimeric unit of **1**. Ellipsoids set at 50% probability and H-atoms removed for clarity (operations: 1–X,1–Y,1–Z).

Lengths (Å): K1–P2' = 3.465(2); K1–Cl1' = 3.213(2); K1–Cl2' = 3.368(2).

*Complex **2***

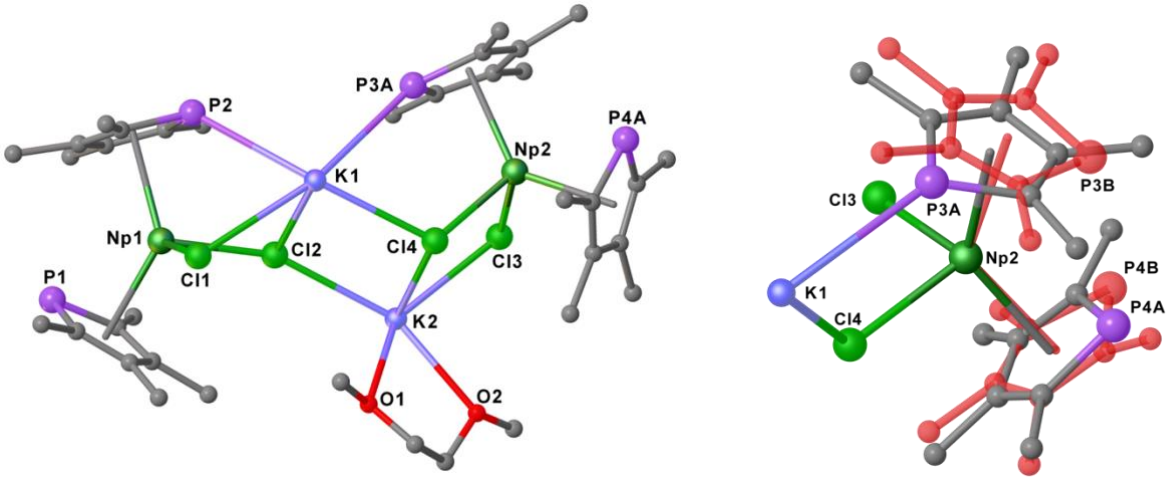

Figure S10. Left: Ball-and-stick representation of the molecular structure of **2**. H-atoms and disordered TMP rings about Np2 removed for clarity, along with a second dimeric unit with identical composition (see below) (operations: X,Y,Z). The data quality is insufficient for meaningful discussion of the metrical parameters. Right: The {Np(TMP)$_2$Cl$_2$K} unit about Np2, showing the disordered TMP ring components with lower occupancy (32%) in red.

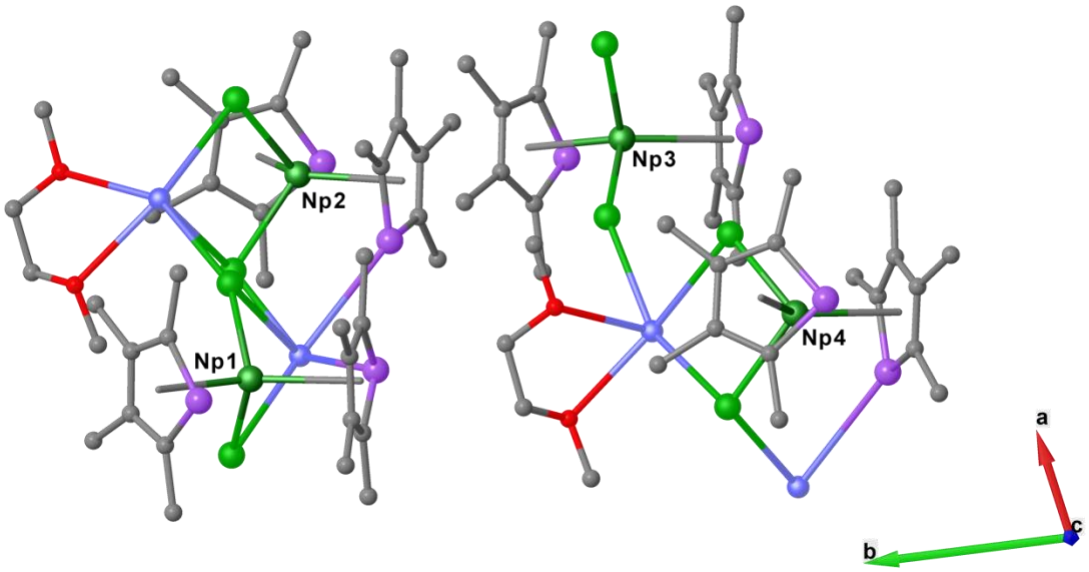

Figure S11. Ball-and-stick representation of the full asymmetric unit for structure of **2**, viewed along the crystallographic *c*-axic. H-atoms removed for clarity, along with two disordered TMP rings about Np2 (operations: X,Y,Z). The data quality is insufficient for meaningful discussion of the metrical parameters.

*Complex **3***

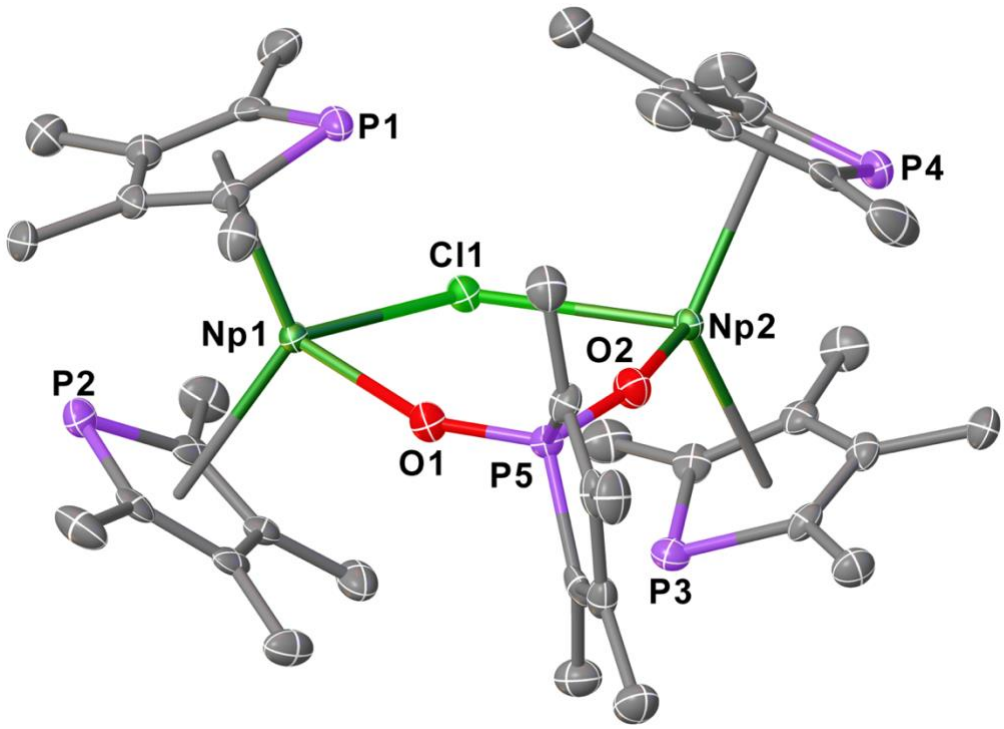

Figure S12. Molecular structure of **3**. Ellipsoids set at 50% probability and H-atoms removed for clarity along with a lattice toluene (operations: X,Y,Z).

Lengths (Å): Np1–P1 = 2.9142(19); Np1–TMP_{cent1} = 2.538(3); Np1–P2 = 2.947(2); Np1–TMP_{cent2} = 2.516(3); Np1–Cl1 = 2.8297(16); Np1–O1 = 2.330(5); Np2–P3 = 2.9371(18); Np2–TMP_{cent3} = 2.535(3); Np2–P4 = 2.964(2); Np2–TMP_{cent4} = 2.540(3); Np2–Cl1 = ; Np2–O2 = 2.304(4); P5–O1 = 1.527(5); P5–O2 = 1.530(5).

Angles (°): TMP_{cent}–Np1–TMP_{cent} = 125.53(10); TMP_{cent}–Np2–TMP_{cent} = 128.84(11); Cl1–Np1–O1 = 86.82(12); Cl1–Np2–O2 = 88.19(12); Np1–Cl1–Np2 = 121.70(6); O1–P5–O2 = 112.9(3).

*Complex **4***

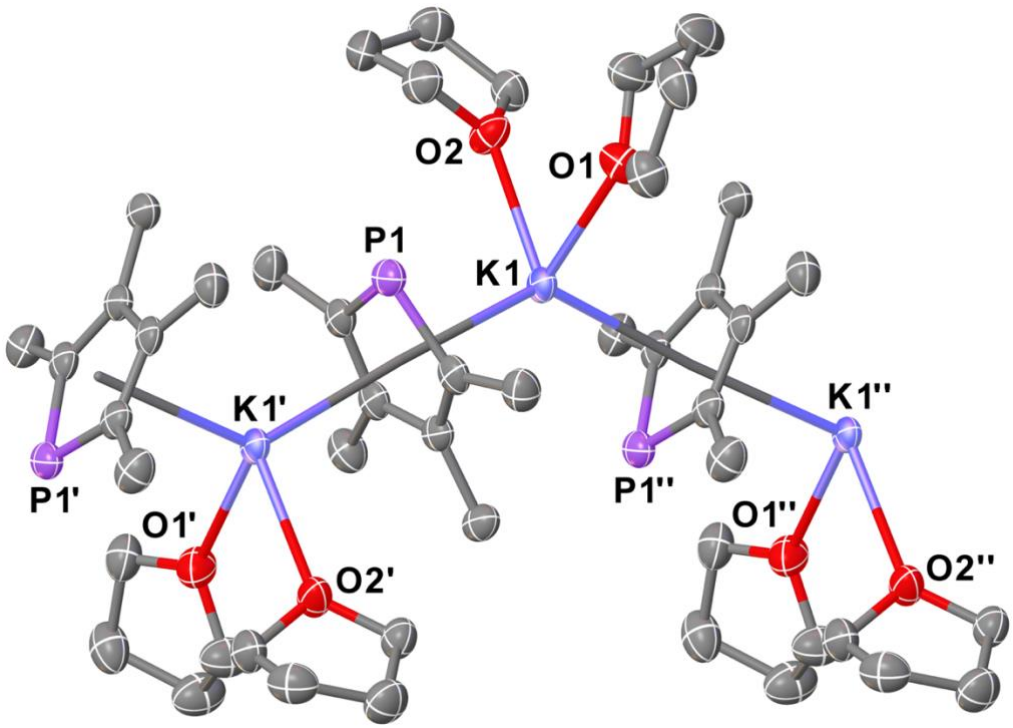

Figure S13. Molecular structure of **4**. Ellipsoids set at 50% probability and H-atoms removed for clarity (operations: X,Y,Z; atom' 3/2–X,1/2+Y,3/2–Z; atom'' 3/2–X,1/2+Y,3/2–Z;).

Lengths (Å): K1–P1 = 3.3285(10); K1–P1'' = 3.3001(11); K1–O1 = 2.702(3); K1–O2 = 2.725(3); K1–TMP_{cen} = 2.8966(14); K1'–TMP_{cent} = 2.9033(14).

Angles (°): K1–TMP_{cent}–K1' = 176.12(5); TMP_{cent}–K1–TMP_{cent} = 132.10(3); O1–K1–O2 = 80.66(9).

*Complex **5***

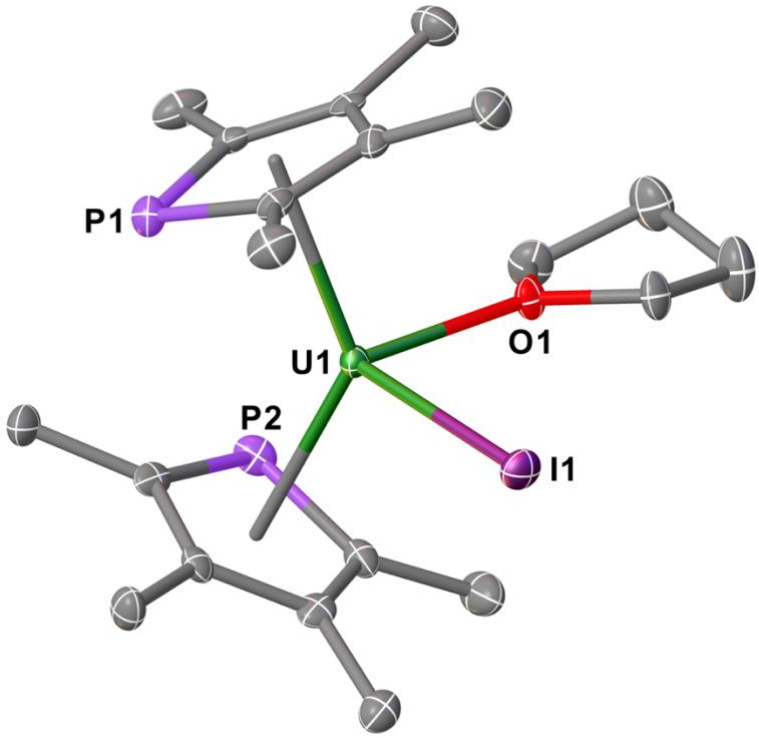

Figure S14. Molecular structure of **5**. Ellipsoids set at 50% probability and H-atoms removed for clarity along with a second molecule of **5** present in the asymmetric unit and which features a disordered THF molecule (operations: X,Y,Z).

Lengths (Å): U1–I1 = 3.0664(5); U1–P1 = 2.9359(14); U1–TMP_{cent1} = 2.527(2); U1–P2 = 2.9760(14); U1–TMP_{cent2} = 2.536(2); U1–O1 = 2.489(3).

Angles (°): TMP_{cent}–U1–TMP_{cent} = 133.50(6); I1–U1–O1 = 92.91(7).

*Complex **6La***

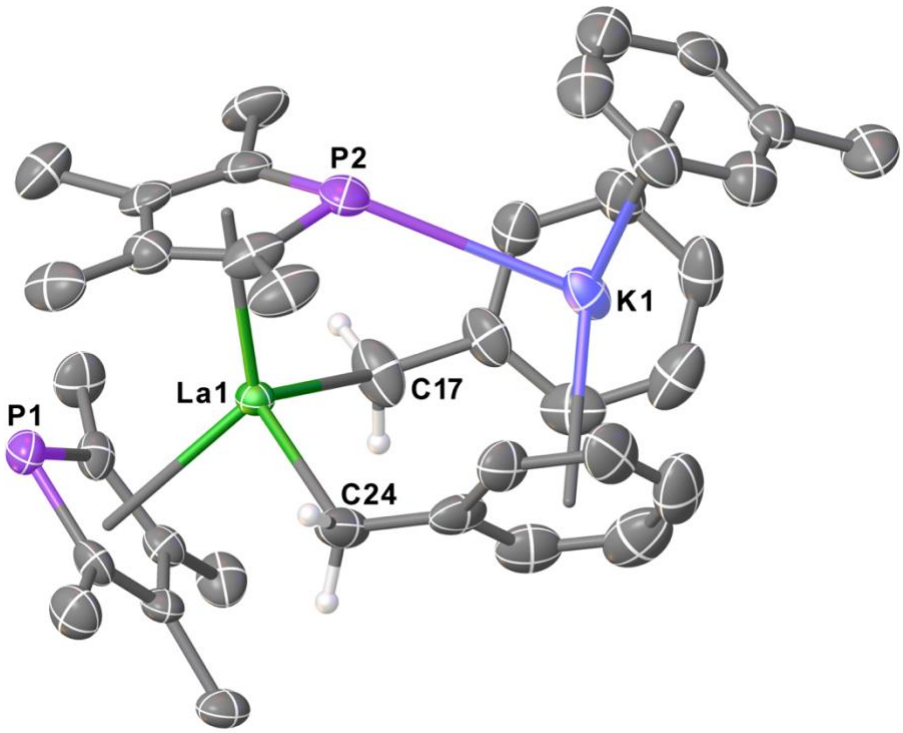

Figure S15. Molecular structure of **6La**. Ellipsoids set at 50% probability and H-atoms (except on C17 and C24) removed for clarity (operations: X,Y,Z).

Lengths (Å): La1–C17 = 2.622(8); La1–C24 = 2.675(9); La1–P1 = 3.0112(12); La1–TMP_{cent1} = 2.650(4); La1–P2 = 3.0407(15); La1–TMP_{cent2} = 2.635(4); K1–P2 = 3.323(2).

Angles (°): C17–La1–C24 = 111.5(4); TMP_{cent}–La1–TMP_{cent} = 127.63(12).

See page S27 (section entitled: “Note on choice of space group and symmetry for **6M** and **7M** series”) for a brief discussion on the choice of space group for this complex.

Complex ***6Ce***

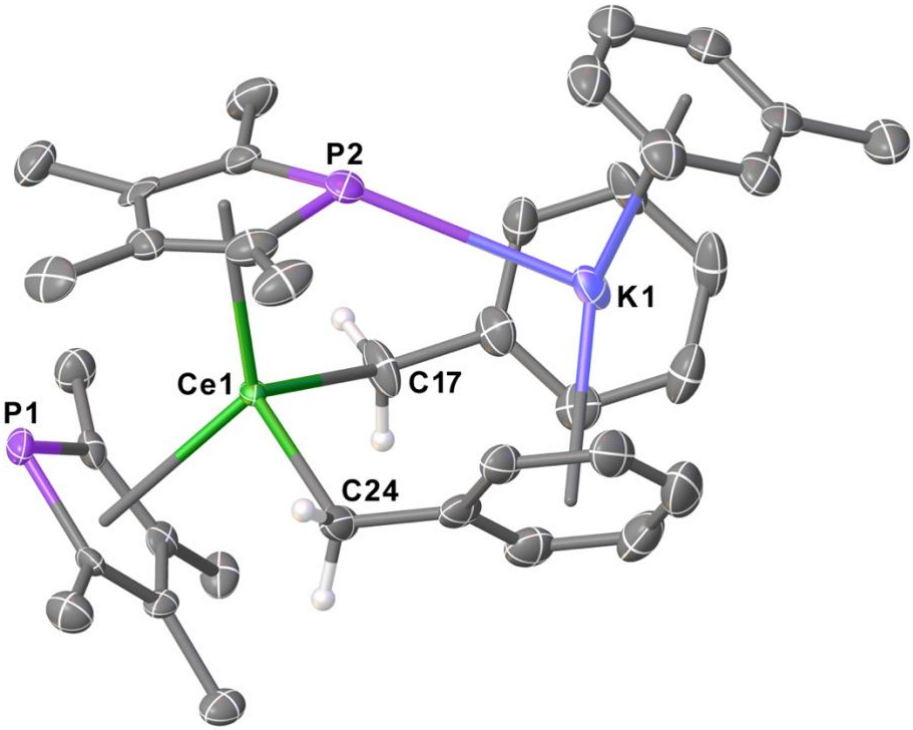

Figure S16. Molecular structure of **6Ce**. Ellipsoids set at 50% probability and H-atoms (except on C17 and C24) removed for clarity (operations: X,Y,Z).

Lengths (Å): Ce1–C17 = 2.619(8); Ce1–C24 = 2.631(10); Ce1–P1 = 2.9863(14); Ce1–TMP_{cent1} = 2.623(3); Ce1–P2 = 3.0197(16); Ce1–TMP_{cent2} = 2.609(4); K1–P2 = 3.313(2).

Angles (°): C17–Ce1–C24 = 111.0(4); TMP_{cent}–Ce1–TMP_{cent} = 127.59(11).

See page S27 (section entitled: “Note on choice of space group and symmetry for **6M** and **7M** series”) for a brief discussion on the choice of space group for this complex.

*Complex **6Pr***

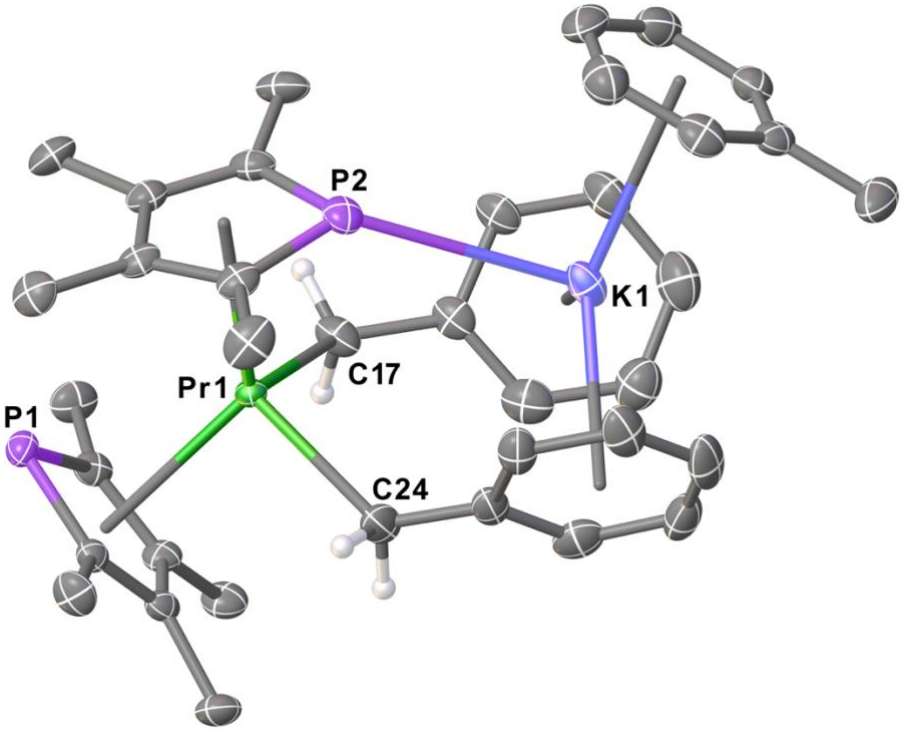

Figure S17. Molecular structure of **6Pr**. Ellipsoids set at 50% probability and H-atoms (except on C17 and C24) removed for clarity (operations: X,Y,Z).

Lengths (Å): Pr1–C17 = 2.592(6); Pr1–C24 = 2.598(5); Pr1–P1 = 2.9672(9); Pr1–TMP_{cent1} = 2.606(2); Pr1–P2 = 3.0034(11); Pr1–TMP_{cent2} = 2.593(2); K1–P2 = 3.3118(16).

Angles (°): C17–Pr1–C24 = 108.1(2); TMP_{cent}–Pr1–TMP_{cent} = 128.07(8).

See page S27 (section entitled: “Note on choice of space group and symmetry for **6M** and **7M** series”) for a brief discussion on the choice of space group for this complex.

*Complex **6U***

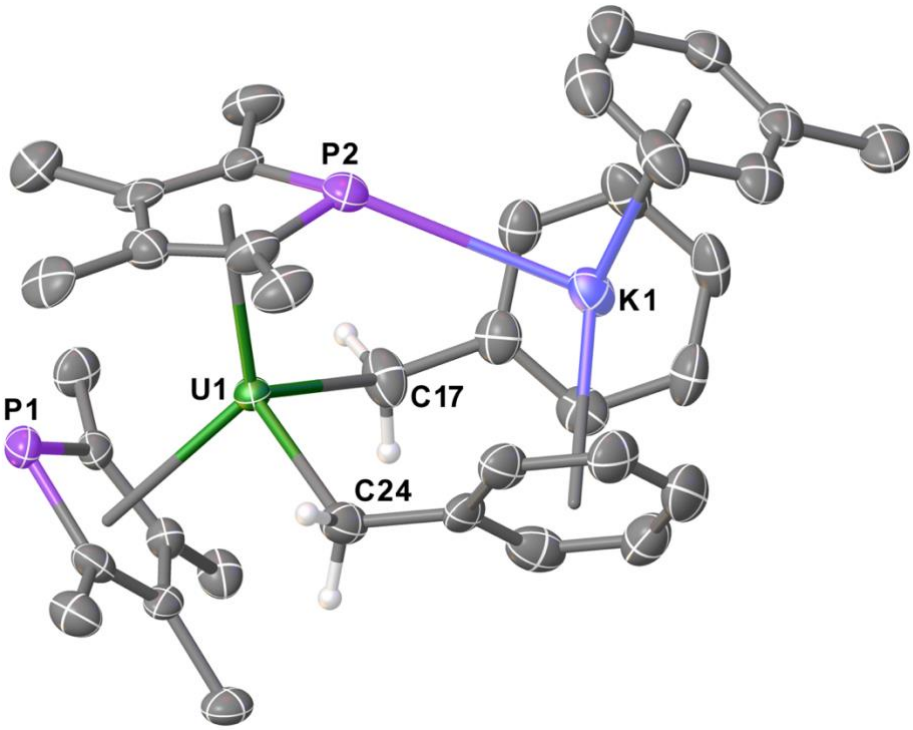

Figure S18. Molecular structure of **6U**. Ellipsoids set at 50% probability and H-atoms (except on C17 and C24) removed for clarity (operations: X,Y,Z).

Lengths (Å): U1–C17 = 2.577(7); U1–C24 = 2.597(7); U1–P1 = 2.9432(11); U1–TMP_{cent1} = 2.580(3); U1–P2 = 2.9766(14); U1–TMP_{cent2} = 2.564(3); K1–P2 = 3.303(2).

Angles (°): C17–U1–C24 = 105.6(3); TMP_{cent}–U1–TMP_{cent} = 128.33(11).

See page S27 (section entitled: “Note on choice of space group and symmetry for **6M** and **7M** series”) for a brief discussion on the choice of space group for this complex.

*Complex **6Np***

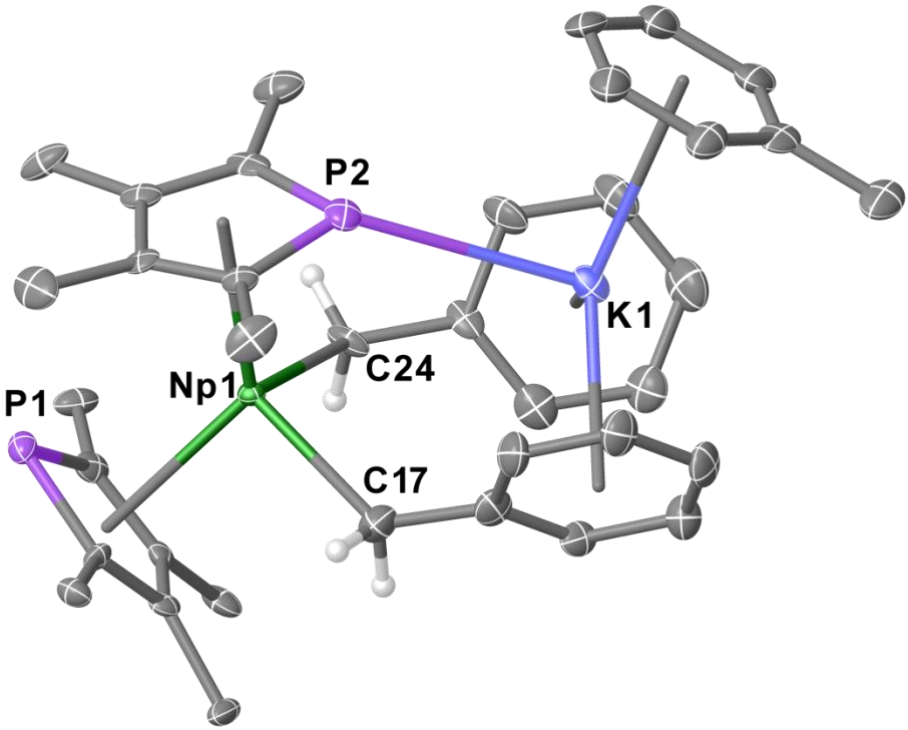

Figure S19. Molecular structure of **6Np**. Ellipsoids set at 30% probability and H-atoms (except on C17 and C24) removed for clarity (operations: X,Y,Z).

Lengths (Å): Np1–C17 = 2.519(18); Np1–C24 = 2.573(15); Np1–P1 = 2.940(2); Np1–TMP_{cent1} = 2.577(9); Np1–P2 = 2.971(3); Np1–TMP_{cent2} = 2.564(8); K1–P2 = 3.317(4).

Angles (°): C17–Np1–C24 = 104.6(5); TMP_{cent}–Np1–TMP_{cent} = 127.8(3).

See page S27 (section entitled: “Note on choice of space group and symmetry for **6M** and **7M** series”) for a brief discussion on the choice of space group for this complex.

*Complex **6Pu***

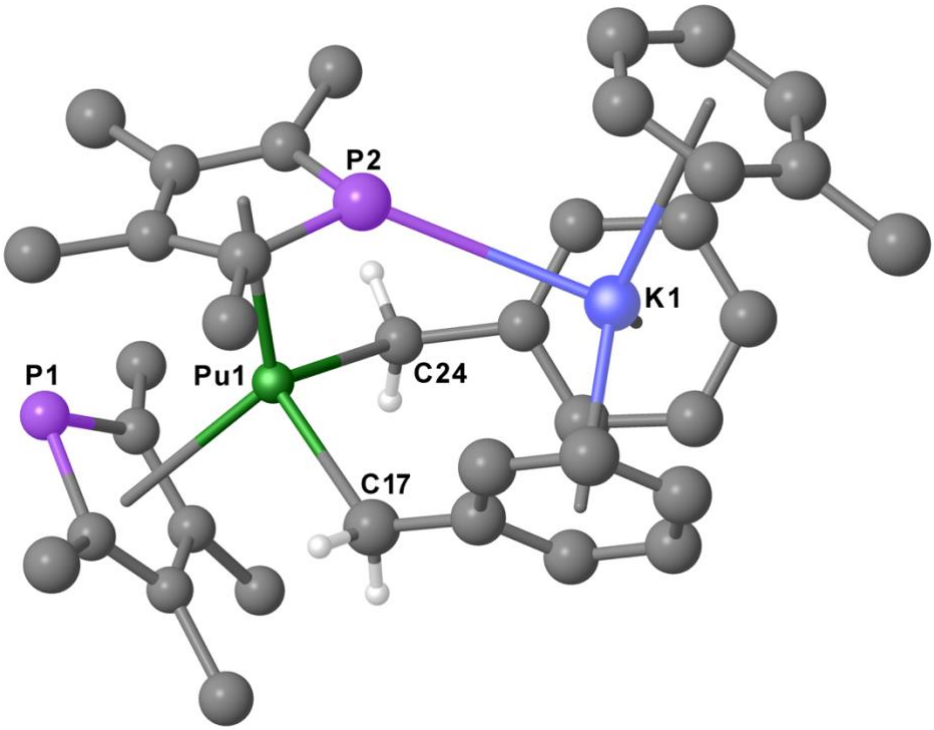

Figure S20. Ball-and-stick representation of the molecular structure of **6Pu**. H-atoms removed for clarity (operations: X,Y,Z). The data quality is insufficient for meaningful discussion of the metrical parameters.

See page S27 (section entitled: “Note on choice of space group and symmetry for **6M** and **7M** series”) for a brief discussion on the choice of space group for this complex.

*Complex **7U***

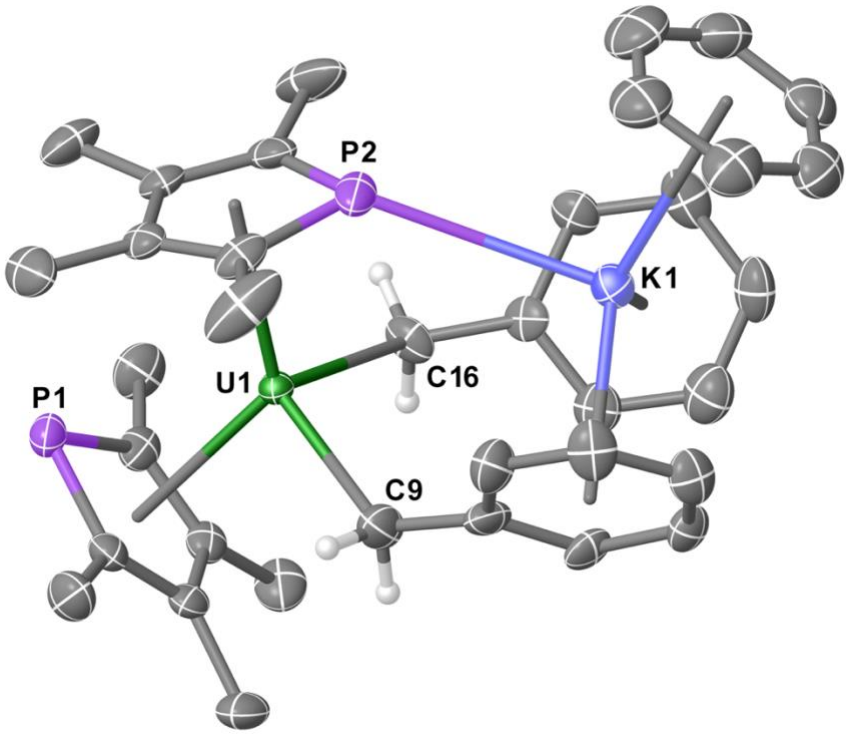

Figure S21. Molecular structure of **7U**. Ellipsoids set at 50% probability and H-atoms (except on C9 and C16) removed for clarity (operations: X,Y,Z; +X,3/2–Y,+Z).

Lengths (Å): U1–C9 = 2.556(17); U1–C16 = 2.654(16); U1–P1 = 2.9576(11); U1–TMP_{cent1} = 2.5915(2); U1–P2 = 2.9857(11); U1–TMP_{cent2} = 2.5816(11); K1–P2 = 3.3275(15).

Angles (°): C9–U1–C16 = 105.6(4); TMP_{cent}–U1–TMP_{cent} = 127.624(9).

See page S27 (section entitled: “Note on choice of space group and symmetry for **6M** and **7M** series”) for a brief discussion on the choice of space group for this complex.

*Complex **7Np***

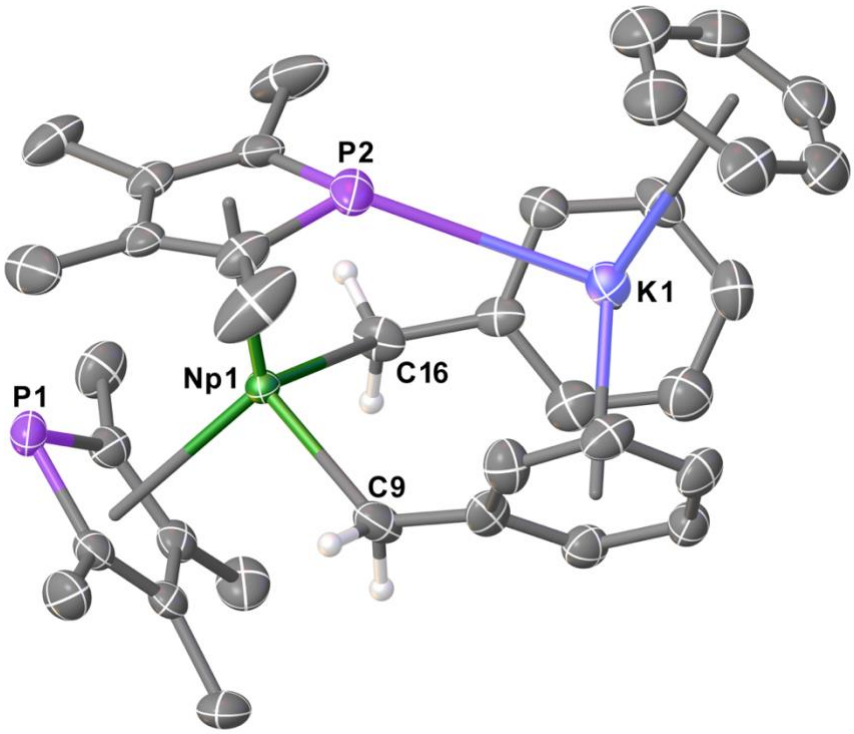

Figure S22. Molecular structure of **7Np**. Ellipsoids set at 50% probability and H-atoms (except on C9 and C16) removed for clarity (operations: X,Y,Z; +X,3/2–Y,+Z).

Lengths (Å): Np1–C9 = 2.479(17); Np1–C16 = 2.603(16); Np1–P1 = 2.9147(11); Np1–TMP_{cent1} = 2.5547(12); Np1–P2 = 2.9403(12); Np1–TMP_{cent2} = 2.5484(12); K1–P2 = 3.2805(16).

Angles (°): C9–Np1–C16 = 105.2(3); TMP_{cent}–Np1–TMP_{cent} = 127.12(4).

See page S27 (section entitled: “Note on choice of space group and symmetry for **6M** and **7M** series”) for a brief discussion on the choice of space group for this complex.

*Complex **7Pu***

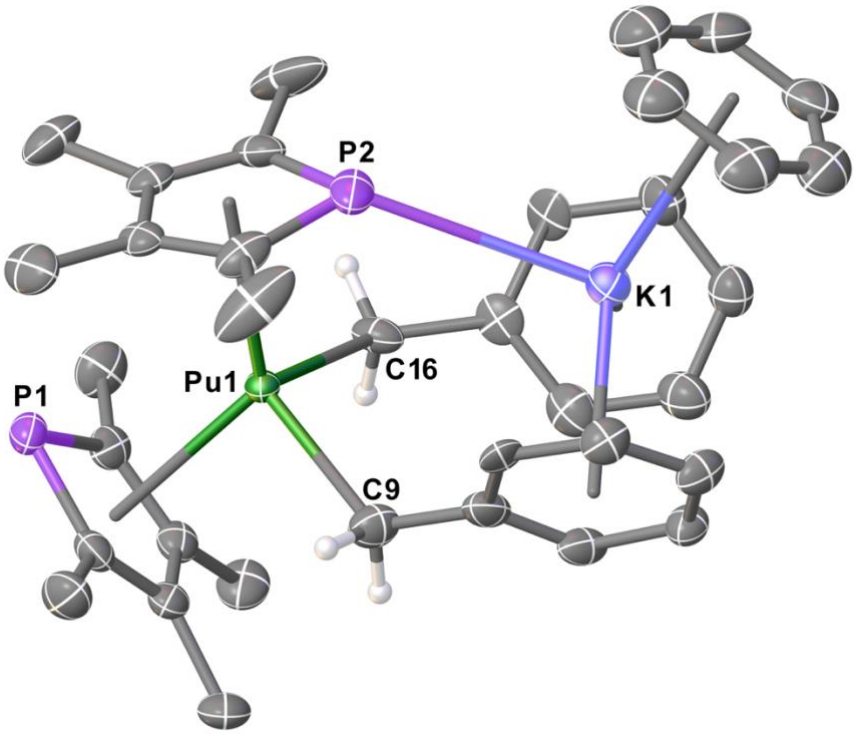

Figure S23. Molecular structure of **7Pu**. Ellipsoids set at 50% probability and H-atoms (except on C9 and C16) removed for clarity (operations: X,Y,Z; +X,1/2–Y,+Z).

Lengths (Å): Pu1–C9 = 2.542(19); Pu1–C16 = 2.614(19); Pu1–P1 = 2.9533(13); Pu1–TMP_{cent1} = 2.5931(15); Pu1–P2 = 2.9816(14); Pu1–TMP_{cent2} = 2.5821(14); K1–P2 = 3.3270(18).

Angles (°): C9–Pu1–C16 = 107.1(4); TMP_{cent}–Pu1–TMP_{cent} = 127.56(5).

See page S27 (section entitled: “Note on choice of space group and symmetry for **6M** and **7M** series”) for a brief discussion on the choice of space group for this complex.

Tables of bond lengths and angles

Table S7. Bond lengths and angles for **6M** (M = U, Np, La, Ce, Pr, Pu) and **7M** (M = U, Np, Pu).

6M	**M–P (Å)**	**M–C_{Bn} (Å)**	**M···TMP_{cent} (Å)**	**K–P (Å)**	**TMP_{cent}···M···TMP_{cent} (°)**	**C_{Bn}···M···C_{Bn} (°)**
La	3.0112(12) 3.0407(15)	2.622(8) 2.675(9)	2.650(4) 2.635(4)	3.323(2)	127.63(12)	111.5(4)
U	2.9432(11) 2.9766(14)	2.577(7) 2.597(7)	2.580(3) 2.564(3)	3.303(2)	128.33(11)	105.6(3)
Ce	2.9863(14) 3.0197(16)	2.619(8) 2.631(10)	2.623(3) 2.609(4)	3.313(2)	127.59(11)	111.0(4)
Np	2.940(2) 2.971(3)	2.519(18) 2.573(15)	2.577(9) 2.564(8)	3.317(4)	127.8(3)	104.6(5)
Pr	2.9672(9) 3.0034(11)	2.592(6) 2.598(5)	2.606(2) 2.593(2)	3.3118(16)	128.07(8)	108.1(2)
7M						
U	2.9576(11) 2.9857(11)	2.556(17) 2.654(16)	2.5915(2) 2.5816(11)	3.3275(15)	127.624(9)	105.6(4)
Np	2.9147(11) 2.9403(12)	2.479(17) 2.603(16)	2.5547(12) 2.5484(12)	3.2805(16)	127.12(4)	105.2(3)
Pu	2.9533(13) 2.9816(14)	2.542(19) 2.614(19)	2.5931(15) 2.5821(14)	3.3270(18)	127.56(5)	107.1(4)

S5. NMR spectroscopy

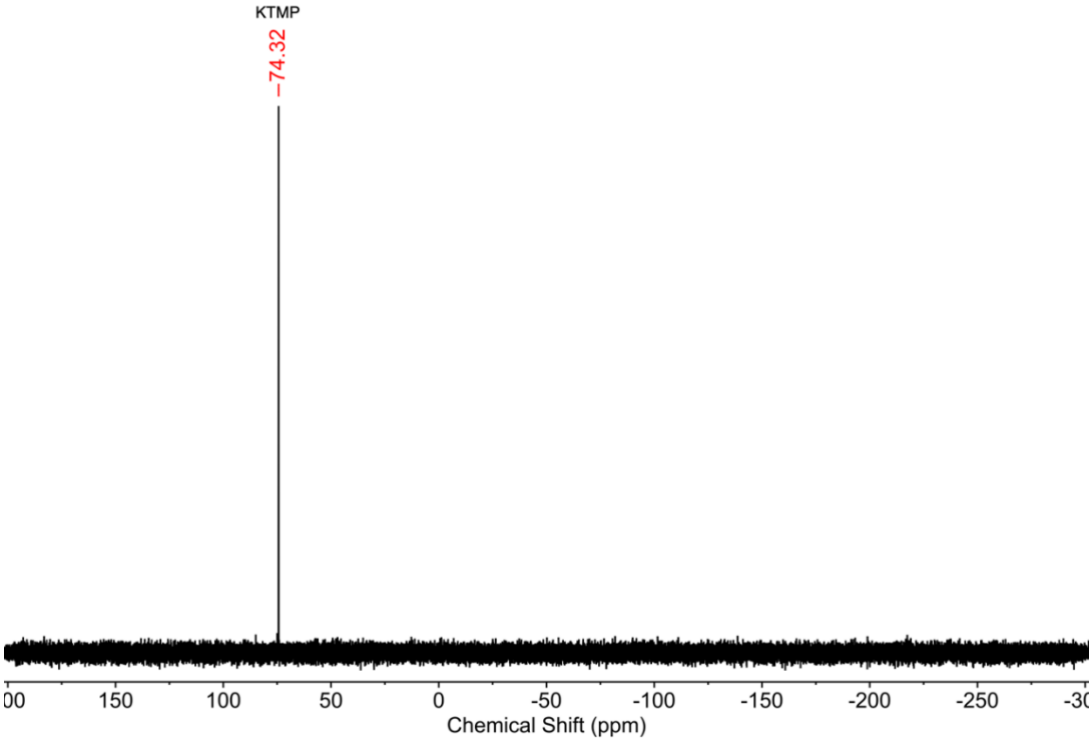

Figure S24. ^{1}H NMR spectrum (at 297 K) of KTMP in C_4H_8O with several drops of C_6D_6.

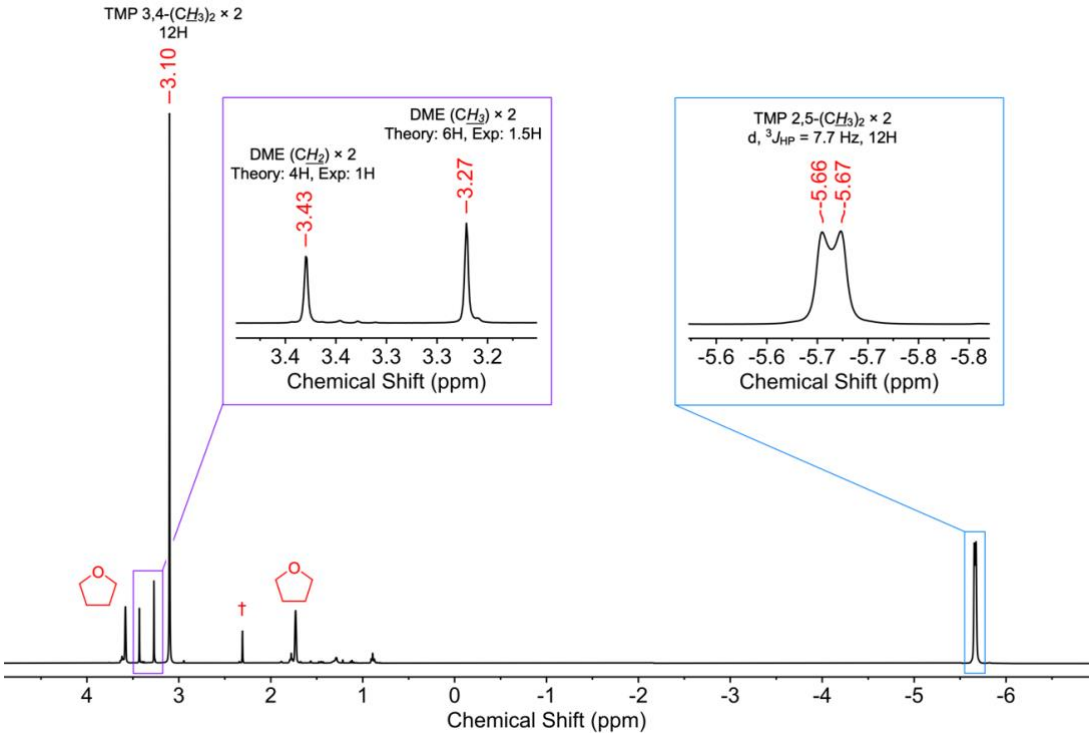

Figure S25. ^{1}H NMR spectrum (at 295 K) of $[Np(TMP)_2Cl_2K(DME)]_n$ (**2**) in C_4D_8O.

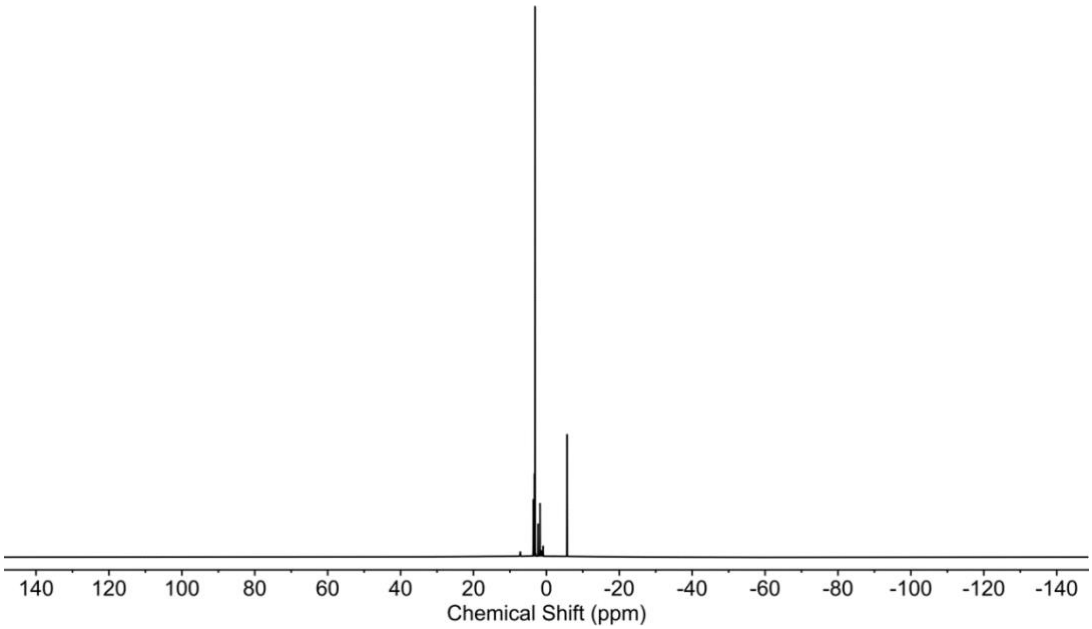

Figure S26. ^{1}H NMR spectrum (at 295 K) of $[Np(TMP)_2Cl_2K(DME)]_n$ (**2**) in C_4D_8O, showing the full range collected.

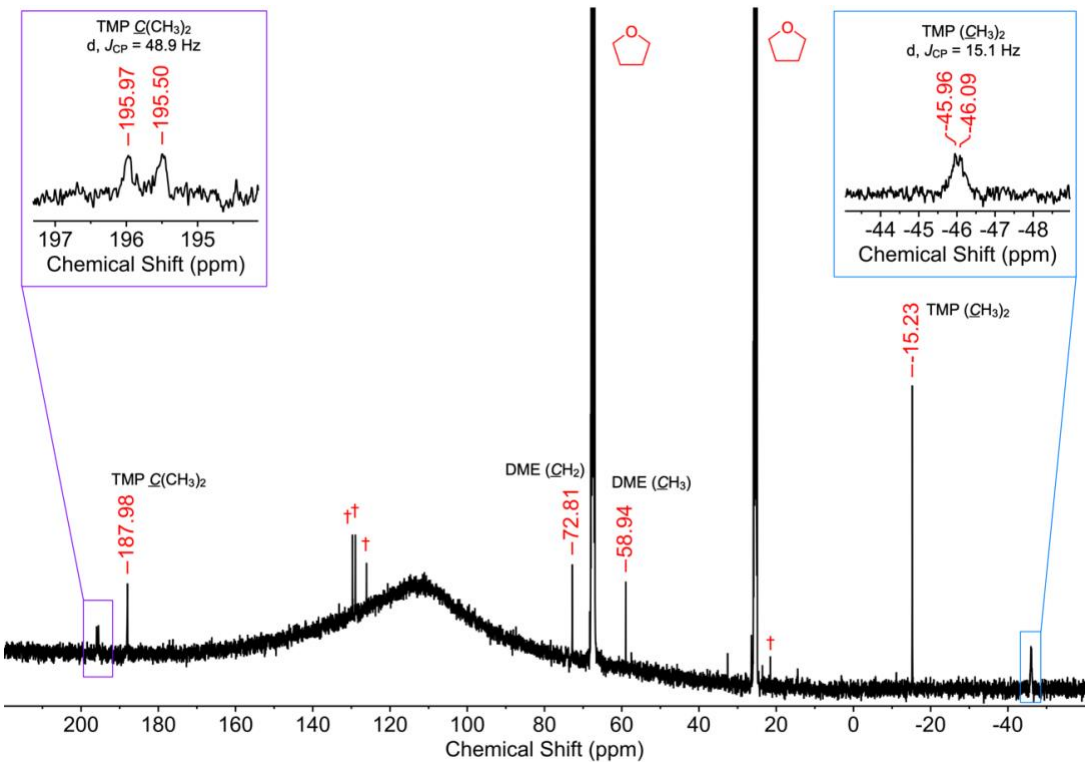

Figure S27. $^{13}C\{^{1}H\}$ NMR spectrum (at 296 K) of $[Np(TMP)_2Cl_2K(DME)]_n$ (**2**) in C_4D_8O. † symbol denotes residual toluene from crystallisation.

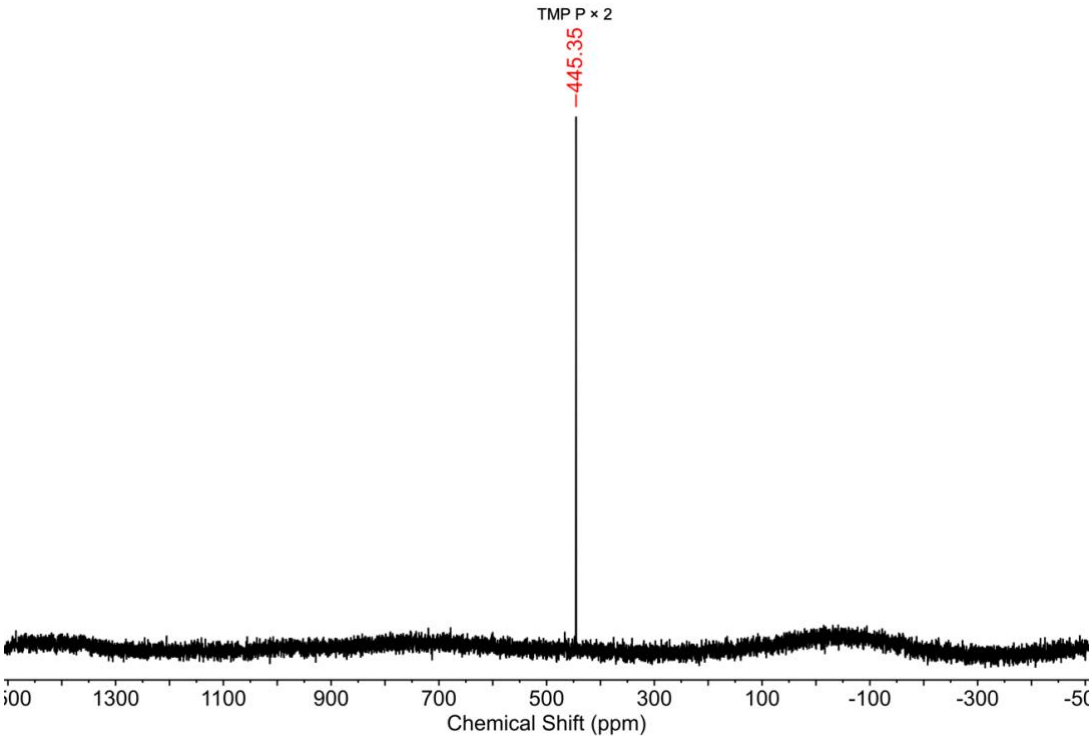

Figure S28. ^{31}P NMR spectrum (at 295 K) of $[Np(TMP)_2Cl_2K(DME)]_n$ (**2**) in C_4D_8O.

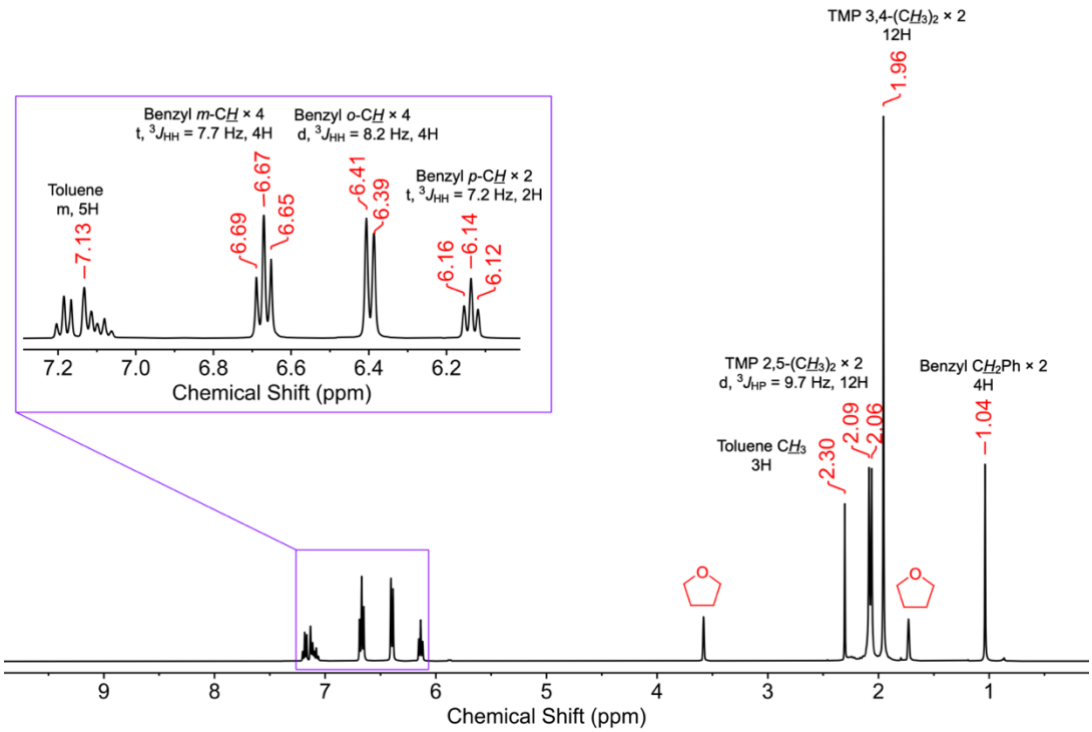

Figure S29. ^{1}H NMR spectrum (at 295 K) of $[La(TMP)_2Bn_2K(toluene)]$ (**6La**) in C_4D_8O.

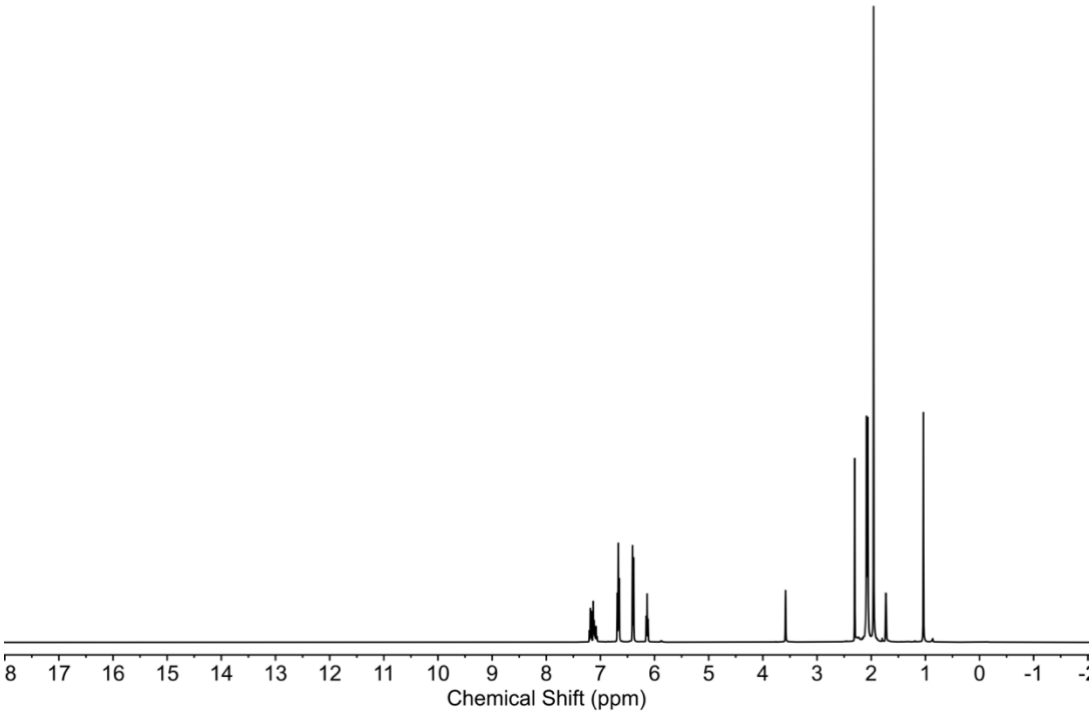

Figure S30. ^{1}H NMR spectrum (at 295 K) of [La(TMP)$_2$Bn$_2$K(toluene)] (**6La**) in C_4D_8O, showing the full range collected.

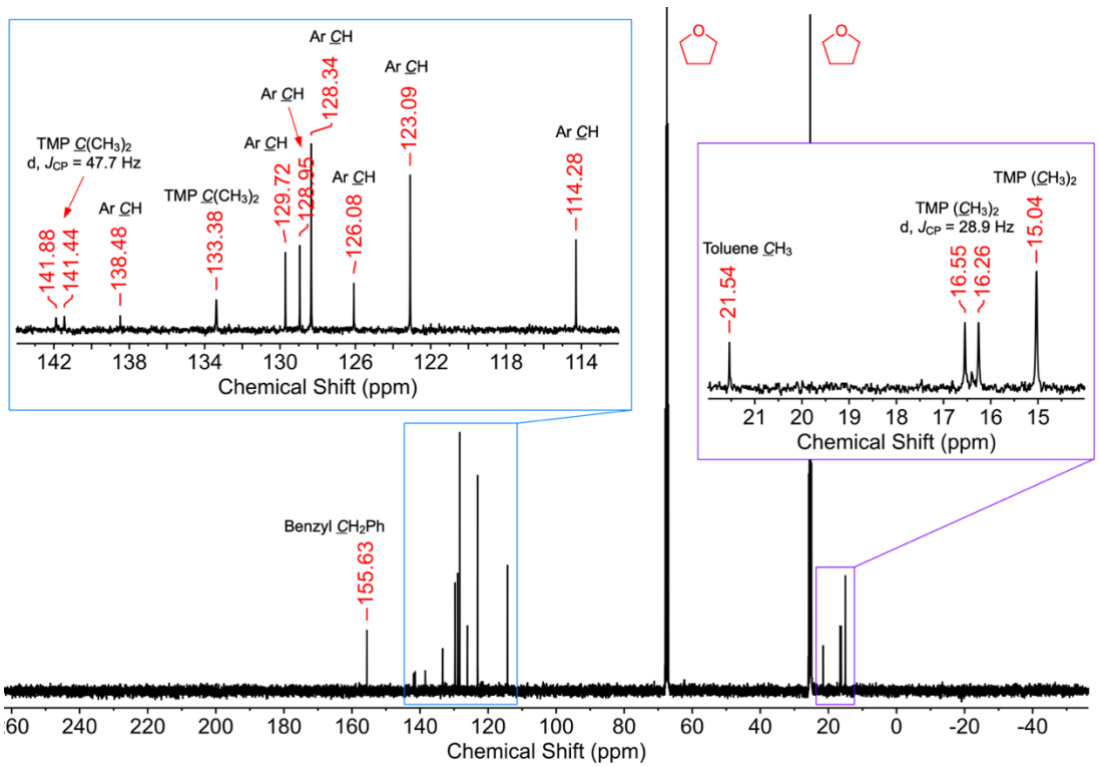

Figure S31. ^{13}C{^{1}H} NMR spectrum (at 296 K) of [La(TMP)$_2$Bn$_2$K(toluene)] (**6La**) in C_4D_8O.

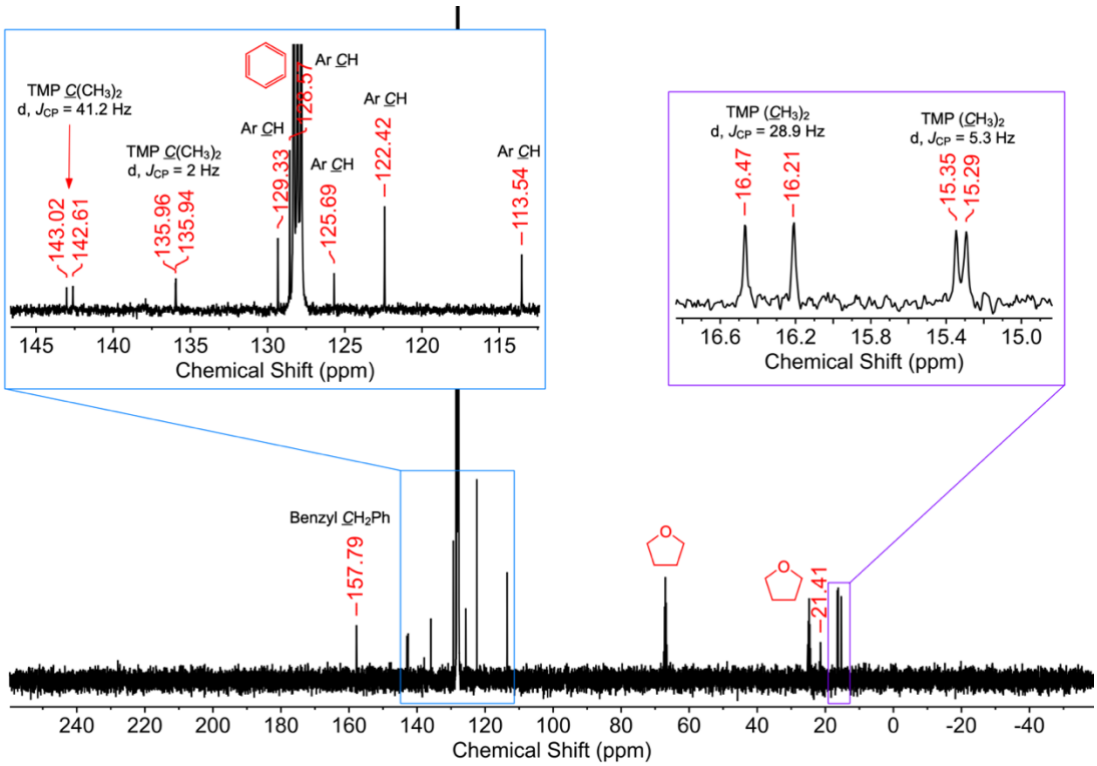

Figure S32. $^{13}C\{^{1}H\}$ NMR spectrum (at 296 K) of [La(TMP)$_2$Bn$_2$K(toluene)] (**6La**) in C_6D_6 with several drops of C_4D_8O to aid with solubility – the ^{13}C–^{31}P coupling on the TMP CH_3 group is resolved here.

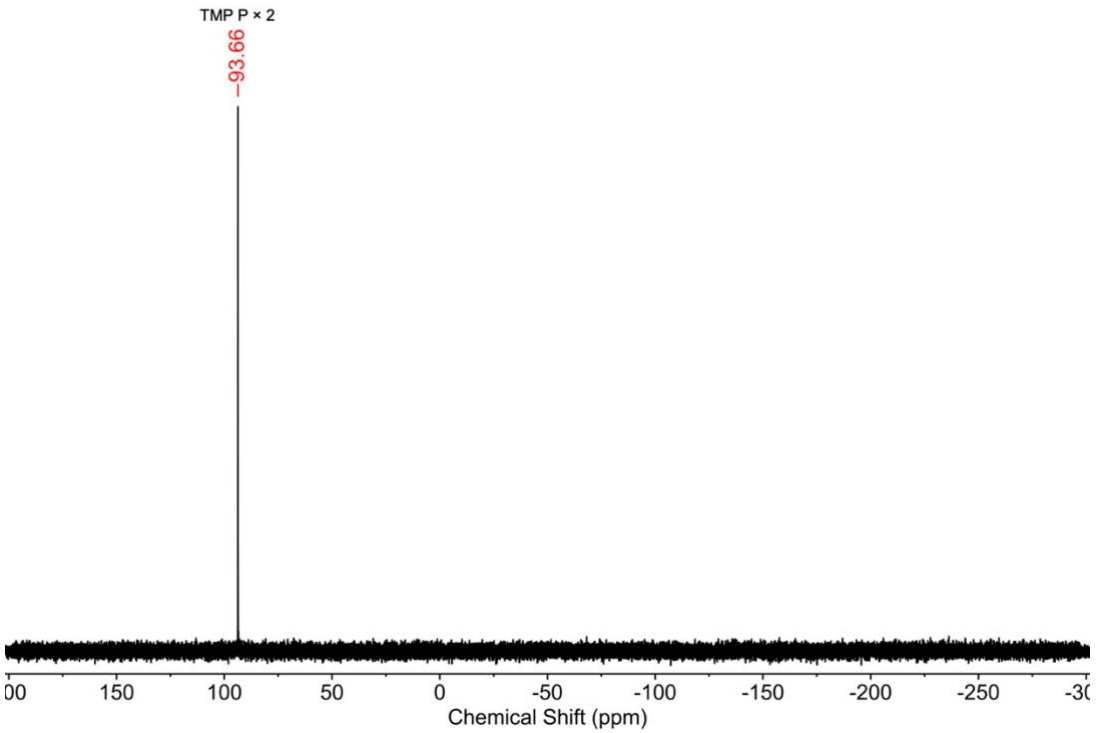

Figure S33. $^{31}P\{^{1}H\}$ NMR spectrum (at 295 K) of [La(TMP)$_2$Bn$_2$K(toluene)] (**6La**) in C_4D_8O.

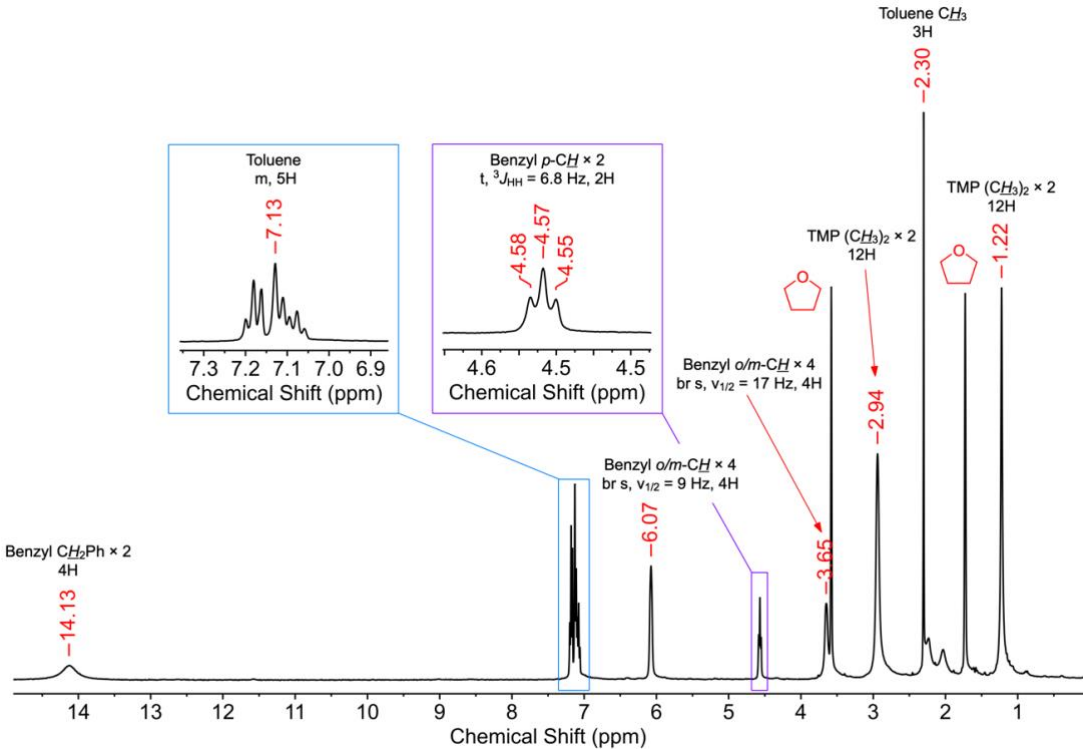

Figure S34. ^{1}H NMR spectrum (at 299 K) of [Ce(TMP)$_2$Bn$_2$K(toluene)] (**6Ce**) in C_4D_8O.

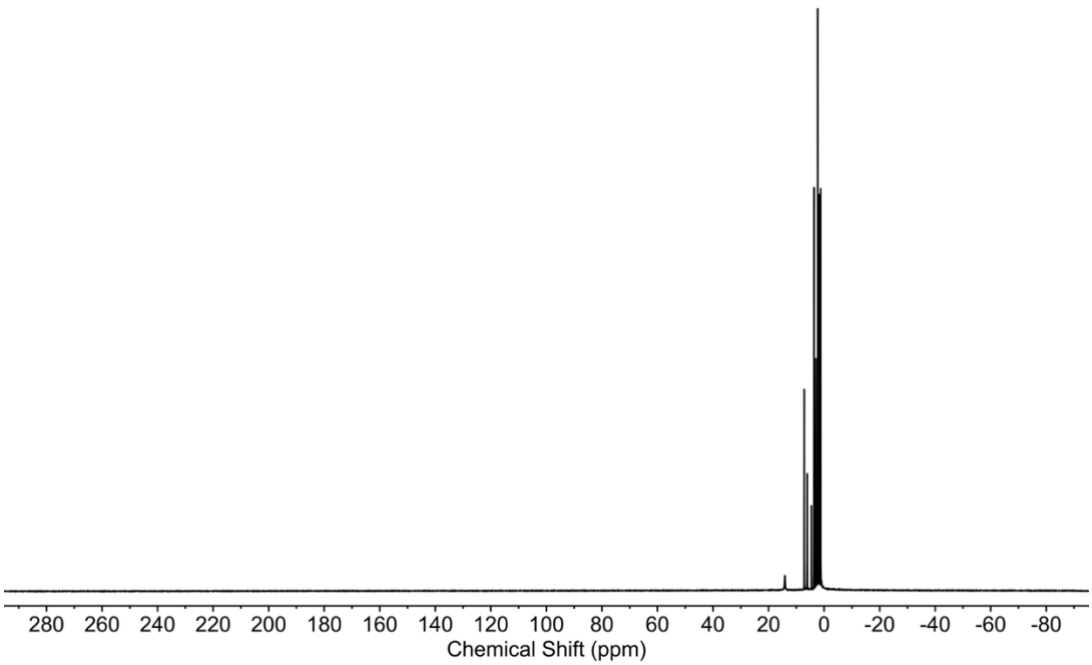

Figure S35. ^{1}H NMR spectrum (at 299 K) of [Ce(TMP)$_2$Bn$_2$K(toluene)] (**6Ce**) in C_4D_8O, showing the full range collected.

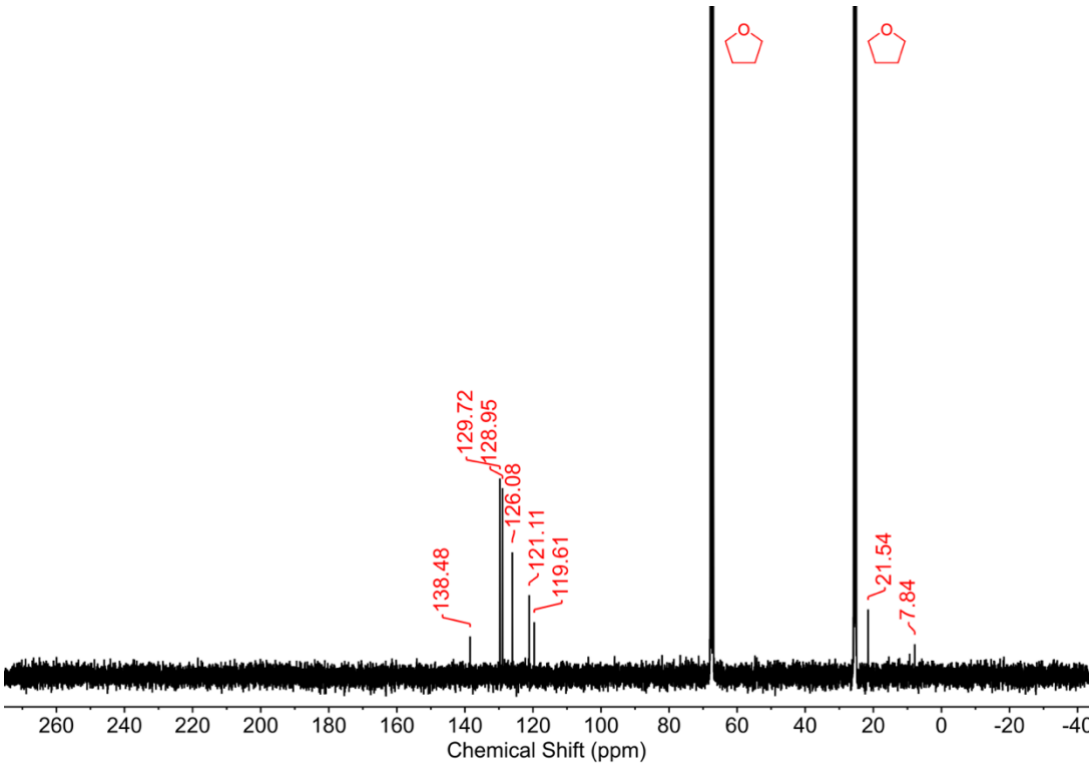

Figure S36. $^{13}C\{^{1}H\}$ NMR spectrum (at 298 K) of [Ce(TMP)$_2$Bn$_2$K(toluene)] (**6Ce**) in C_4D_8O.

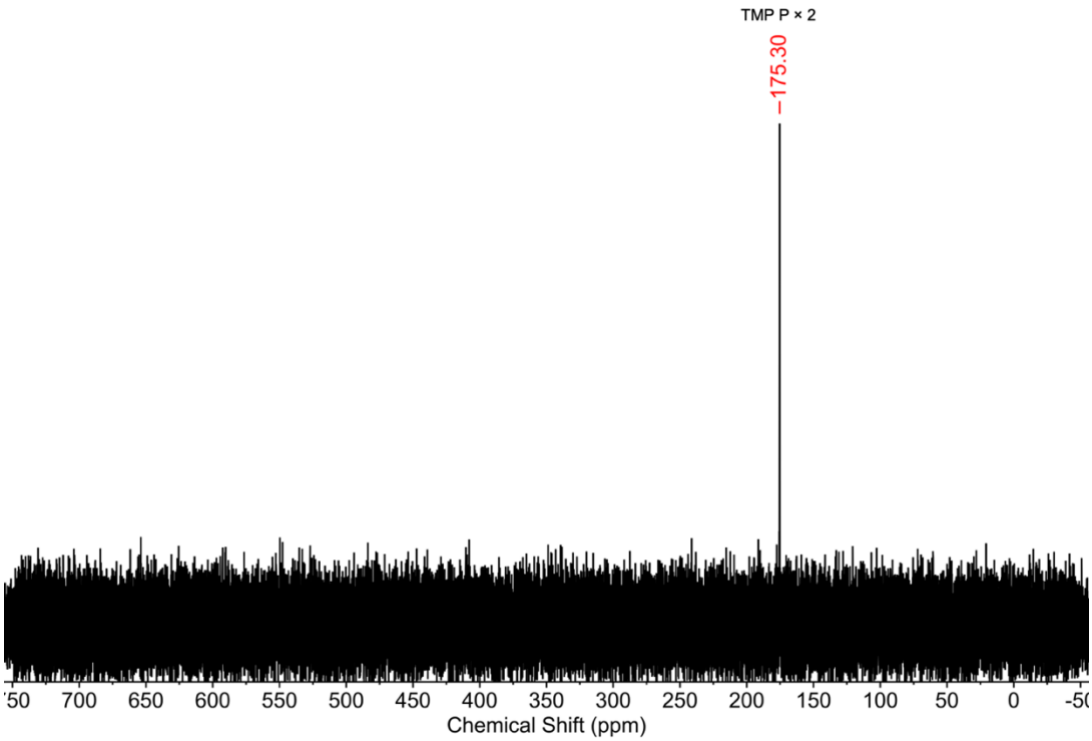

Figure S37. $^{31}P\{^{1}H\}$ NMR spectrum (at 299 K) of [Ce(TMP)$_2$Bn$_2$K(toluene)] (**6Ce**) in C_4D_8O.

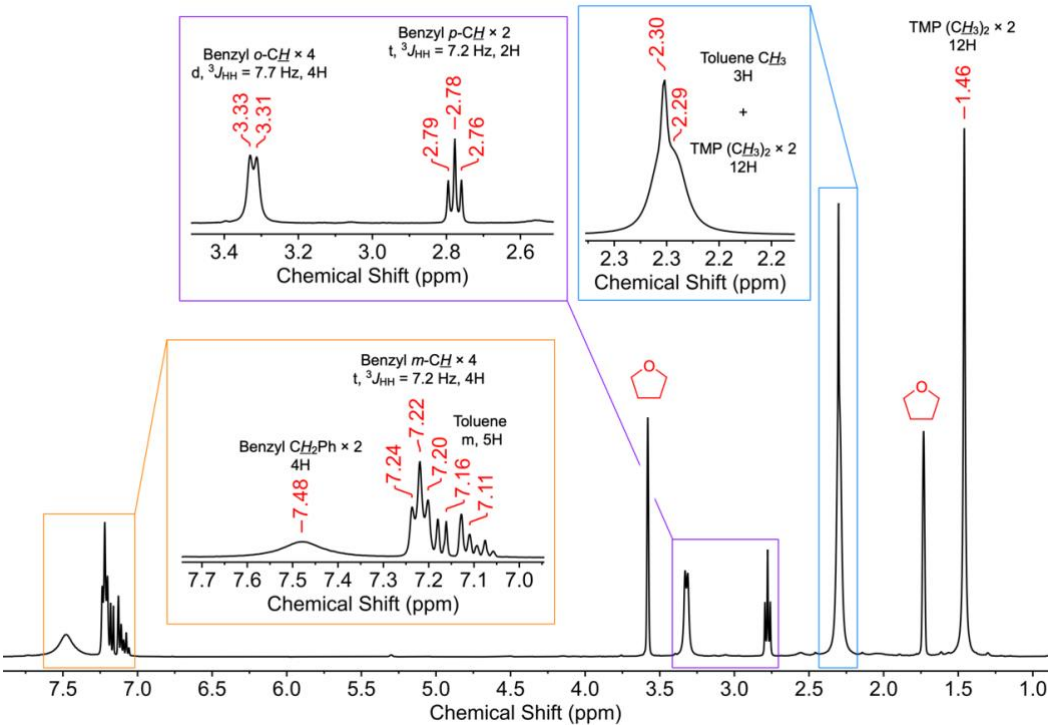

Figure S38. ^{1}H NMR spectrum (at 299 K) of [Pr(TMP)$_2$Bn$_2$K(toluene)] (**6Pr**) in C_4D_8O.

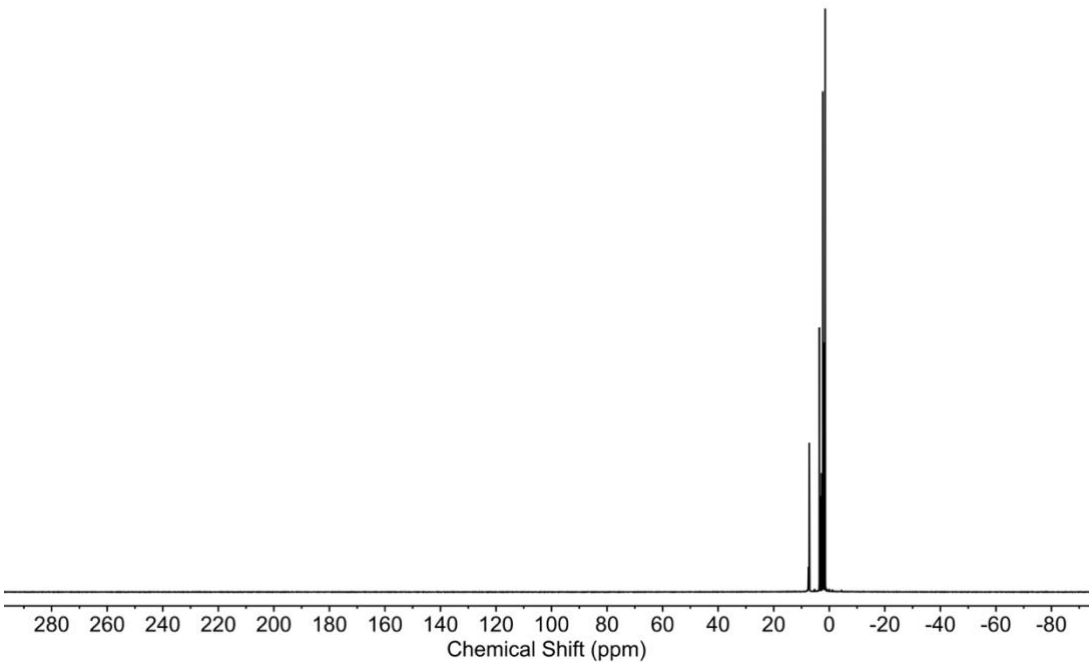

Figure S39. ^{1}H NMR spectrum (at 299 K) of [Pr(TMP)$_2$Bn$_2$K(toluene)] (**6Pr**) in C_4D_8O, showing the full range collected.

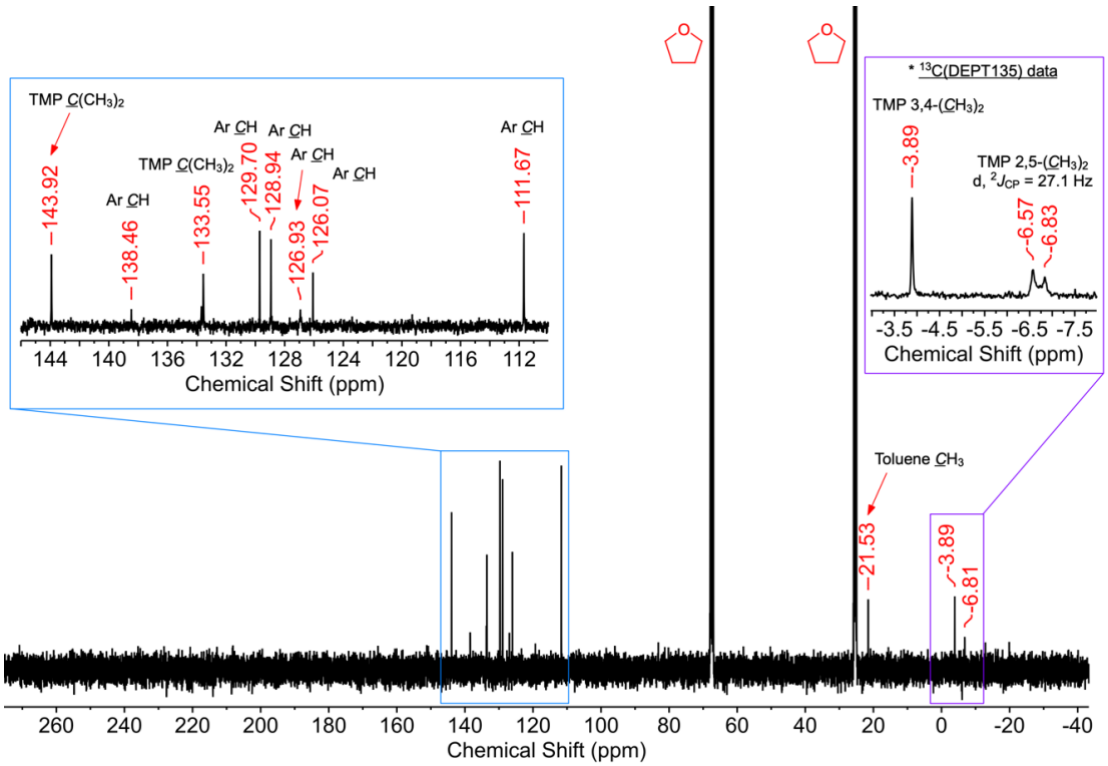

Figure S40. $^{13}C\{^{1}H\}$ NMR spectrum (at 298 K) of [Pr(TMP)$_2$Bn$_2$K(toluene)] (**6Pr**) in C_4D_8O.

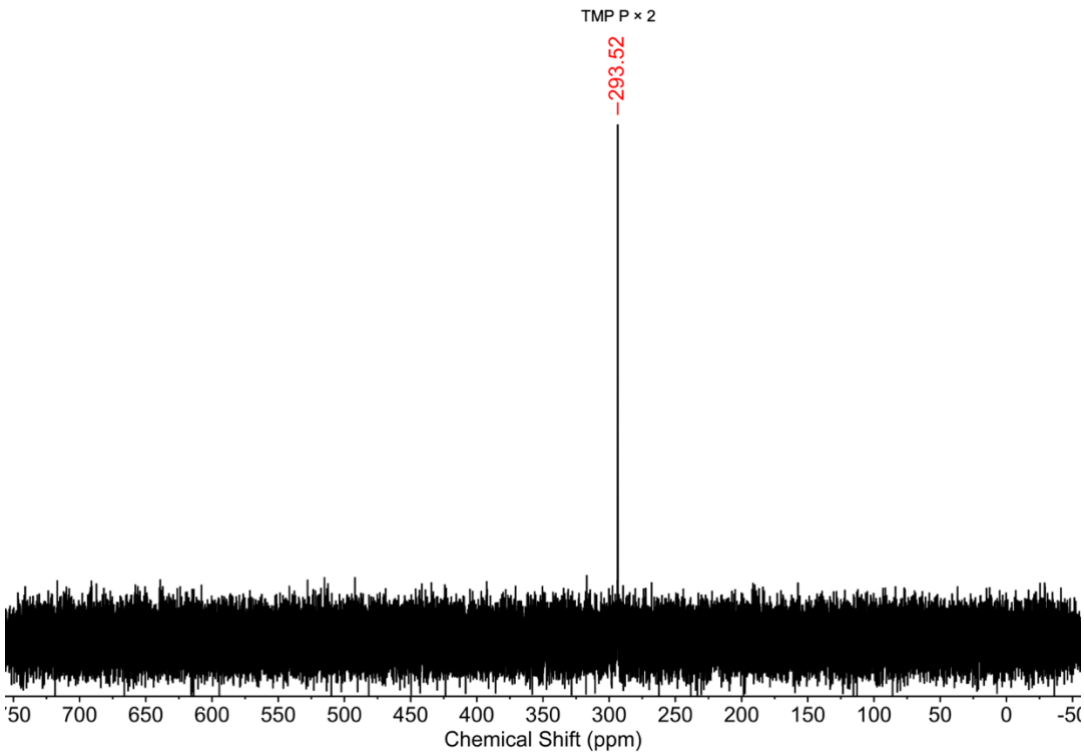

Figure S41. $^{31}P\{^{1}H\}$ NMR spectrum (at 299 K) of [Pr(TMP)$_2$Bn$_2$K(toluene)] (**6Pr**) in C_4D_8O.

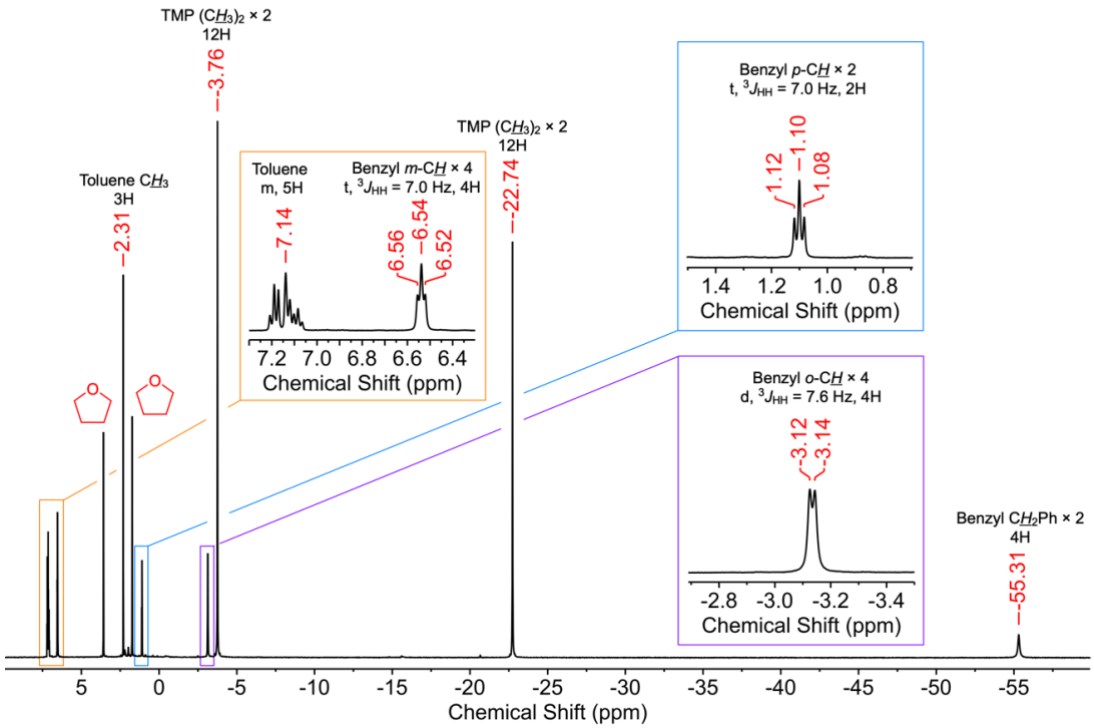

Figure S42. ^{1}H NMR spectrum (at 299 K) of [U(TMP)$_2$Bn$_2$K(toluene)] (**6U**) in C_4D_8O.

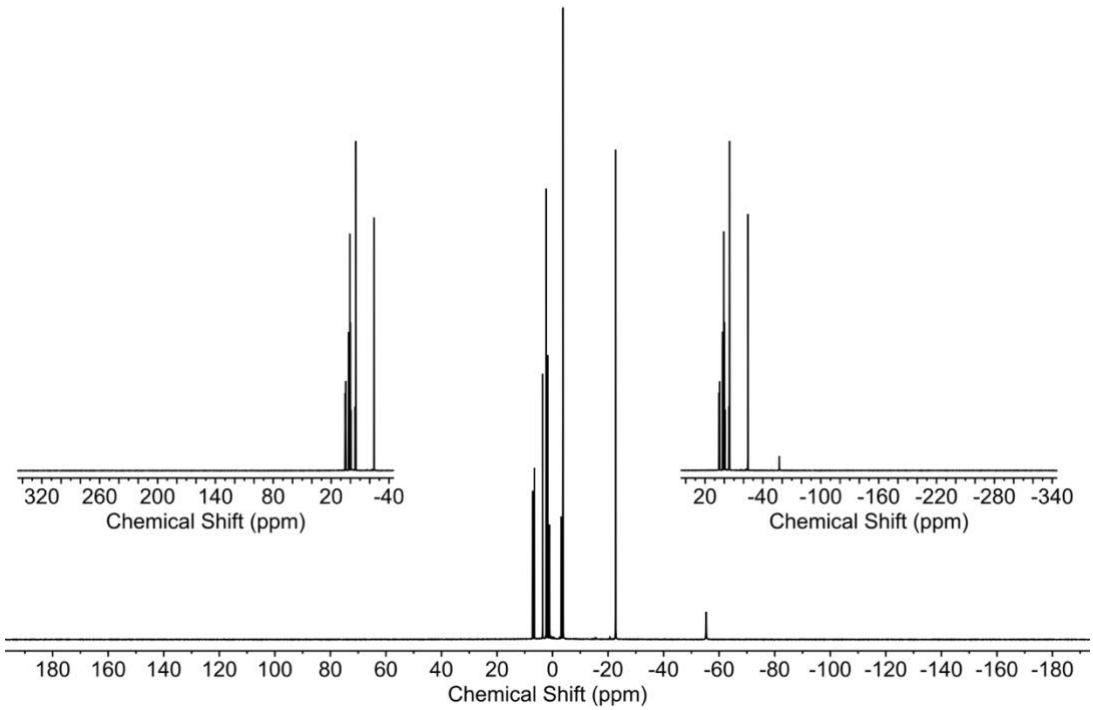

Figure S43. ^{1}H NMR spectrum (at 299 K) of [U(TMP)$_2$Bn$_2$K(toluene)] (**6U**) in C_4D_8O, showing the full range collected.

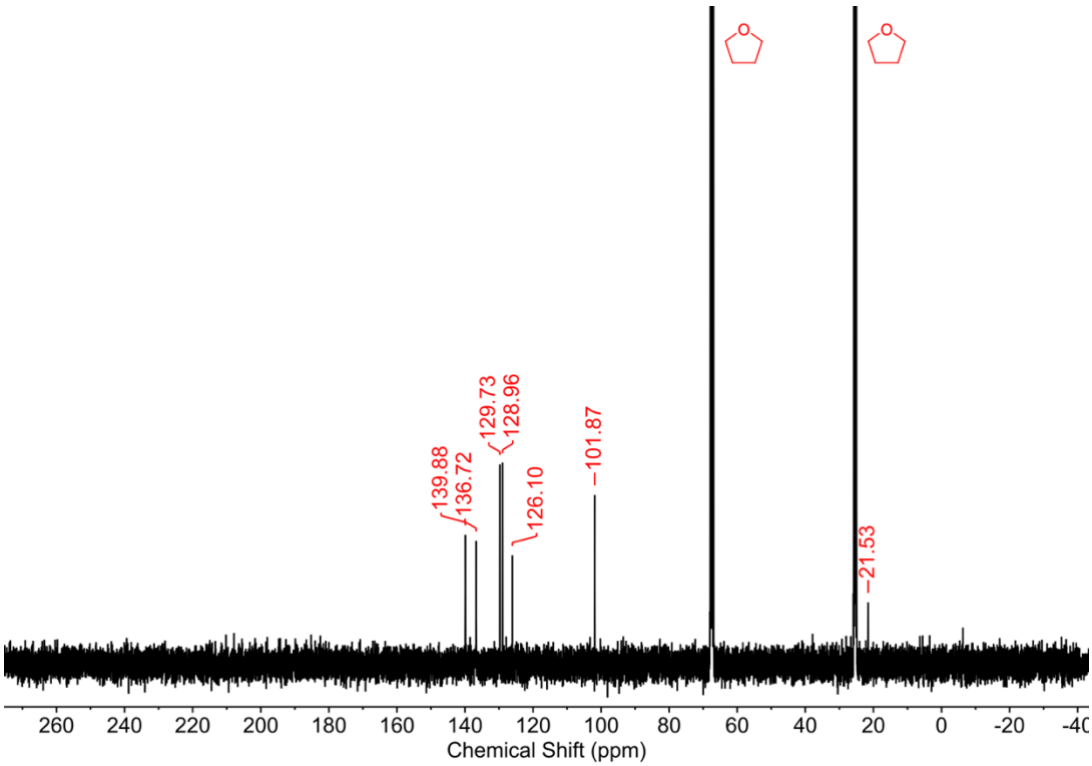

Figure S44. $^{13}C\{^{1}H\}$ NMR spectrum (at 298 K) of [U(TMP)$_2$Bn$_2$K(toluene)] (**6U**) in C_4D_8O.

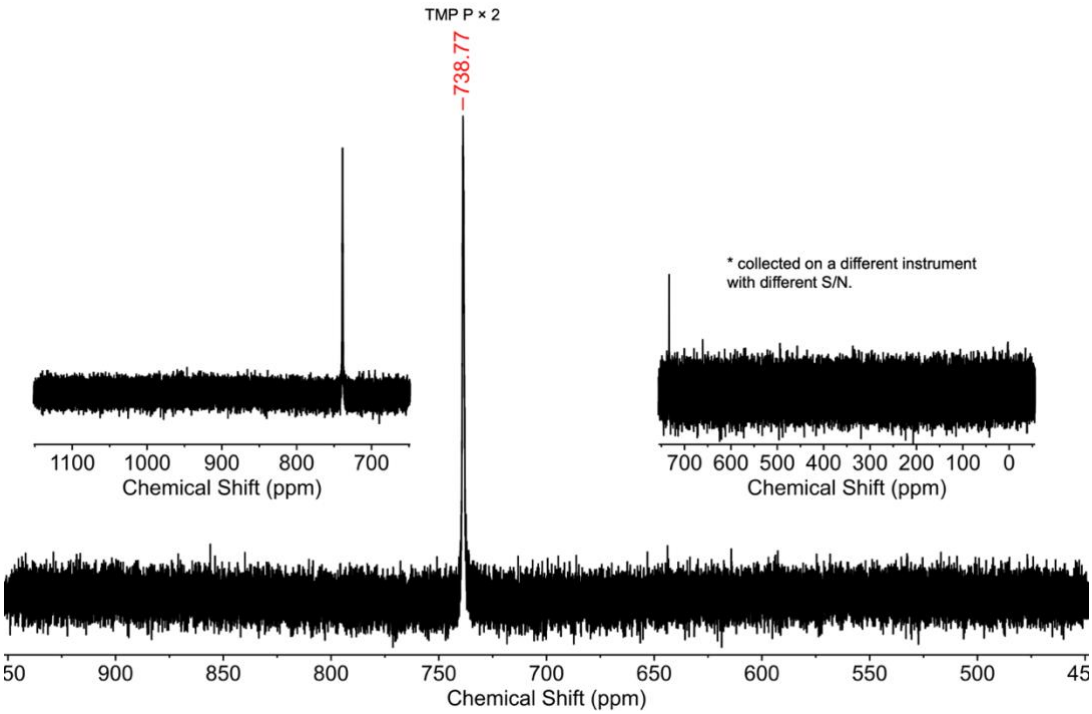

Figure S45. $^{31}P\{^{1}H\}$ NMR spectrum (at 298 K, 299 K for top right inset) of [U(TMP)$_2$Bn$_2$K(toluene)] (**6U**) in C_4D_8O, showing the full range collected.

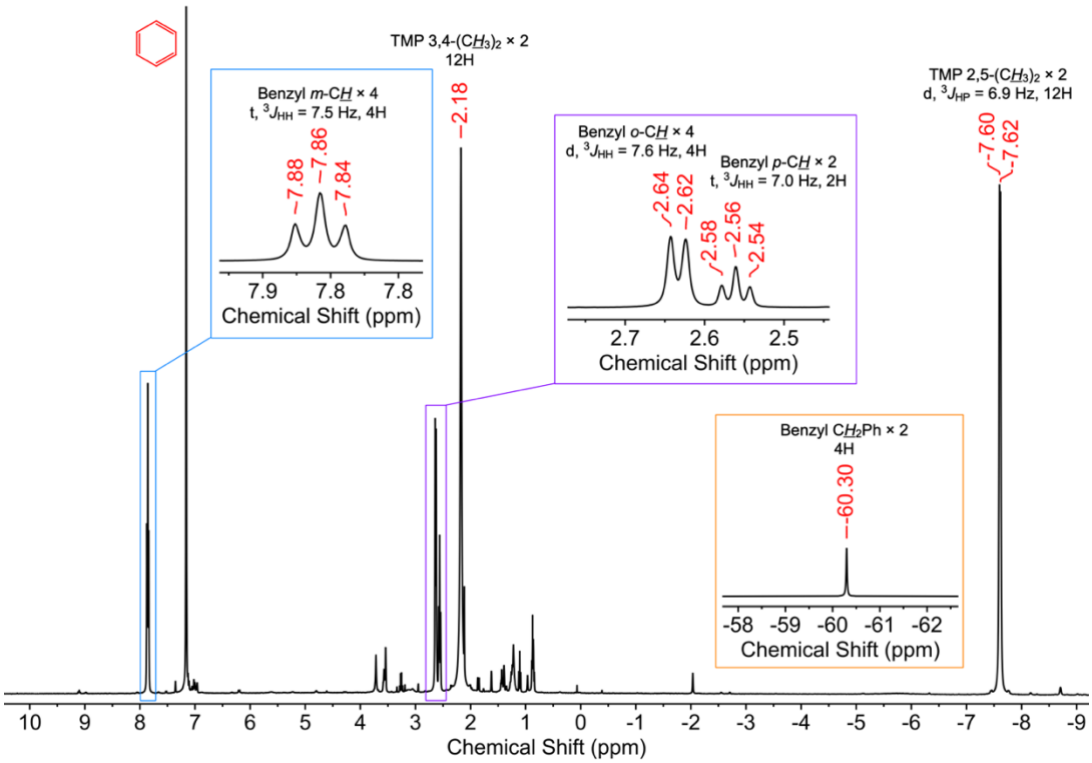

Figure S46. ^{1}H NMR spectrum (at 295 K) of [Np(TMP)$_2$Bn$_2$K(toluene)] (**6Np**) in C_6D_6 with several drops of C_4D_8O.

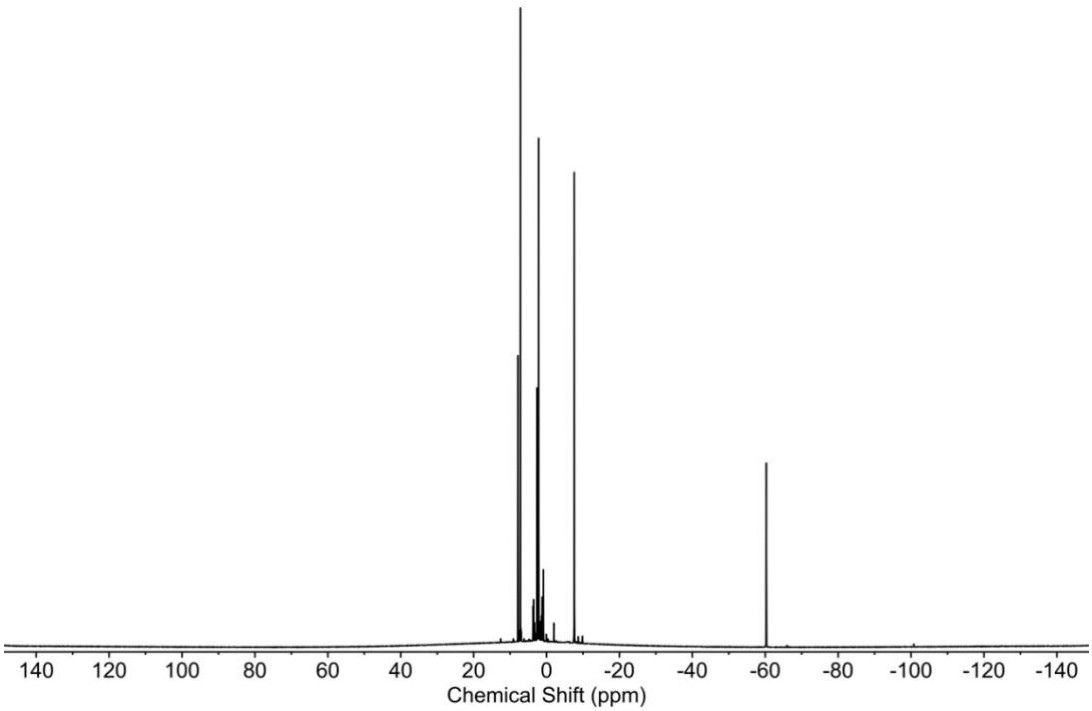

Figure S47. ^{1}H NMR spectrum (at 295 K) of [Np(TMP)$_2$Bn$_2$K(toluene)] (**6Np**) in C_6D_6 with several drops of C_4D_8O, showing the full range collected.

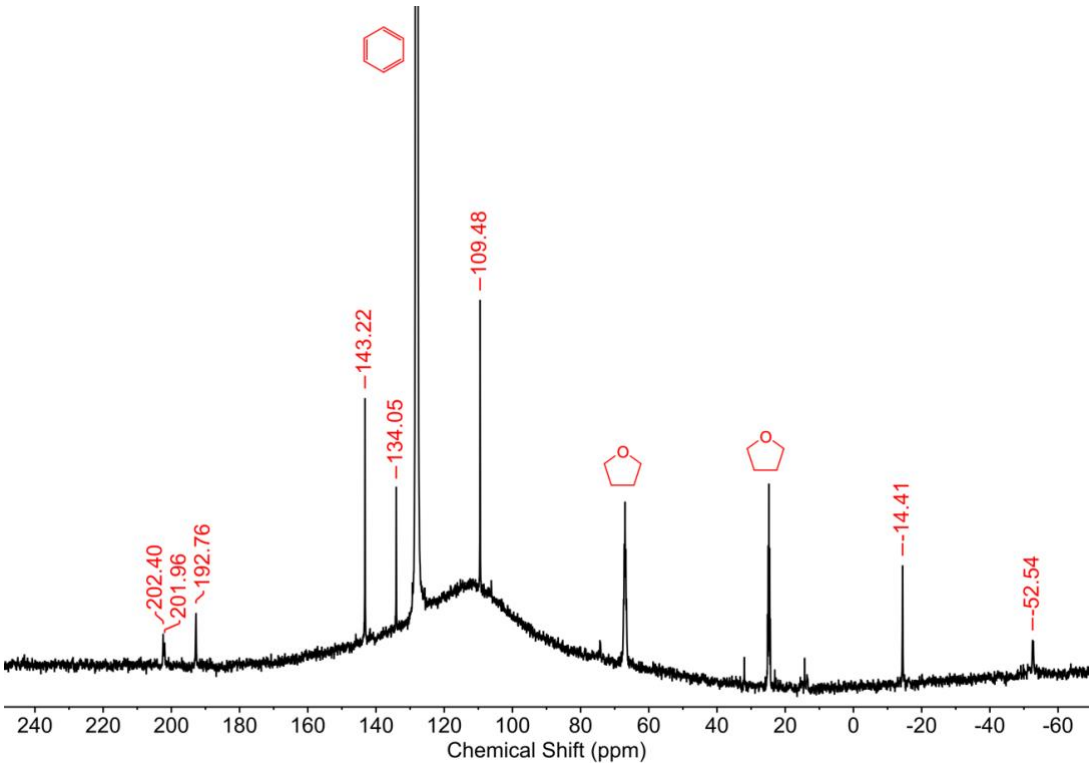

Figure S48. $^{13}C\{^{1}H\}$ NMR spectrum (at 295 K) of [Np(TMP)$_2$Bn$_2$K(toluene)] (**6Np**) in C_6D_6 with several drops of C_4D_8O. Broad feature *ca*. 110 ppm is due to the fluorinated ethylene propylene NMR tube liner.

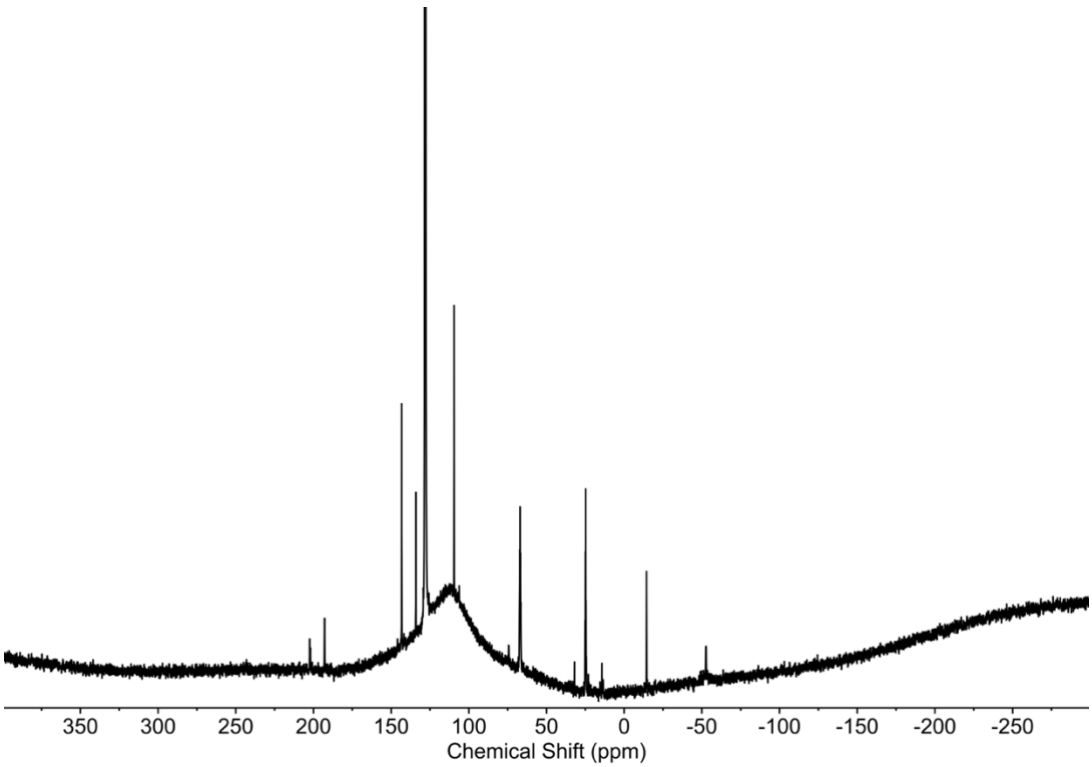

Figure S49. $^{13}C\{^{1}H\}$ NMR spectrum (at 295 K) of [Np(TMP)$_2$Bn$_2$K(toluene)] (**6Np**) in C_6D_6 with several drops of C_4D_8O, showing the full range collected.

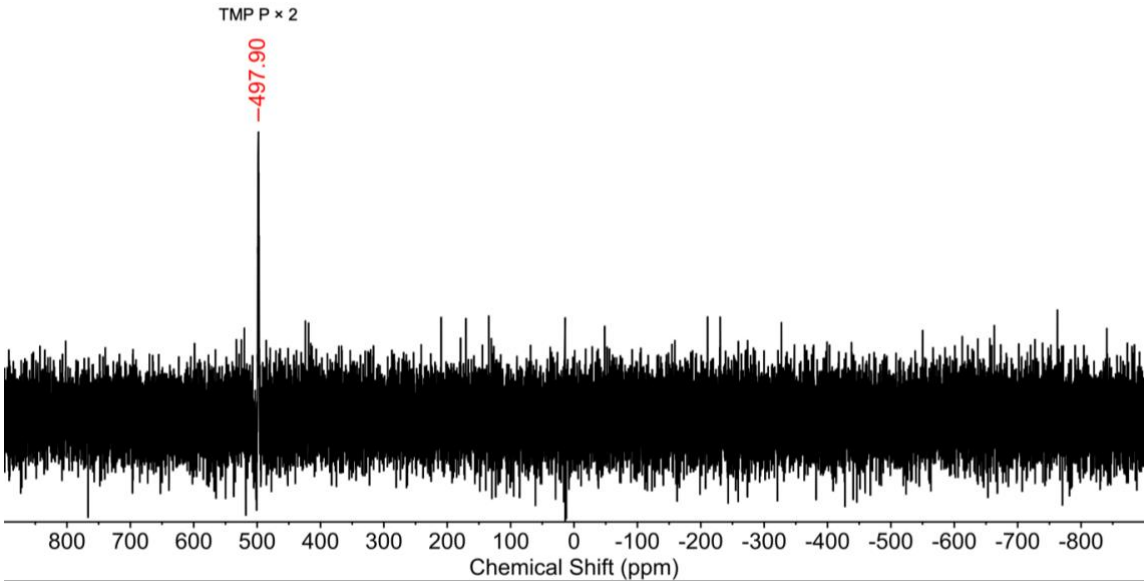

Figure S50. $^{31}P\{^{1}H\}$ NMR spectrum (at 296 K) of [Np(TMP)$_2$Bn$_2$K(toluene)] (**6Np**) in C_6D_6 with several drops of C_4D_8O.

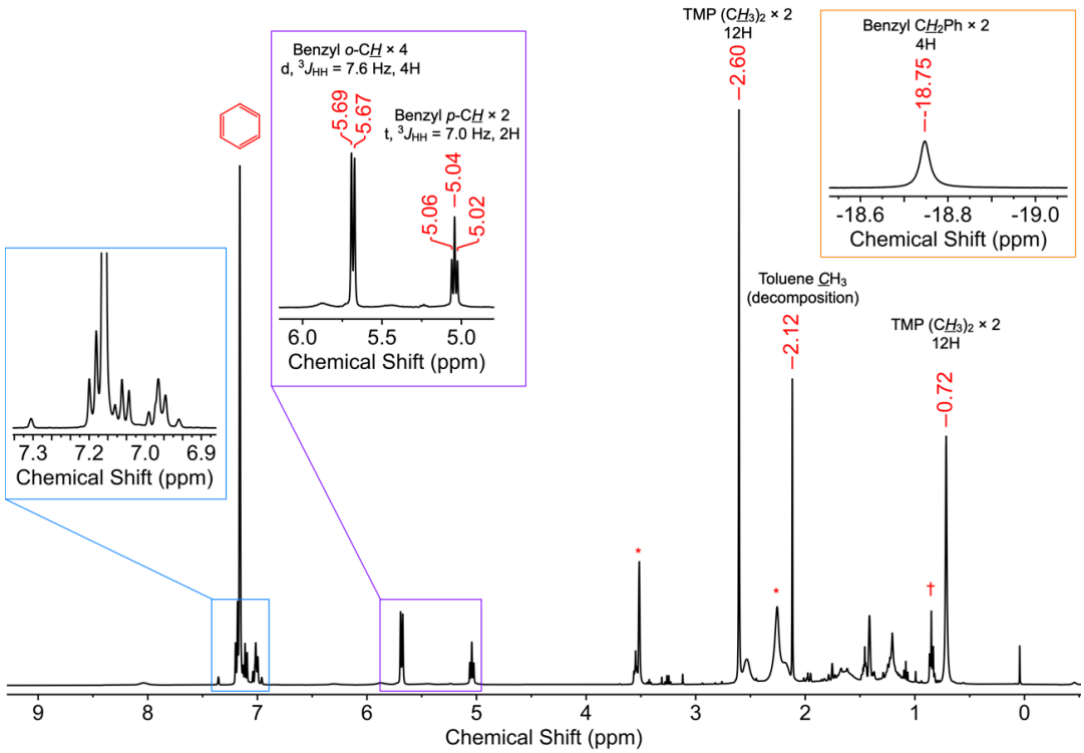

Figure S51. ^{1}H NMR spectrum (at 296 K) of [Pu(TMP)$_2$Bn$_2$K(toluene)] (**6Pu**) in C_6D_6 with several drops of C_4D_8O. * symbols denote unknown impurities; † symbol denotes a triplet ascribable to either the benzyl *m*-CH groups, or to trace *n*-pentane from the glovebox atmosphere due to sample preparation requirements.

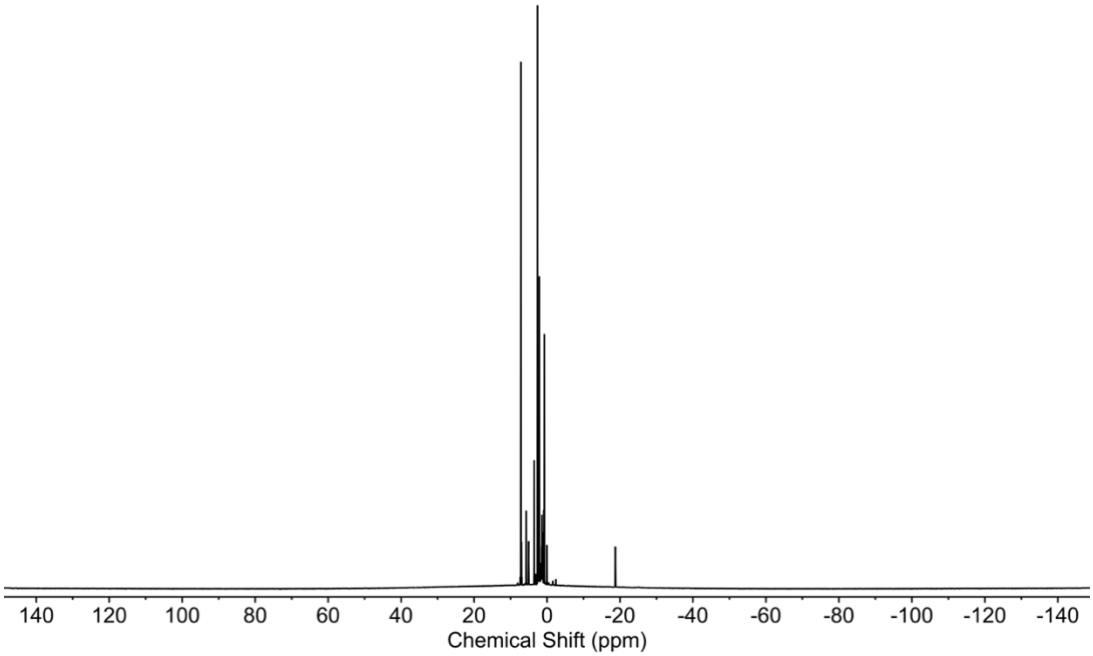

Figure S52. ^{1}H NMR spectrum (at 296 K) of [Pu(TMP)$_2$Bn$_2$K(toluene)] (**6Pu**) in C_6D_6, showing the full range collected.

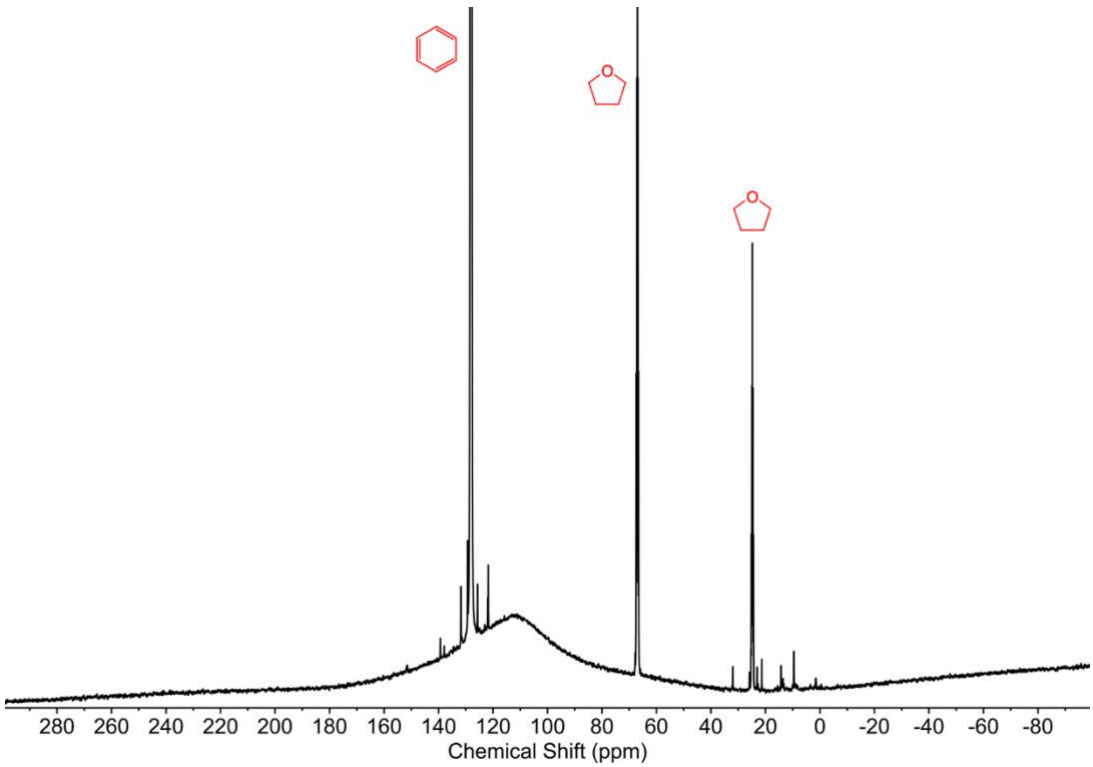

Figure S53. ^{13}C{^{1}H} NMR spectrum (at 296 K) of [Pu(TMP)$_2$Bn$_2$K(toluene)] (**6Pu**) in C_6D_6 with several drops of C_4D_8O, showing the full range collected.

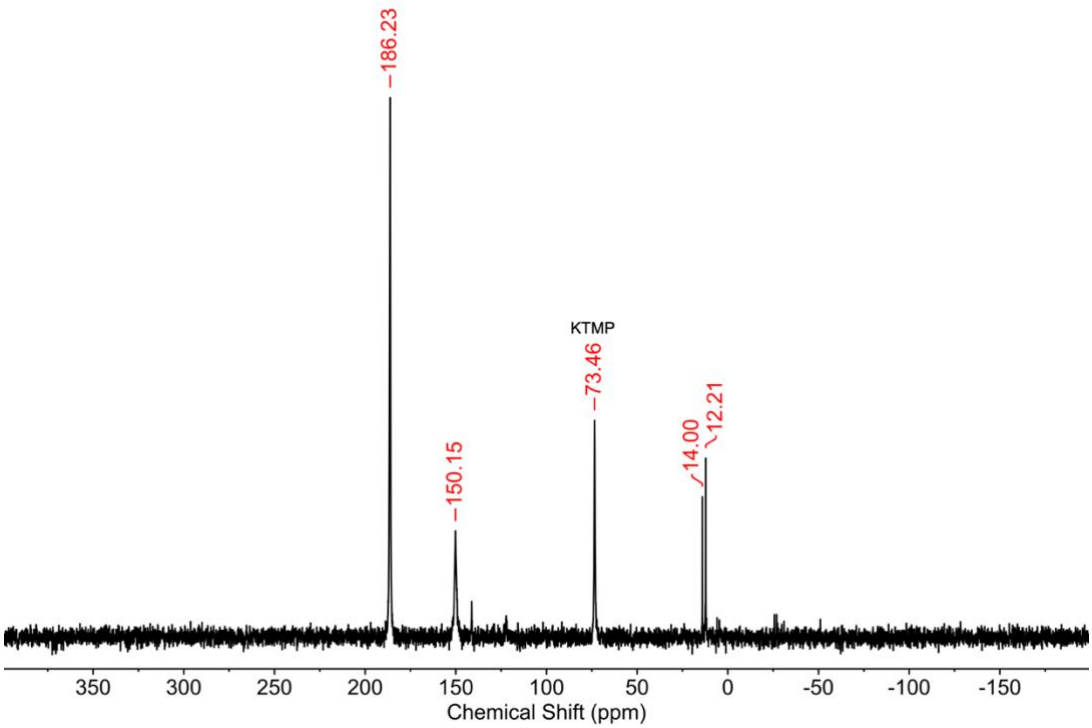

Figure S54. $^{31}P\{^{1}H\}$ NMR spectrum (at 296 K) of $[Pu(TMP)_2Bn_2K(toluene)]$ (**6Pu**) in C_6D_6 with several drops of C_4D_8O. The only identifiable peak is KTMP, presumably from disassociation/decomposition of **6Pu** from diffusion of unavoidable traces of atmospheric gases during the sealing procedure and long collection time.

Table of chemical shifts

Table S8. Some ^{1}H, and ^{31}P of chemical shifts for groups in [M(TMP)$_2$Bn$_2$K(toluene)] (**6M**, M = La, Ce, Pr, U, Np, and Pu).

	^{1}H C$\underline{H_2}$Ph (ppm)	**^{1}H Bn *o*-CH (ppm)**	**^{1}H Bn *m*-CH (ppm)**	**^{1}H Bn *p*-CH (ppm)**	**^{1}H TMP C$\underline{H_3}$ (ppm)**	**^{31}P TMP P (ppm)**
KTMP	-	-	-	-	[a]	74.32
6La	1.04	6.40	6.67	6.14	1.96 / 2.08	93.66
6Ce	1.22	3.65 / 6.07	3.65 / 6.07	4.57	2.94	175.30
6Pr	7.48	3.32	7.22	2.78	1.46 / 2.29	293.52
6U	–55.31	–3.13	6.54	1.10	–22.74/ –3.76	738.77
6Np	–60.30	2.63	7.86	2.56	–7.61 / 2.18	–497.90
6Pu	–18.75	5.68	[b]	5.04	0.72 / 2.60	[b]

[a] See elsewhere for the ^{1}H NMR chemical shift of KTMP, the data here was gathered in a mixture of C_4H_8O and C_6D_6 for comparison to **6M** complexes.

[b] These peaks could not be unambiguously located and so are not stated. Please see relevant figures.

Magnetic moments determined by NMR spectroscopy (Evans method)

Table S9. Data for the determination of the magnetic moments of [M(TMP)$_2$Bn$_2$K(toluene)] (**6M**, M = Ce, Pr, U, and Np).

Sample (peak)	μ_{eff} (μ_B mol^{-1}) [a]	Sample mass (g)	Solvent mass (g)	Solvent [d]	M_r (g mol^{-1})	Δ peak (Hz) [e]
6Ce (3.85 peak) [b]	2.625(10)	0.0162(1)	0.5242(1)	C_4D_8O	731.90	175.30
6Ce (1.72 peak) [b]	2.955(12)					229.00
6Pr (3.85 peak) [b]	3.697(16)	0.0157(1)	0.5164(1)	C_4D_8O	732.69	366.40
6Pr (1.72 peak) [b]	3.953(17)					422.45
6U (3.85 peak) [b]	3.231(14)	0.0152(1)	0.5450(1)	C_4D_8O	829.81	219.17
6U (1.72 peak) [b]	3.579(15)					274.06
6Np [c]	2.42(3)	0.0057(1)	0.3990(1)	C_6D_6	828.78	55.83

[a] Error reported as the standard deviation calculated from the min/max μ_{eff} values corresponding to the error of the masses.
[b] Masses gathered on a balance with internal calibration to 0.1 mg.
[c] Masses gathered on a balance externally validated with an external 0.1 mg check-weight.
[d] C_4D_8O = 0.985 g mL^{-1}, ρ C_6D_6 = 0.950 g mL^{-1}.
[e] Spectrometer frequency 400.130 MHz. Simple diamagnetic correction of M_r / −2,000,000 applied.[17]

Numerical averages and values to 3 significant figures

6Ce = 2.79(1) μ_B mol^{-1}

6Pr = 3.83(2) μ_B mol^{-1}

6U = 3.41(2) μ_B mol^{-1}

6Np = 2.42(3) μ_B mol^{-1} (*Note:* This is not an average as benzene rather than THF was used for **6Np**, thus only one peak is shifted).

Numerical average, $\bar{x} = 1/n\,(\sum_{i=1}^{n} x_i)$, calculated using the min/max μ_{eff} values based on the error of the masses. Error calculated per Equation S2 using individual standard deviation values.

S6. UV-vis-NIR spectroscopy

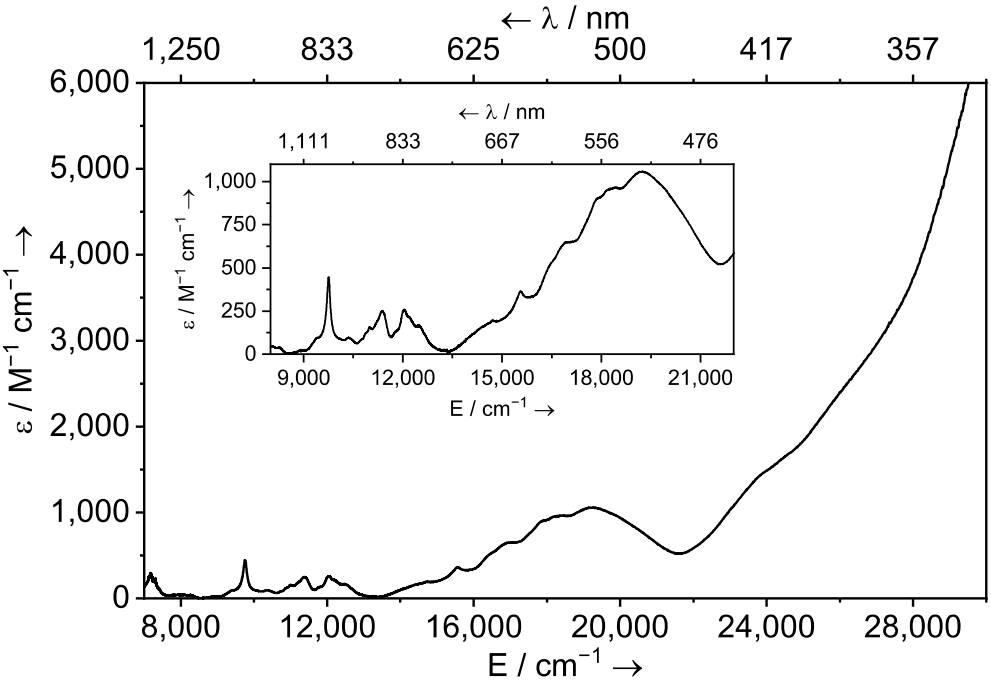

Figure S55. UV-vis-NIR spectrum of $[Np(TMP)_2Cl_2K(DME)]_n$ (**2**) in THF (0.34 mM) at room temperature.

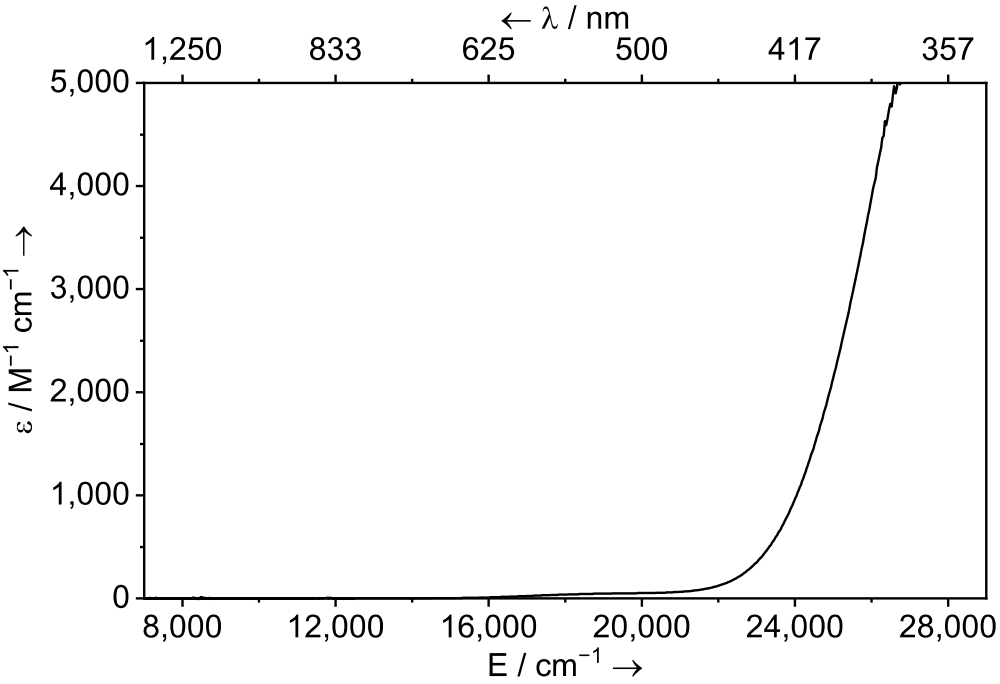

Figure S56. UV-vis-NIR spectrum of $[La(TMP)_2Bn_2K(toluene)]$ (**6La**) in THF (0.98 mM) at room temperature.

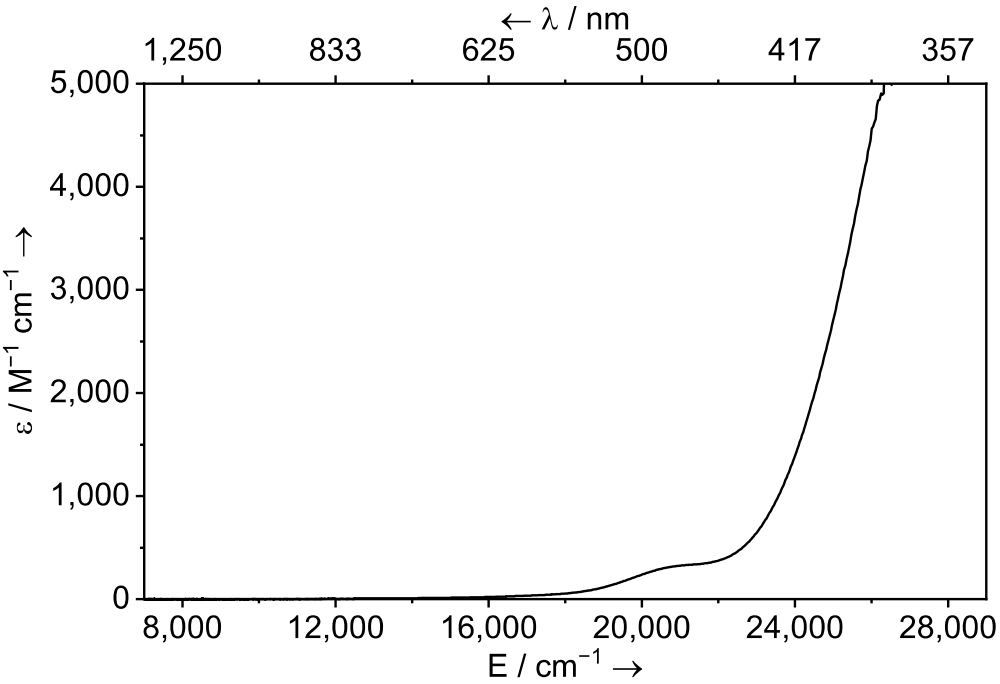

Figure S57. UV-vis-NIR spectrum of [Ce(TMP)$_2$Bn$_2$K(toluene)] (**6Ce**) in THF (0.99 mM) at room temperature.

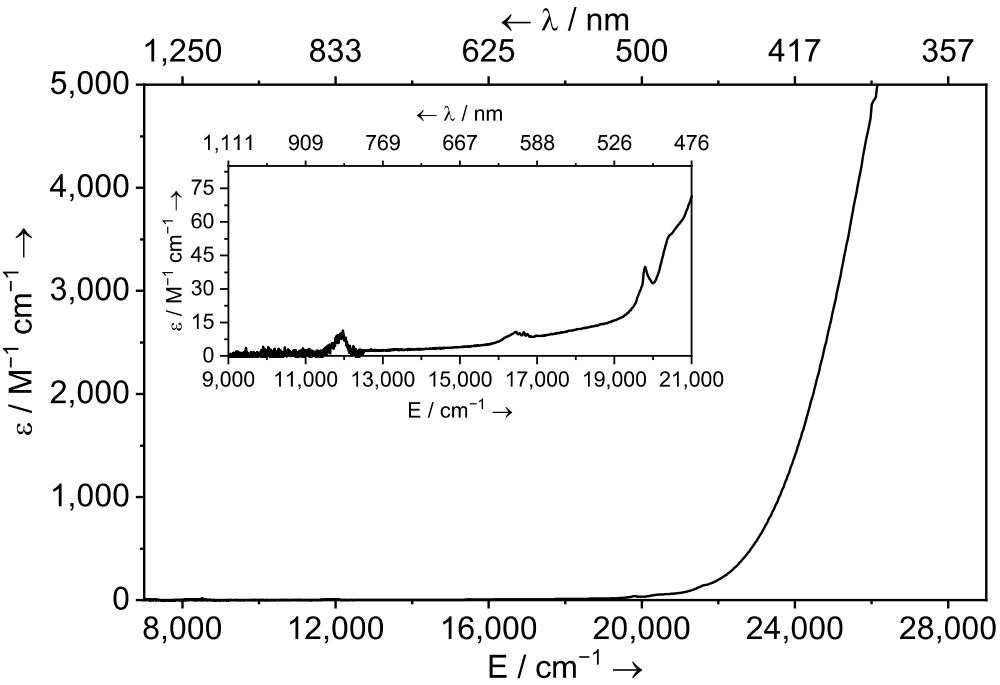

Figure S58. UV-vis-NIR spectrum of [Pr(TMP)$_2$Bn$_2$K(toluene)] (**6Pr**) in THF (0.97 mM) at room temperature.

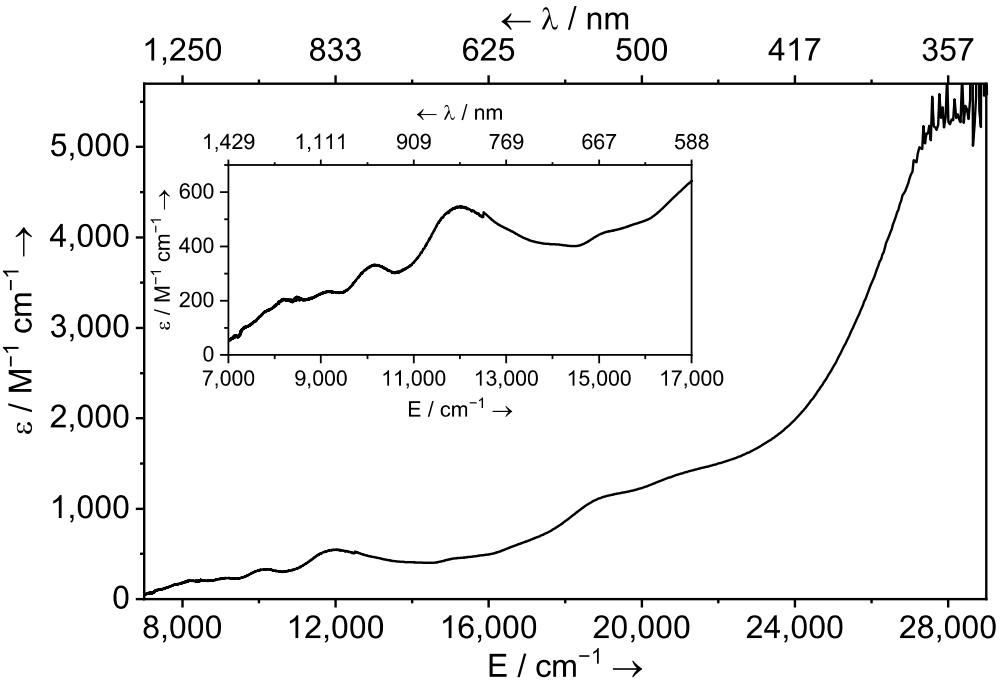

Figure S59. UV-vis-NIR spectrum of [U(TMP)$_2$Bn$_2$K(toluene)] (**6U**) in THF (0.97 mM) at room temperature.

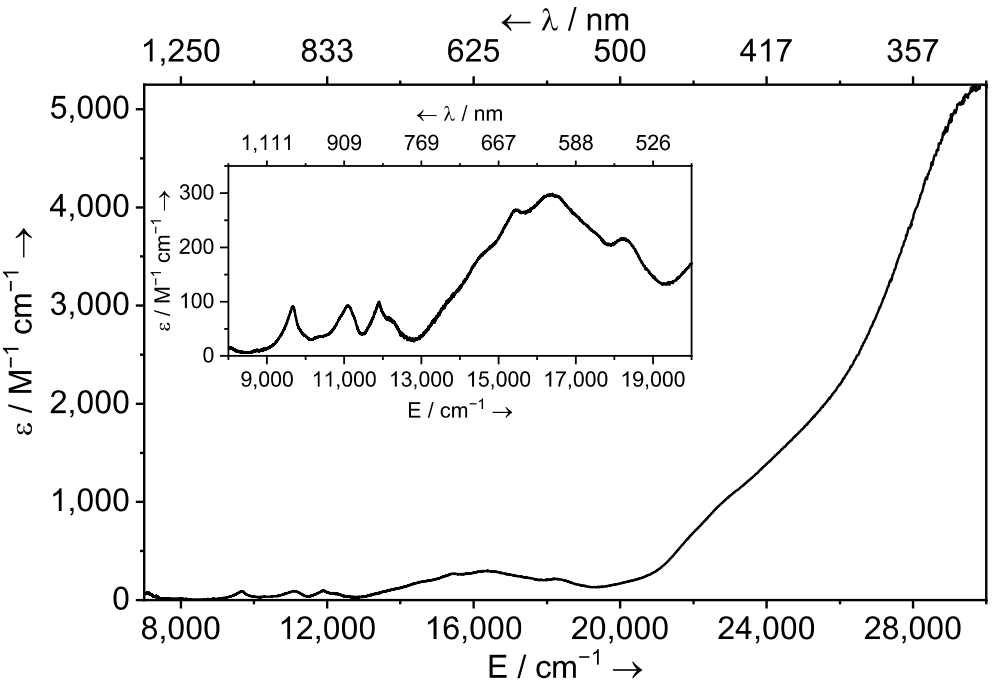

Figure S60. UV-vis-NIR spectrum of [Np(TMP)$_2$Bn$_2$K(toluene)] (**6Np**) in toluene (0.50 mM) at room temperature.

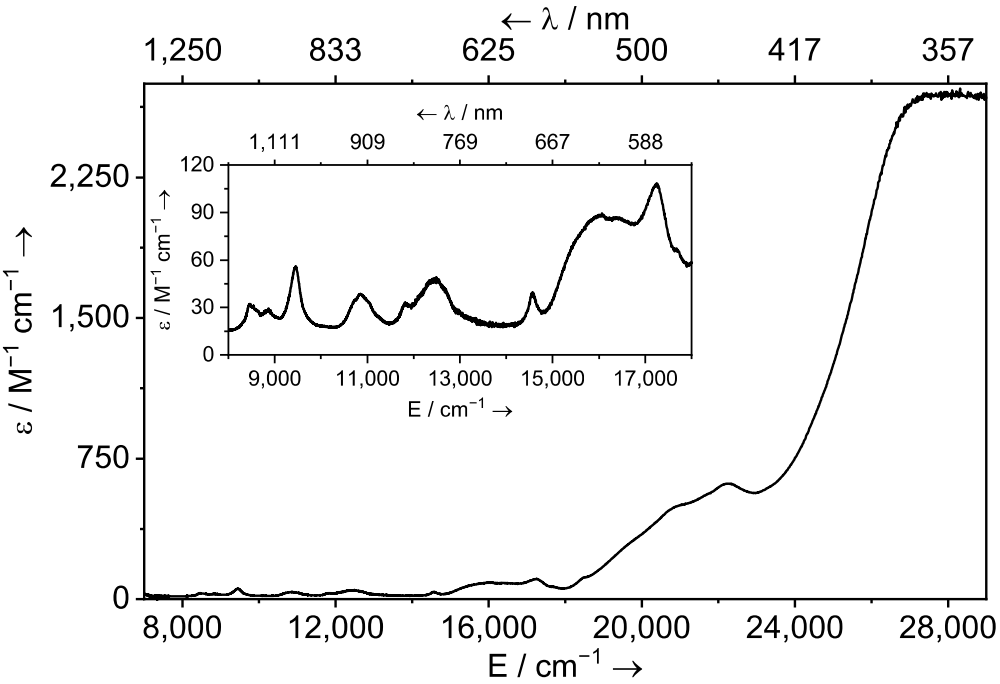

Figure S61. UV-vis-NIR spectrum of [Pu(TMP)$_2$Bn$_2$K(toluene)] (**6Pu**) in toluene (1.0 mM) at room temperature.

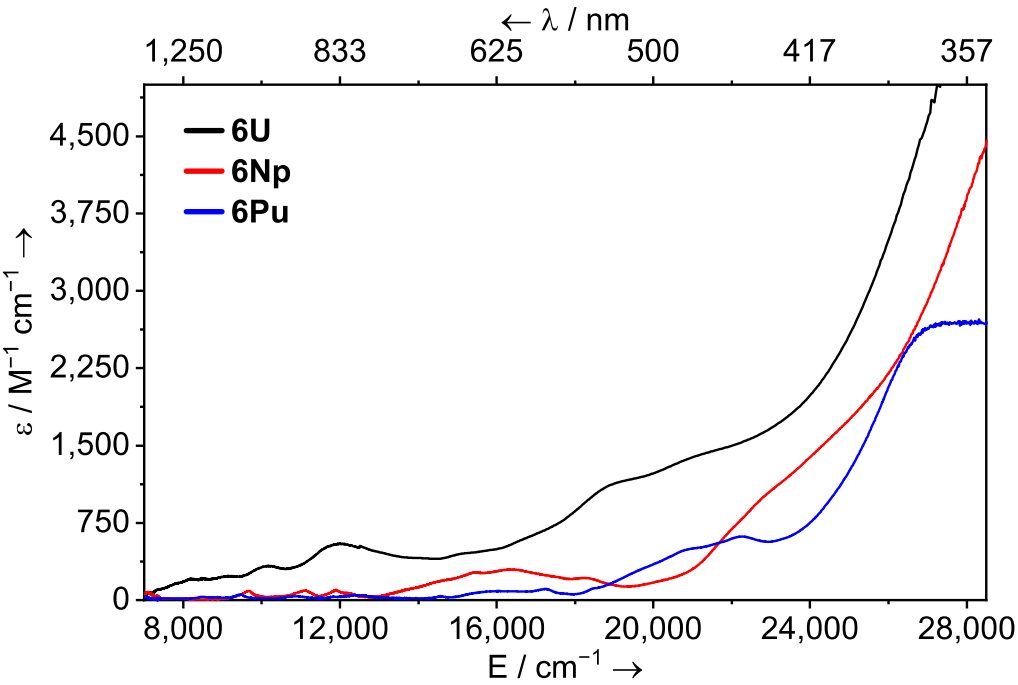

Figure S62. Combined UV-vis-NIR spectra of [U(TMP)$_2$Bn$_2$K(toluene)] (**6U**, black line) in THF (0.97 mM), and [Np(TMP)$_2$Bn$_2$K(toluene)] (**6Np**, red line) in toluene (0.50 mM), and [Pu(TMP)$_2$Bn$_2$K(toluene)] (**6Pu**, red line) in toluene (1.00 mM) at room temperature.

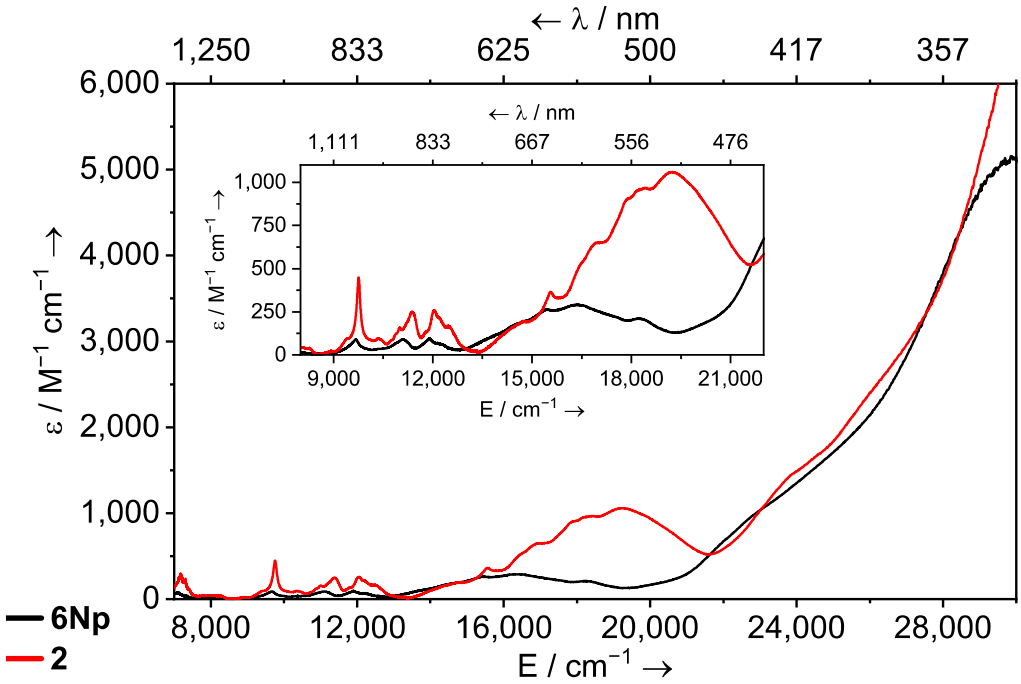

Figure S63. Combined UV-vis-NIR spectra of [Np(TMP)$_2$Cl$_2$K(DME)] (**2**, red line) in THF (0.34 mM) and [Np(TMP)$_2$Bn$_2$K(toluene)] (**6Np**, black line) in toluene (0.50 mM) at room temperature. To show the similarities in the 5*f*→5*f* transitions.

S7. ATR-IR / FTIR spectroscopy

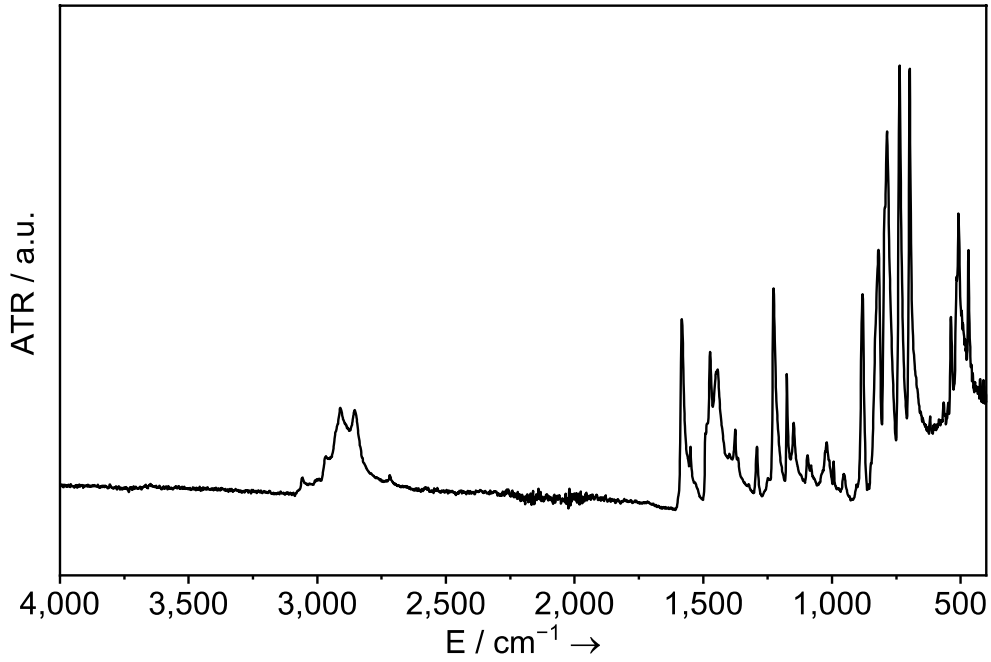

Figure S64. ATR-IR spectrum of [La(TMP)$_2$Bn$_2$K(toluene)] (**6La**).

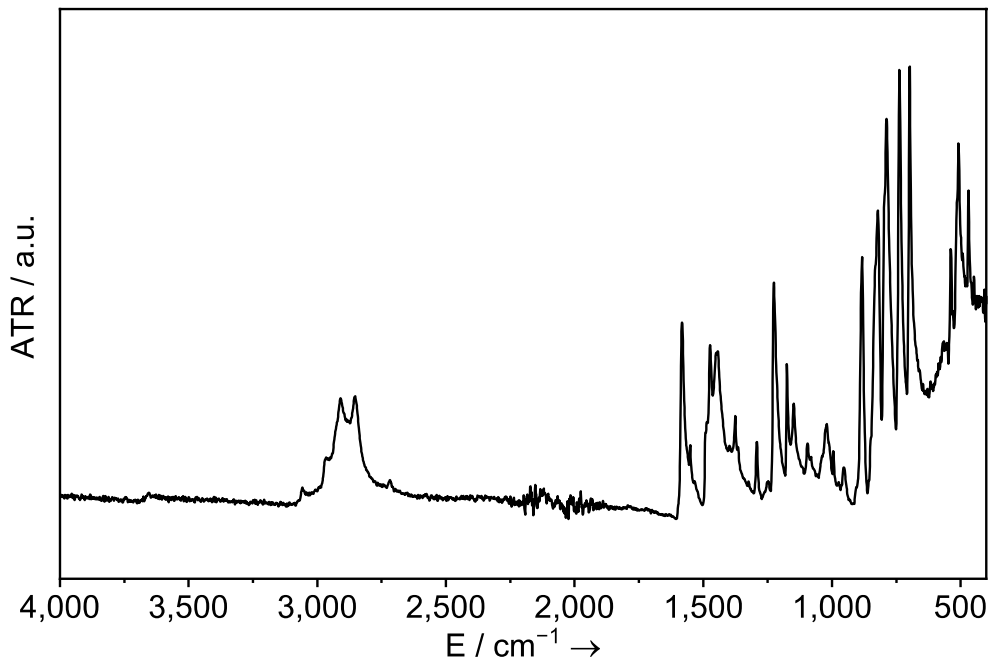

Figure S65. ATR-IR spectrum of [Ce(TMP)$_2$Bn$_2$K(toluene)] (**6Ce**).

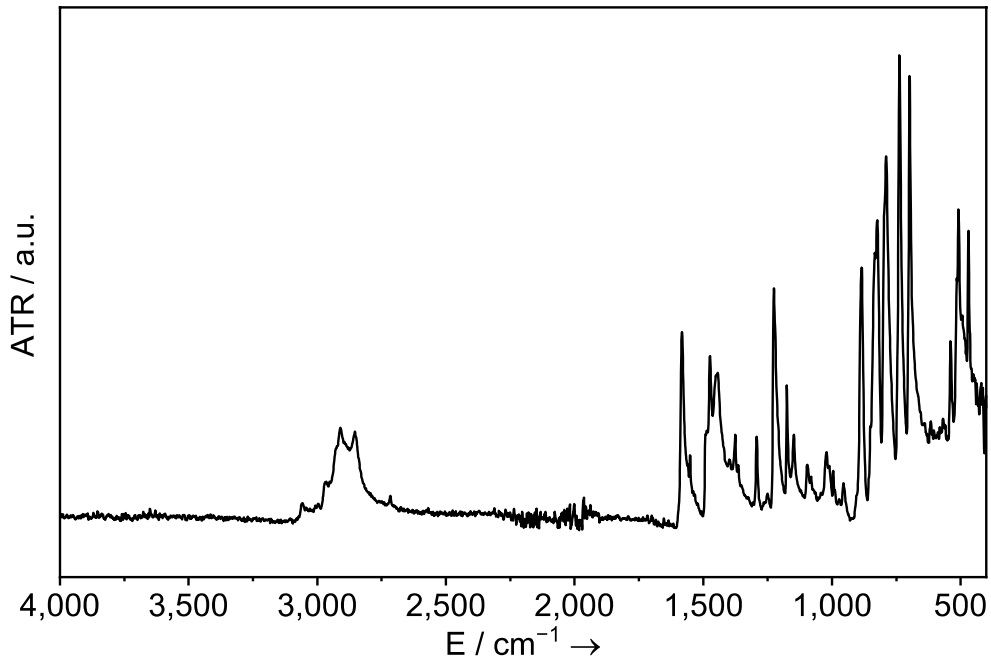

Figure S66. ATR-IR spectrum of [Pr(TMP)$_2$Bn$_2$K(toluene)] (**6Pr**).

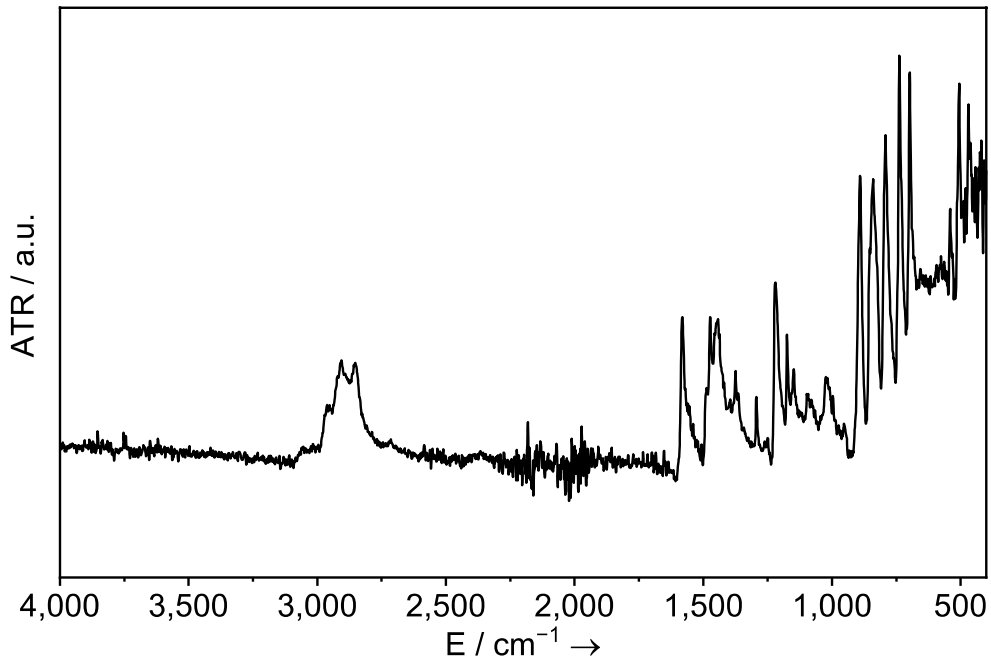

Figure S67. ATR-IR spectrum of [U(TMP)$_2$Bn$_2$K(toluene)] (**6U**).

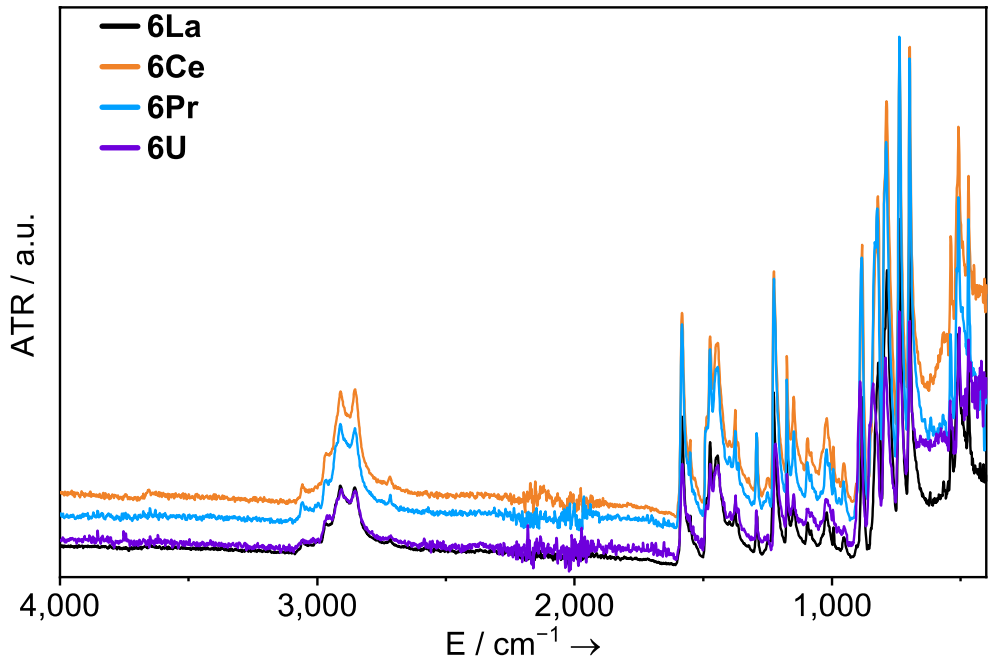

Figure S68. Combined ATR-IR spectra of [M(TMP)$_2$Bn$_2$K(toluene)] (**6M**, M = La, Ce, Pr, and U).

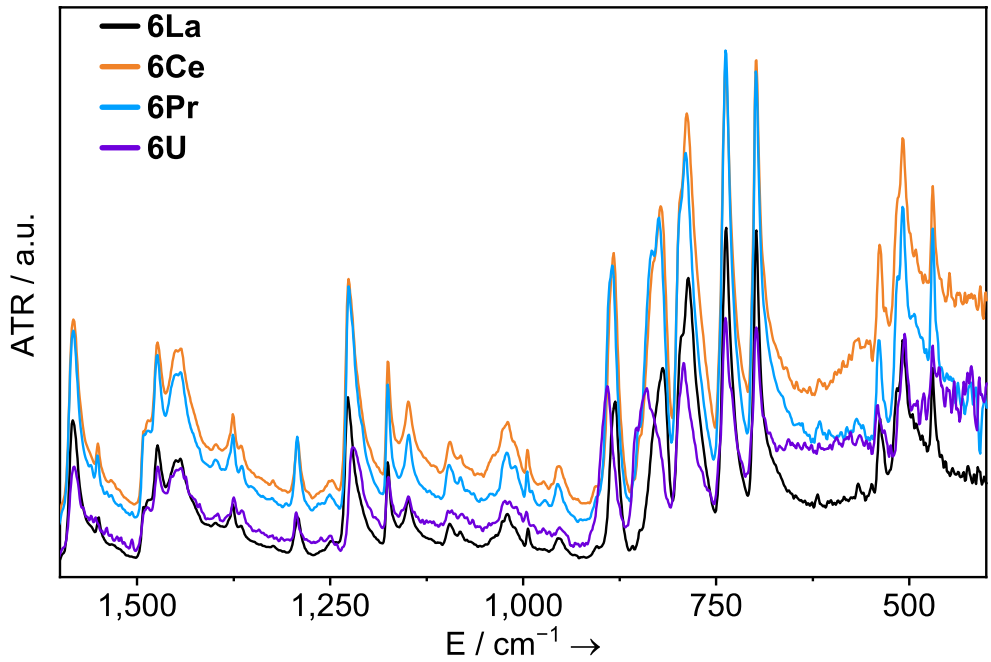

Figure S69. Combined ATR-IR spectra of [M(TMP)$_2$Bn$_2$K(toluene)] (**6M**, M = La, Ce, Pr, and U) zoomed to show just the fingerprint region.

S8. SQUID Magnetometry

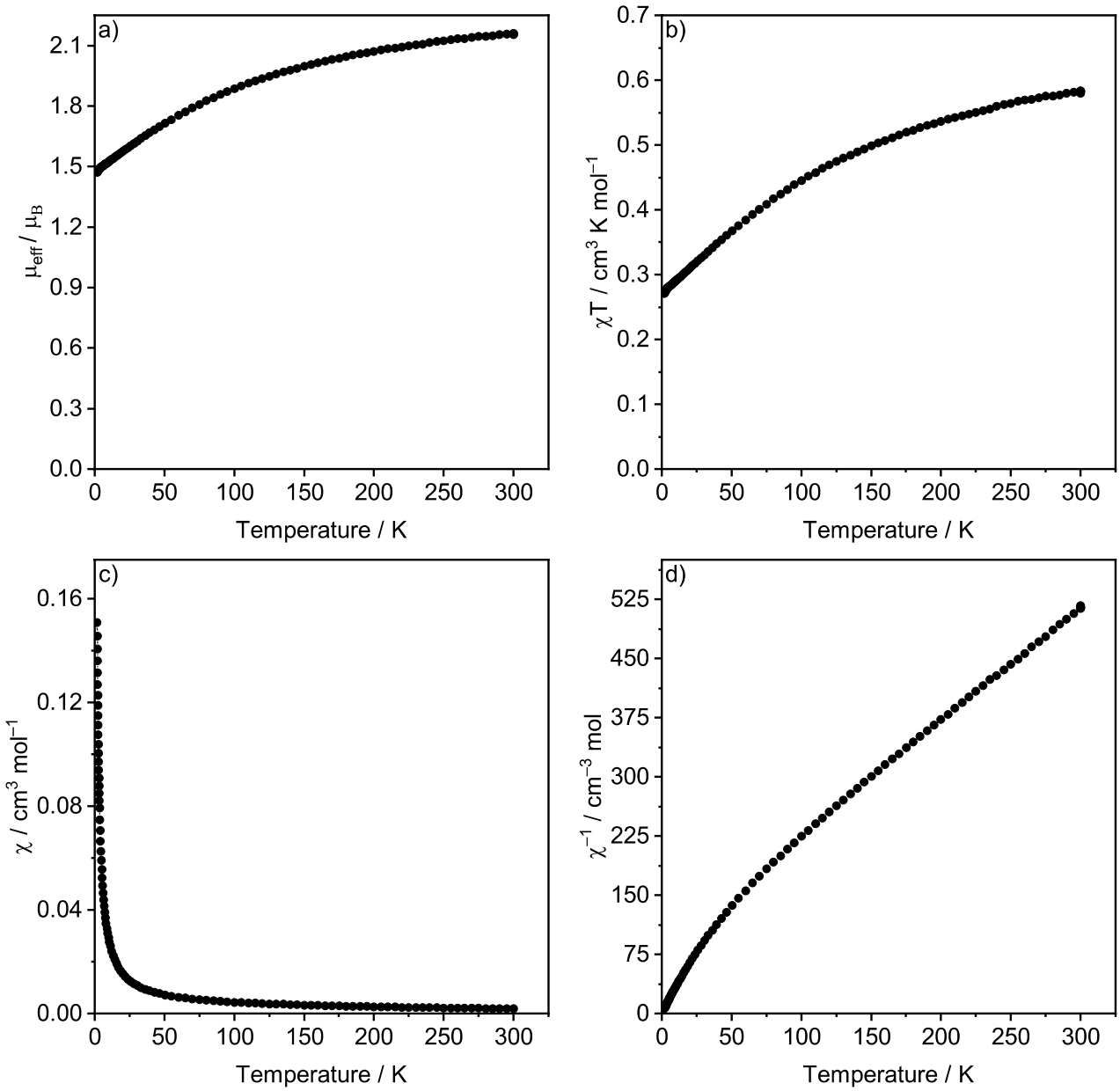

Figure S70. Variable-temperature SQUID magnetometry data of a powdered sample of **6Ce** in a 0.5 T external field over the temperature range 300–1.8 K: a) μ_{eff} *vs* T; b) χT *vs* T; c) χ *vs* T; d) χ^{-1} *vs* T.

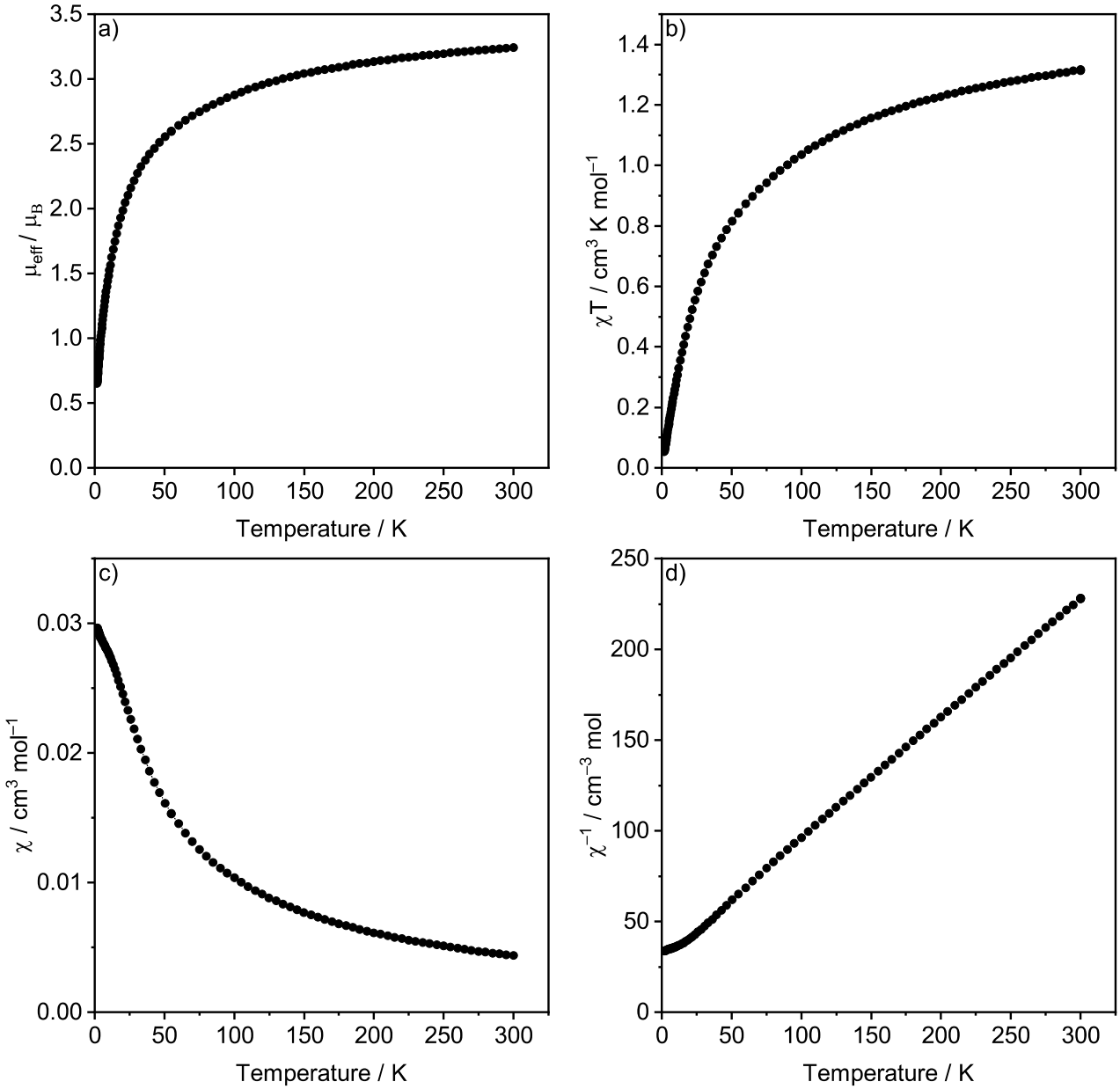

Figure S71. Variable-temperature SQUID magnetometry data of a powdered sample of **6Pr** in a 0.5 T external field over the temperature range 300–1.8 K: a) μ_{eff} *vs* T; b) χT *vs* T; c) χ *vs* T; d) χ^{-1} *vs* T.

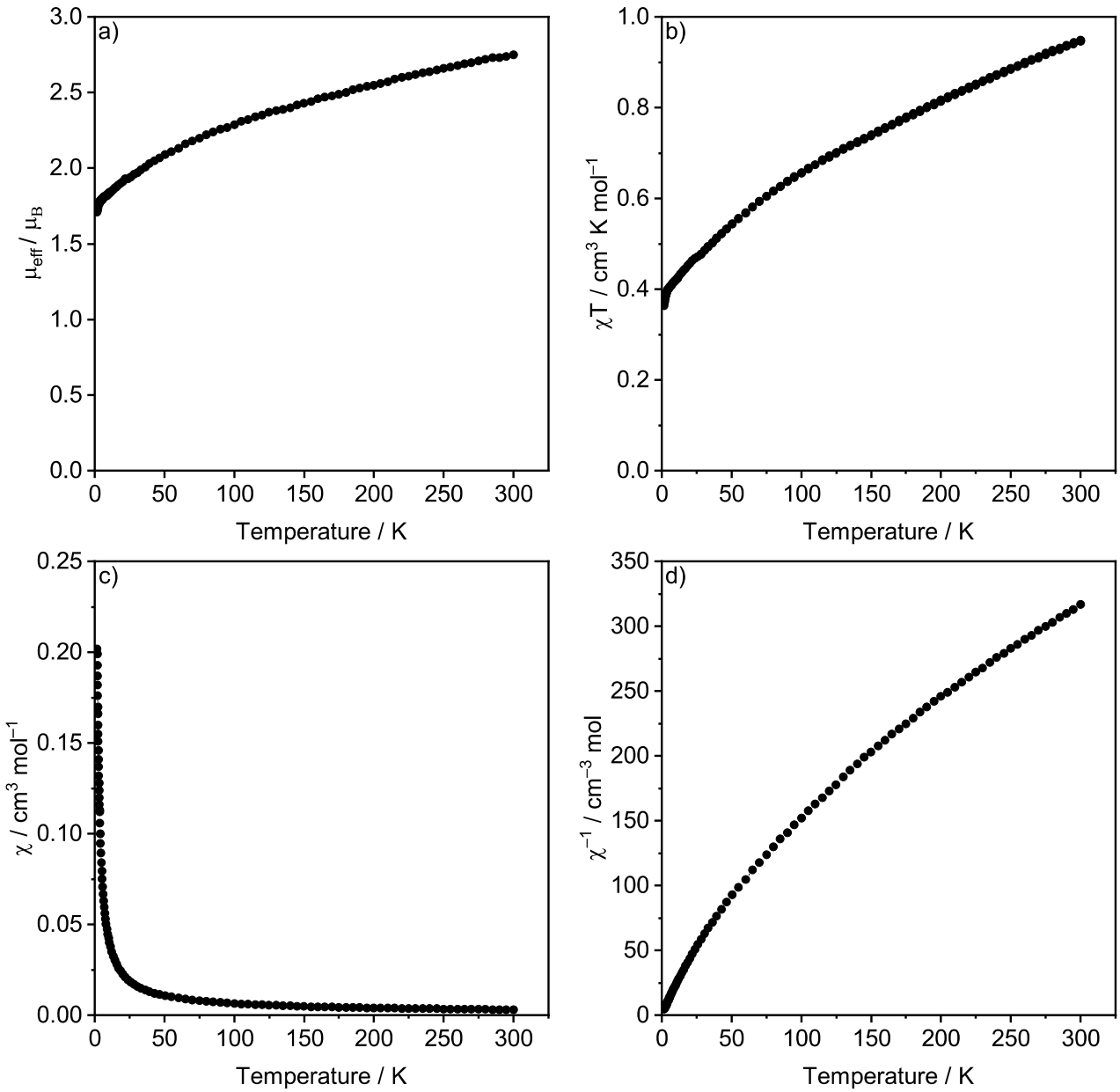

Figure S72. Variable-temperature SQUID magnetometry data of a powdered sample of **6U** in a 0.5 T external field over the temperature range 300–1.8 K: a) μ_{eff} *vs* T; b) χT *vs* T; c) χ *vs* T; d) χ^{-1} *vs* T.

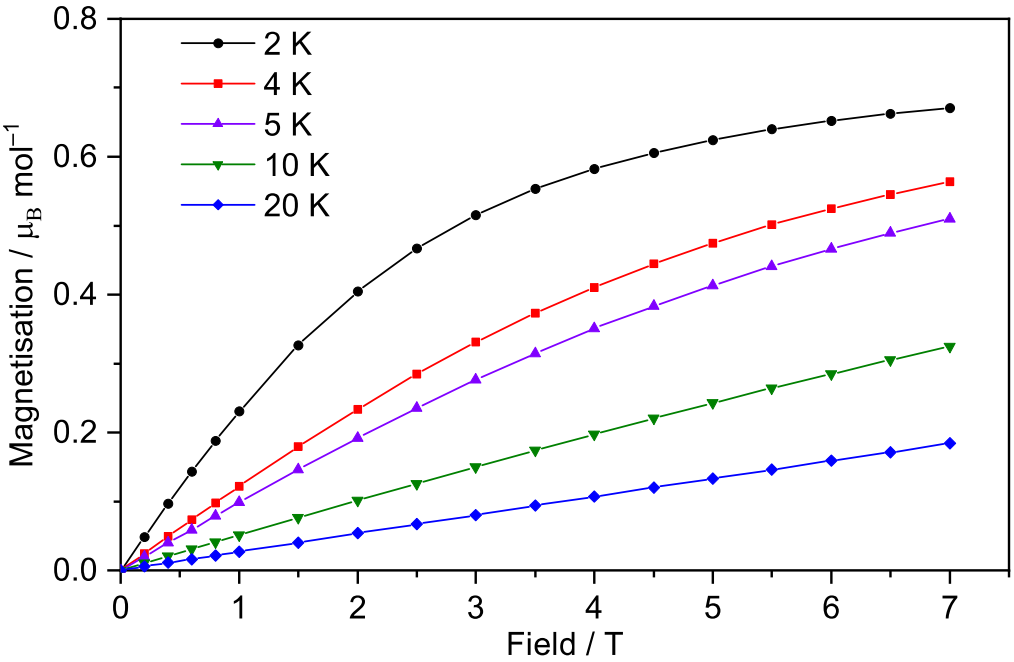

Figure S73. Variable-field molar magnetisation for **6Ce** up to 7 T at multiple temperatures.

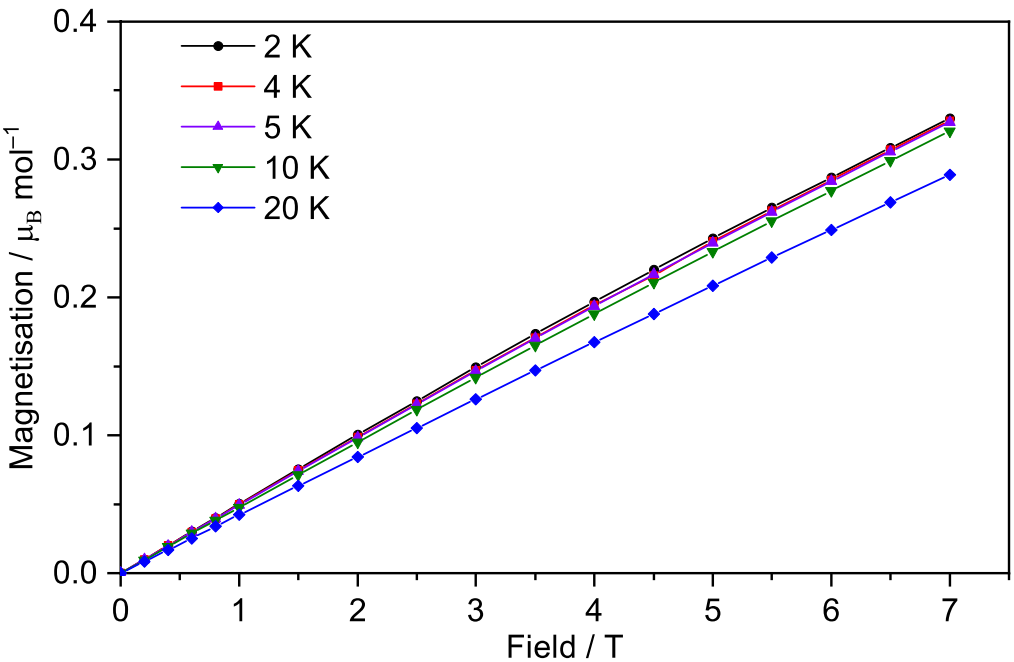

Figure S74. Variable-field molar magnetisation for **6Pr** up to 7 T at multiple temperatures.

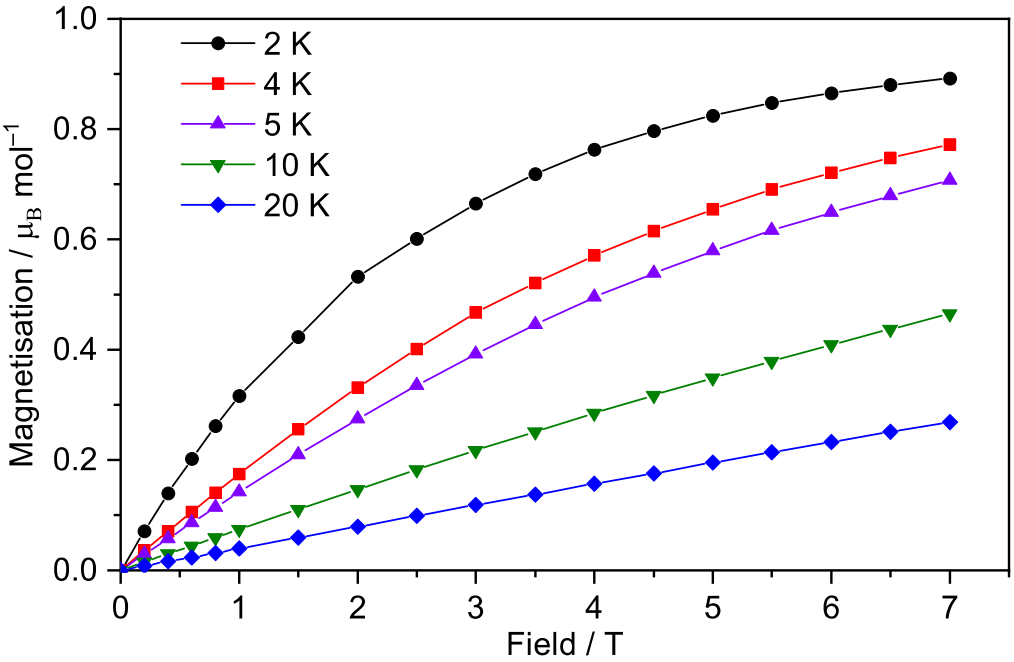

Figure S75. Variable-field molar magnetisation for **6U** up to 7 T at multiple temperatures.

S9. References

[1] K. Izod, S. T. Liddle, W. Clegg, A convenient route to lanthanide triiodide THF solvates. Crystal structures of $LnI_3(THF)_4$ [Ln = Pr] and $LnI_3(THF)_{3.5}$ [Ln = Nd, Gd, Y]. *Inorg. Chem.* **2004**, *43*, 214-218. https://doi.org/10.1021/ic034851u.

[2] T. V. Fetrow, J. P. Grabow, J. Leddy, S. R. Daly, Convenient Syntheses of Trivalent Uranium Halide Starting Materials without Uranium Metal. *Inorg. Chem.* **2021**, *60*, 7593-7601. https://doi.org/10.1021/acs.inorgchem.1c00598.

[3] C. A. P. Goodwin, M. T. Janicke, B. L. Scott, A. J. Gaunt, $[AnI_3(THF)_4]$ (An = Np, Pu) preparation bypassing An^0 metal precursors: access to Np^{3+}/Pu^{3+} nonaqueous and organometallic complexes. *J. Am. Chem. Soc.* **2021**, *143*, 20680-20696. https://doi.org/10.1021/jacs.1c07967.

[4] C. D. Carmichael, N. A. Jones, P. L. Arnold, Low-valent uranium iodides: straightforward solution syntheses of UI_3 and UI_4 etherates. *Inorg. Chem.* **2008**, *47*, 8577-8579. https://doi.org/10.1021/ic801138e.

[5] S. M. Greer, Ö. Üngor, R. J. Beattie, J. L. Kiplinger, B. L. Scott, B. W. Stein, C. A. P. Goodwin, Low-spin 1,1'-diphosphametallocenates of Chromium and Iron. *Chem. Commun.* **2020**, *57*, 595-598. https://doi.org/10.1039/D0CC06518H.

[6] B. L. Scott, Actinide Research Quarterly, Los Alamos National Laboratory, **2015**, pp. 6-9. https://doi.org/10.2172/1188164.

[7] D. Parker, E. A. Suturina, I. Kuprov, N. F. Chilton, How the Ligand Field in Lanthanide Coordination Complexes Determines Magnetic Susceptibility Anisotropy, Paramagnetic NMR Shift, and Relaxation Behavior. *Acc. Chem. Res.* **2020**, *53*, 1520-1534. https://doi.org/10.1021/acs.accounts.0c00275.

[8] N. Muller, P. C. Lauterbur, J. Goldenson, Nuclear Magnetic Resonance Spectra of Phosphorus Compounds. *J. Am. Chem. Soc.* **2002**, *78*, 3557-3561. https://doi.org/10.1021/ja01596a002.

[9] S. A. Pattenaude, N. H. Anderson, S. C. Bart, A. J. Gaunt, B. L. Scott, Non-aqueous neptunium and plutonium redox behaviour in THF - access to a rare Np(III) synthetic precursor. *Chem. Commun.* **2018**, *54*, 6113-6116. https://doi.org/10.1039/C8CC02611D.

[10] M. A. Whitefoot, D. Perales, M. Zeller, S. C. Bart, Synthesis of Non-Aqueous Neptunium(III) Halide Solvates from NpO_2. *Chem. Eur. J.* **2021**, *27*, 18054-18057. https://doi.org/10.1002/chem.202103265.

[11] Rigaku Oxford Diffraction, (2022), CrysAlisPro Software system, version 1.171.42, Rigaku Corporation, Wroclaw, Poland.

[12] O. V. Dolomanov, L. J. Bourhis, R. J. Gildea, J. A. K. Howard, H. Puschmann, OLEX2: a complete structure solution, refinement and analysis program. *J. Appl. Crystallogr.* **2009**, *42*, 339-341. https://doi.org/10.1107/s0021889808042726.

[13] G. M. Sheldrick, Crystal structure refinement with SHELXL. *Acta Crystallogr. C* **2015**, *71*, 3-8. https://doi.org/10.1107/S2053229614024218.

[14] G. M. Sheldrick, A short history of SHELX. *Acta Crystallogr. A* **2008**, *64*, 112-122. https://doi.org/10.1107/S0108767307043930.

[15] Inkscape: Open Source Scalable Vector Graphics Editor. https://inkscape.org/.

[16] W. Clegg, A. J. Blake, J. M. Cole, J. S. O. Evans, P. Main, S. Parsons, D. J. Watkin, *Crystal Structure Analysis*, 2nd ed., Oxford University Press, Oxford, **2009**. http://doi.org/10.1093/acprof:oso/9780199219469.001.0001.

[17] G. A. Bain, J. F. Berry, Diamagnetic Corrections and Pascal's Constants. *J. Chem. Educ.* **2008**, *85*, 532-536. https://doi.org/10.1021/ed085p532.